

POLITECNICO DI TORINO

CORSO DI LAUREA MAGISTRALE in INGEGNERIA BIOMEDICA

TESI DI LAUREA MAGISTRALE

“Development of multifunctional mesoporous silica nanoparticles with antioxidant properties for treating inflammatory-related diseases”



**Politecnico
di Torino**

Candidato

Anna Rossanese

305590

Relatori

Prof.ssa Chiara Tonda-Turo

Prof.ssa Irene Carmagnola

Prof. Piergiorgio Gentile

Ottobre 2023

Abstract

Post-traumatic stress disorder (PTSD) is a long-lasting debilitating condition that impacts a wide range of people across the world, and it is characterized by different kind of symptoms, like re-experiencing the traumatic event, avoidance of trauma-related stimuli, negative thoughts or emotions associated with the traumatic event, general changes in mood and cognition, and hyperarousal symptoms. In addition to the severe psychological issues, a lot of studies have discovered a connection between PTSD and an increased risk of serious physical diseases, which are all known to have an inflammatory component.

This inflammatory component is also found in skin infection since the immune system fights it by stimulating inflammation in both the injured tissue and the body. Generally, *Staphylococcus aureus* is the leading cause of skin and soft tissue infections (SSTI), and the burden of diseases from *S. aureus* SSTI, particularly those caused by methicillin-resistant isolates (MRSA), is extremely high.

To reduce this inflammation state, the aim of this project was to create a natural polymer-based nanocarrier system for the delivery of antioxidant extracts as an innovative approach to target and reduce inflammation. To do that, the “Layer by Layer” technique was used to build a polyelectrolyte multilayer that could encapsulate antioxidant. Two natural polymers, Pectin (PEC) and Chitosan (CH) were alternately used to coat mesoporous silica nanoparticles (MNPs) exploiting their opposite charge to create electrical interactions. Chitosan and Pectin were chosen to be used respectively as polycation and polyanion after the measurement of their Zeta Potential using the Dynamic Light Scattering (DLS), (PE -39 mV and CH +40 mV). Due to the negative charge of the MNPs’ surface, the first layer was the Chitosan, then the Pectin and so on to reach 5 total layers.

The anti-inflammatory component was obtained using antioxidants extracted from seaweed. Through the optimization of several extraction parameters such as temperature (°C), time (min) and liquid/solid ratio (mg/mL), carried out thanks to the design of experiment (DOEs), it was possible to optimize an

ultrasound assisted extraction using a 50% ethanol solution for 6 different types of seaweed. To evaluate the total phenolic content (TPC), the Folin-Ciocalteu reagent was used: the seaweed extract with the highest TPC was chosen and it was mixed with the Pectin at two different ratios (Antioxidant Extract:Pectin 4:1 and 10:1). Furthermore, the FTIR/ATR was used to detect the presence of different functional groups. Finally, to characterize the MNPs chemistry and morphology, different analyses were performed, such as the TEM, the XPS and the FTIR analyses.

To test the cytocompatibility of the MNPs, Live&Dead and PrestoBlue assays were used on fibroblasts, while the antibacterial activity of the antioxidant extracts was evaluated through some bacterial tests.

Declaration

This report is being submitted as a requirement for the completion of the Master's Degree in Biomedical Engineering at Politecnico di Torino. It has not been previously submitted for any other degree at this university or any other academic institution. The research described in this report was conducted at the University of Newcastle upon Tyne and is fully documented in a Project Logbook, which is available for examination. I am fully aware of the consequences of plagiarism, fabrication, and failure to acknowledge sources, and I hereby affirm that this report is free from any such violations.

Acknowledgments

First, I would like to thank Professor Chiara Tonda Turo and Professor Irene Carmagnola for giving me the opportunity to carry out this project. Furthermore, I would like to express my gratitude to Piergiorgio Gentile, for the availability to teach and help me through all the work at Newcastle University. Your guidance has been fundamental during this experience. Thank you.

Sommario

Abstract

Declaration

Acknowledgment

1	INTRODUCTION	10
1.1	POST TRAUMATIC STRESS DISORDER (PTSD)	10
1.1.1	INFLAMMATION AND PTSD	11
1.1.2	REACTIVE OXYGEN SPECIES (ROS)	13
1.1.3	GENDER'S INFLUENCE IN PTSD	14
1.1.4	TREATMENTS	15
1.2	SKIN INFECTION	16
1.2.1	OVERVIEW	16
1.2.2	BACTERIAL INFECTIONS	19
1.2.2.1	SKIN IMMUNE SYSTEM.....	20
1.3	NATURAL ANTIOXIDANTS.....	23
1.3.1	SEAWEEEDS	27
1.3.1.1	BROWN ALGAL POLYSACCHARIDES.....	27
1.3.1.2	RED ALGAL POLYSACCHARIDES	28
1.3.1.3	GREEN ALGAL POLYSACCHARIDES	28
1.3.2	EXTRACTION OF ANTIOXIDANTS.....	29
1.4	ANTIOXIDANTS DELIVERY VIA NANOCARRIERS.....	30
1.5	LAYER BY LAYER TECHNIQUE (LBL).....	32
1.5.1	LBL ASSEMBLY WITH NATURAL POLYMERS	33
2	AIM AND OBJECTIVES	36
3	MATERIALS AND METHODS	38
3.1	MATERIALS	38
3.2	METHODS	39
3.2.1	ULTRASOUND ASSISTED EXTRACTION TECHNIQUE	39
3.2.2	CHARACTERIZATION OF ANTIOXIDANTS EXTRACT	40
3.2.2.1	METABOLITES EVALUATION - METABOLOMICS.....	40
3.2.2.2	FOLIN-CIOCALTEU METHOD TO EVALUATE THE TOTAL PHENOLIC CONTENT	42

3.2.2.3	FERRIC REDUCING ANTIOXIDANT POWER METHOD TO EVALUATE THE ANTIOXIDANT ACTIVITY	43
3.2.2.4	FOURIER-TRANSFORM INFRARED SPECTROSCOPY (FTIR-ATR) TO DETERMINE SURFACE FUNCTIONAL GROUPS	44
3.2.3	PREPARATION OF NANOPARTICLES.....	44
3.2.3.1	POLYELECTROLYTES PREPARATION.....	44
3.2.3.2	LAYER BY LAYER FUNCTIONALIZATION	45
3.2.4	CHARACTERIZATION OF NANOPARTICLES	46
3.2.4.1	DYNAMIC LIGHT SCATTERING TO MEASURE THE ζ -POTENTIAL.....	46
3.2.4.2	TRANSMISSION ELECTRON MICROSCOPE (TEM) FOR THE MORPHOLOGY CHARACTERIZATION.....	46
3.2.4.3	X-RAY PHOTOELECTRON SPECTROSCOPY (XPS) ANALYSIS.....	47
3.2.4.1	FOLIN-CIOCALTEU METHOD.....	47
3.2.4.2	FTIR ANALYSIS	48
3.2.5	CELL CULTURE	48
3.2.6	BACTERIAL TESTS	50
4	RESULTS AND DISCUSSION.....	52
4.1	ULTRASOUND-ASSISTED EXTRACTION TECHNIQUE.....	52
4.1.1	EFFECT OF TEMPERATURE, TIME AND RATIO ON TOTAL PHENOLIC CONTENT (TPC) ..	52
4.1.2	MINITAB EQUATIONS	Errore. Il segnalibro non è definito.
4.1.1	METABOLOMICS	Errore. Il segnalibro non è definito.
4.1.2	EVALUATION OF RELIABILITY OF THE FITTED MODELS.....	57
4.2	CARACTERIZATION OF ANTIOXIDANT EXTRACT	64
4.2.1	FTIR	64
4.2.2	TOTAL PHENOLIC CONTENT (TPC) AND ANTIOXIDANT ACTIVITY EVALUATION	66
4.2.2.1	FOLIN-CIOCALTEU METHOD.....	66
4.2.2.2	FERRIC REDUCING ANTIOXIDANT POWER METHOD (FRAP)	67
4.3	CHARACTERIZATION OF NANOPARTICLES.....	68
4.3.1	ζ -POTENTIAL ANALYSIS.....	68
4.3.1.1	MESOPOROUS SILICA NANOPARTICLES (MNPs)	68
4.3.1.2	POLYELECTROLYTES SOLUTION	69
4.3.1.2.1	Chitosan solution.....	Errore. Il segnalibro non è definito.
4.3.1.2.2	Pectin solution.....	Errore. Il segnalibro non è definito.
4.3.1.3	ANTIOXIDANT SOLUTIONS	70
4.3.1.4	LBL	72
4.3.2	XPS	83

4.3.3	TEM.....	83
4.3.4	FTIR.....	76
4.3.5	FOLIN.....	Errore. Il segnalibro non è definito.
5	CONCLUSIONS.....	99
6	FUTURE DEVELOPMENTS.....	100

1 INTRODUCTION

1.1 POST TRAUMATIC STRESS DISORDER (PTSD)

Post-traumatic stress disorder (PTSD) is a long-lasting debilitating condition that impacts a wide range of people across the world¹. It often emerges because of a traumatic experience², and commonly develops in comorbidity with other diseases such as depression, anxiety and substance abuse that can lead to suicide. PTSD is characterized by different kind of symptoms, like re-experiencing the traumatic event, avoidance of trauma-related stimuli, negative thoughts or emotions associated with the traumatic event, general changes in mood and cognition, and hyperarousal symptoms³.

War veterans are at a particularly high risk of developing PTSD. A big part of soldiers returning from conflicts suffer from this disease⁴: Military personnel face a high risk of developing PTSD due to their combat exposure. Studies indicate that close to 20% of US Vietnam veterans experienced this disorder during their lifetime and that about 10% still had PTSD a decade after exposure. Similar numbers have been observed for soldiers returning from wars in Iraq and Afghanistan⁵. Moreover, Australian Vietnam veterans have reported a lifetime prevalence of PTSD reaching up to 30%⁶. However, PTSD is not exclusive to military personnel and can also affect civilians who have experienced natural disasters, sexual trauma, or the loss of family members. In the current medical field, the diagnosis of PTSD is mostly dependent on the clinical symptomatology, that includes evaluating cognitive, behavioral, and emotional aspects to determine if the individual meets the criteria for the disorder⁷. In addition to the traditional symptoms, individuals with PTSD, on average, tend to have a higher rate of cardiovascular disease, metabolic syndrome (MetS), diabetes and autoimmune diseases, suggesting that there are physical implications associated with PTSD. So, in addition to lifestyle related factors (e.g., decreased physical activity, obesity, tobacco and substance use, medications)⁸, certain processes intrinsic to PTSD pathophysiology could be contributing to somatic disease risk, like accelerated biological aging, sympathetic and glucocorticoid dysregulation, metabolic changes, inflammation, and others⁹.

1.1.1 INFLAMMATION AND PTSD

As previously said, diagnostic symptoms of PTSD consist of three main groups¹⁰:

1. **Re-experiencing**: the traumatic event is constantly reexperienced through recurrent recollections of the trauma and distressing dreams of the event.
2. **Avoidance**: the patient persistently attempts to avoid stimuli associated with the traumatic event, such as thoughts, feelings, or conversations related to the trauma and avoiding people, activities, and places that arouse memories of the trauma.
3. **Increased arousal**: patients may have difficulty falling or staying asleep and concentrating, they may also show irritability and may exhibit hypervigilance.

In addition to the severe psychological issues, a lot of studies have discovered a connection between PTSD and an increased risk of serious physical diseases, including cardiovascular diseases and autoimmune disorders. While the exact molecular mechanisms of these comorbidities are unclear, these diseases are all known to have an inflammatory component, so that suggests that the immune system is dysregulated in PTSD⁷. However, there is a relatively limited understanding of the specific risk associated with PTSD and autoimmune disorders¹¹.

PTSD is linked with different biological abnormalities that could raise the risk for autoimmune disorders. First, individuals with PTSD appear characterized by lower levels of the immunomodulatory glucocorticoid hormone cortisol¹². Second, more and more evidence links PTSD with increased inflammatory activity, as indexed by elevated levels of proinflammatory cytokines and higher signaling through proinflammatory nuclear factor- κ B transcriptional control pathways¹³. An increasing number of studies have shown that individuals with PTSD exhibit significantly elevated blood levels of inflammatory markers, such as interleukin-1 β (IL-1 β), interleukin-6 (IL-6), tumor necrosis factor α (TNF- α),

and C-reactive protein (CRP). Among these, TNF α is a cytokine that has a vital function in inflammatory and immune processes by regulating immune cells: increased levels of this cytokine are indicators of increased inflammation. TNF α has been implicated in psychiatric and medical disorders, some of which are comorbid with PTSD⁶.

Third, it has been observed an altered patterns of gene expression in immune cells and reduced methylation of immune-related genes in patients with PTSD¹⁴. Finally, some studies suggest that PTSD may accelerate immune cell aging, as indicated by shorter age-adjusted telomere length, which has been linked with elevated inflammation in vivo and in vitro.

Moreover, a large body of research indicates that PTSD is associated with the dysregulation of two systems known to influence inflammatory activity, the sympathetic nervous system (SNS) and the hypothalamic-pituitary adrenal (HPA) axis, which relay signals to the peripheral organs and the immune system.¹²

Particularly, as shown in *Figure 1*, upon acute exposure to stress, corticotrophin-releasing hormone (CRH) is secreted from the hypothalamus, thereby activating the HPA axis¹⁵. The binding of CRH to its receptor on pituitary corticotropes triggers the release of adrenocorticotrophic hormone (ACTH) from the anterior pituitary into the systemic circulation, stimulating cortisol synthesis from the adrenal cortex.

In parallel, stress exposure also triggers the SNS to release catecholamines such as epinephrine and norepinephrine, which are responsible for physiological changes, such as increases in heart rate and blood pressure¹⁶. In response to norepinephrine, monocytes are mobilized from the bone marrow into the periphery, where they encounter danger-associated molecular patterns (DAMPs), activating nuclear factor kappa B (NF- κ B) mediated production of pro-inflammatory cytokines. Indeed, individuals with PTSD exhibited increased peripheral NF- κ B activity and NF- κ B-mediated transcriptional changes in monocytes, which contribute to the inflammatory environment¹⁷.

In PTSD, HPA axis hyperactivity following repeated trauma may disrupt glucocorticoid signaling, which leads to peripheral and central nervous system inflammation¹⁸. Normally, following the binding of glucocorticoids to the glucocorticoid receptor (GR), the stress response is dampened via a negative-feedback loop. The glucocorticoid-GR complex also suppresses inflammatory responses either by stimulating the transcription of anti-inflammatory genes in the nucleus or by inhibiting the expression of proinflammatory proteins in the cytosol. However, chronic exposure to stress may result in glucocorticoid resistance, wherein cortisol cannot inhibit NF- κ B-mediated pro-inflammatory cytokine release, dampening glucocorticoid negative feedback of the HPA axis. Overall, the inflammatory state in PTSD is propagated through a combination of glucocorticoid resistance along with increased sympathetic and decreased parasympathetic nervous system activity¹⁹.

To evaluate the inflammatory response in PTSD from a deeper perspective, some techniques of neurological assessments including magnetic resonance imaging (MRI) and positron emission tomography (PET) have emerged. For instance, some MRI-based studies demonstrated significant structural²⁰ and neurochemical alterations in specific regions of the brain in association with stress or trauma. Further research that investigates these neurological alterations in PTSD in association with inflammatory responses as well as specific clinical symptoms of PTSD using up-to-date methods of clinical assessment may further reveal the underlying pathways of the disorder in a multi-level perspective.⁷

1.1.2 REACTIVE OXYGEN SPECIES (ROS)

Chronic exposure to trauma and stress can also stimulate the production and release of mitochondrial reactive oxygen species (ROS)¹⁹. ROS are characterized as oxygen-carrying molecules having reactive properties which consist of radicals like O_2^- (superoxide), $HO\cdot$ (hydroxyl) and non-radicals including H_2O_2 (hydrogen peroxide)²¹. These ROS molecules originate from oxygen which is utilized in several metabolic responses in the mitochondria and endoplasmic reticulum (ER) along with peroxisomes. Around 2% of the

oxygen is utilized through mitochondria to generate O_2^- . Therefore, mitochondria are recognized as an utmost source of ROS. The ER provides an oxidizing environment for proper folding of proteins increasing ROS levels, while peroxisomes are responsible for the scavenging of ROS through the catalytic degradation of H_2O_2 and the generation of ROS via β -oxidation of the fatty acids. Coordination of ROS/redox homeostasis is central in the regulation of normal biological functions including cell growth, senescence, cell survival and aging. Low/moderate levels ROS is important for proliferation, differentiation, migration, and survival, while excessive ROS levels are harmful²². Alteration in the H_2O_2 or ROS has a potential effect on cellular functions because they are susceptible to the redox environment²³.

1.1.3 GENDER'S INFLUENCE IN PTSD

After experiencing a traumatic event, women have twice the probability of developing PTSD compared to men. This difference in PTSD prevalence mirrors the sex difference for comorbid disorders such as major depression and anxiety disorders. It has been hypothesized that the high prevalence of PTSD in women may be due to a greater vulnerability to trauma²⁴, abnormal immune responses or dysregulation of neuroendocrine pathways involved in fear processing²⁵.

The neuroendocrine axis provides the structural and functional basis for interactions between the brain, hormones, and glands that allows the organism to respond to external stimuli like stress with complex physiological changes. As previously said, PTSD is associated with dysfunction in the HPA axis and physiologic responses to stress. Particularly, HPA axis has been found to be more sensitive and to respond more strongly to acute stress in females than males²⁶, with HPA axis activity fluctuating with the ovarian cycle. Interactions between circulating estradiol and the HPA axis might be one key mediator of the observed sex differences in PTSD susceptibility. Estradiol especially seems to exert modulating effects on HPA functioning, for example, high estradiol has been shown to result in elevated cortisol response to stress. Overall, these data seem to indicate that morphological and functional

changes of the brain areas involved in the stress response, associated with dysfunction of the HPA axis, leads to blunted glucocorticoid negative feedback that contribute to the high risk of PTSD in women following a traumatic event.²⁷

1.1.4 TREATMENTS

Nowadays there are numerous evidence-based treatments for PTSD, including pharmacotherapy and various forms of trauma-focused psychotherapy²⁸.

Multiple treatment guidelines recommend trauma-focused cognitive-behavioral therapy (TF-CBT) as the first line of treatment for PTSD, which is a manualized therapy originally designed for trauma associated with sexual assault and later adapted for other trauma types, typically comprising twelve 60–90 min sessions once or twice per week with a focus on trauma memories and reducing distress via written exposures and cognitive restructuring around themes of safety, trust, power/control, esteem, and intimacy²⁸. More specifically, CPT focuses on helping patients understand and reconceptualize their trauma by modifying some kind of assessment that disrupt recovery through promotion of avoidance behaviors²⁸.

For what concern the pharmacotherapy, during the last two decades, only 2 medications, paroxetine and sertraline, have been approved for the treatment of PTSD²⁹. Both are in the class of selective serotonin reuptake inhibitors (SSRIs), which affect the neurotransmitter serotonin, that plays an important role in regulating mood, anxiety, appetite, sleep, and other body functions.

Although SSRIs are associated with an overall response rate of approximately 60% in patients with PTSD, only 20% to 30% of patients achieve complete remission¹⁰.

Unfortunately, responsiveness to these first-line pharmacotherapies is suboptimal at 50–60%.

1.2 SKIN INFECTION

1.2.1 OVERVIEW

The human skin is the largest organ in the whole body, and it has a unique multi-layer structure distinct from any other organ³⁰. Starting from the outside in, the skin is composed primarily of three layers: (*Figure 1*).

1. The epidermis
2. The dermis
3. The hypodermis

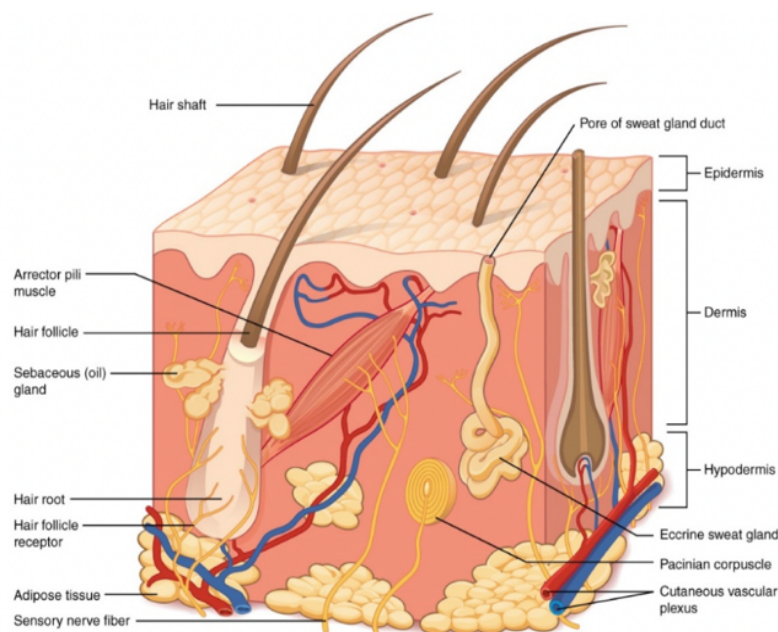


Figure 1: Representation of the three different layers of the skin

The outermost layer of the skin is called the epidermis, which consists of five strata: stratum germinativum, spinosum, granulosum, lucidum, and corneum. The epidermis lacks its own blood supply, and nutrients are supplied through diffusion from underlying layers. The primary cells that make up the epidermis are mainly keratinocytes, along with other types of cells like melanocytes, Langerhans cells, and Merkel cells. These additional cells are responsible for functions like pigmentation, immune responses, and tactile sensitivity. Keratinocytes are involved in synthesizing keratin, a structural protein, and they originate from the deepest layer, the stratum germinativum. Throughout

their life, keratinocytes undergo a continuous process of renewal and turnover known as “keratinization”. This process involves a synthesis phase followed by a degradative phase, leading to changes in the shape and content of the cells. As they progress toward the skin's surface, the keratinocytes transform from living polygonal cells into flattened, dead squamous cells³¹.

The region where the epidermis and dermis meet is called the dermal-epidermal junction. Its primary functions are to hold the two layers together and facilitate the exchange of nutrients between them.³²

The dermis is approximately 1000µm thick and contains a rich capillary plexus that nurtures the skin. Sensor nerves for pain, temperature, and pressure are all found within the dermis, as is a rich lymphatic network. It provides great structural support to the skin through the dense meshwork of collagen and elastin, amongst other structural fibers and ground substance: these components are responsible for providing the skin with its elasticity and tensile strength. The dermis consists of two layers: the papillary dermis, located just below the epidermis and relatively thin, and the reticular dermis, which is thicker and lies between the papillary dermis and the hypodermis (the deepest layer of the skin)³³.

Additionally, within the dermis, you can find glands, nerve endings, hair follicles, blood vessels, and touch receptors, all of which play essential roles in different aspects of skin function and sensation.

Beneath the dermis there is the hypodermis containing blood vessels and adipocytes. It is thicker than the dermis and it consists of loose connective tissue and fat. The main role of this skin layer is to store lipids for energy (though it can serve as a reservoir of fatty acids that produce other bioactive lipid mediators)³⁴.

The skin performs important functions³⁵:

1. **Barrier function:** the skin serves as a protective barrier for the body, shielding it from mechanical, chemical, and thermal impacts.

Furthermore, it acts as a defense against harmful UV radiation, microbes, and excess loss of body fluid.

2. **Sensorial function:** in the skin there are many receptors all over the body, forming the somatosensory system. Those receptors can be distinguished in mechanoreceptors, able to feel pressure, vibrations and texture; thermoreceptors; proprioceptors, which can determine the relative position of different segments of the body and the absolute position of the body in the surrounding environment; and pain receptors.
3. **Temperature regulation and insulation:** The skin plays a crucial role in regulating body temperature, accounting for approximately 90% of heat loss in the human body. The rate of heat loss depends on two main factors: the transfer of heat from internal tissues to the skin through blood vessels and the conduction of heat from the skin to the environment via various mechanisms like evaporation, conduction, convection, and radiation. To maintain a constant body temperature of around 37°C, necessary for optimal enzymatic activity in cells, the skin collaborates with blood vessels, hair, sweat glands, and adipose tissue. When the body temperature rises, the skin responds by dilating blood vessels, leading to increased blood flow near the skin's surface, and by triggering sweating to dissipate heat through evaporation. Conversely, in colder conditions, the skin engages in vasoconstriction, reducing blood flow to the surface, and hair stands erect to create a layer of trapped air, thus preserving heat. By managing these processes, the skin effectively regulates body temperature and helps to maintain the body's internal environment at an ideal level for proper physiological functioning.
4. **Immunological defence:** the first line of defense, also called innate immunity, consists of antimicrobial substances, phagocytic cells and natural killer cells, cytokines, and the complement system³⁶. The most important roles of the innate immunity are recognizing the microbial organisms, restricting the infection, and activating the adaptive immunity response. This kind of response is generally quick, poorly specific, and does not have memory³⁷. The adaptive immune response

is activated by the detection of an antigen; it can be humoral (B-lymphocytes) or cell-mediated (T-lymphocytes); it is very specific, and it possesses a memory. The two types of immunity are not independent; they collaborate with the aid of a variety of immune cells that are taking part to the process.

1.2.2 BACTERIAL INFECTIONS

Bacterial skin and soft tissues infections (SSTI) often determine acute disease and frequent emergency recovering, and they are one of the most common causes of infection among groups of different ages³⁸. SSTIs can ensue from the imbalance between the pathogenic power of a microorganism and the immunological defenses of the host. Various physical and chemical alterations of the skin can induce disruption of the cutaneous barrier, then predisposing to bacteria penetration, growth, and multiplication³⁹. Once the bacteria have penetrated the skin layers and their virulence factors have overcome local host's defenses, tissue invasion occurs. Subsequent dissemination of microorganisms in viable tissue triggers a series of systemic host responses. The microbial causes of SSTIs in hospitalized patients have been recorded over some years and the results show that the predominant pathogens included *Staphylococcus aureus* (ranked first in all geographic regions), *Pseudomonas aeruginosa*, *Escherichia coli* and *Enterococcus spp*³⁹.

As previously said, the cutaneous barrier can be disrupted by wounding, thus allowing microbial pathogens to invade the underlying tissue. After wounding, a complex wound healing process is initiated which comprises three phases (*Figure 2*).

1. *The inflammatory phase*: dominated by blood clot formation and invasion of immune cells such as neutrophils and macrophages.
2. *The proliferation phase*: it comprises tissue formation with angiogenesis and re-epithelialization.
3. *The remodeling phase*: it includes remodeling with collagen synthesis⁴⁰.

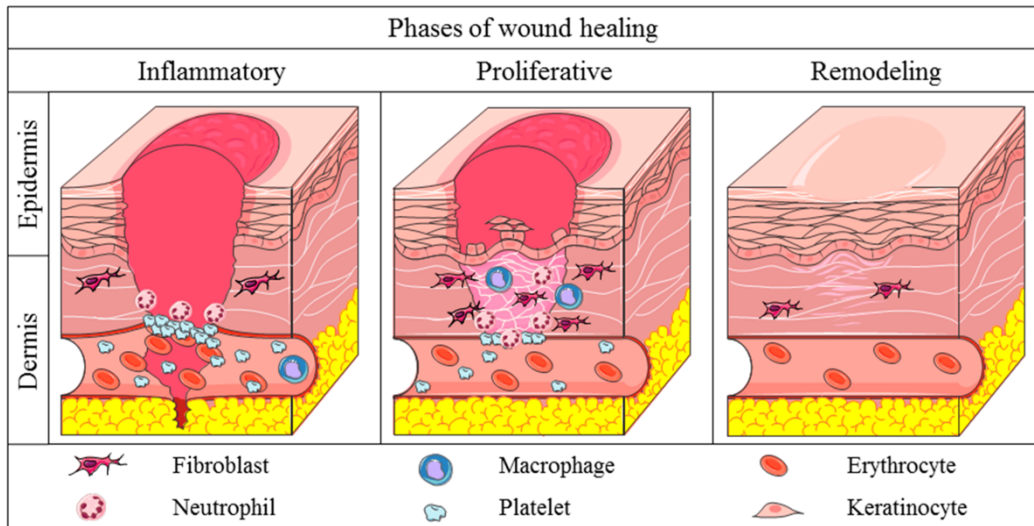


Figure 2: Wound healing process

Adequate wound closure is a prerequisite for maintaining skin homeostasis since failures during wound recovery can cause the formation of chronic wounds which often remain in the inflammatory stage and are challenging to heal⁴¹. Chronic wounds like diabetic, pressure and venous leg ulcers are mainly polymicrobial and most frequently caused by *S. aureus* and *P. aeruginosa*. While *S. aureus* is usually located in the top layer of the skin, *P. aeruginosa* is detected in the deepest region of the wound bed. Infection of wounds is accompanied by high mortality and morbidity.⁴²

1.2.2.1 SKIN IMMUNE SYSTEM

The skin is an immunologically complex organ that can respond to infectious and noninfectious aggressive agents through innate and adaptive immunity mechanisms⁴³. In addition to the immune cells themselves, certain skin cells, such as keratinocytes and melanocytes, may also affect local immune responses by releasing cytokines, which can modulate inflammatory responses⁴⁴.

- 1. Keratinocytes:** they can distinguish between the microbiota and potentially pathogenic agents, and they can recognize highly conserved structures known as pathogen-associated molecular patterns (PAMPs)⁴⁵. The recognition of PAMP ensures that there is no activation

of mechanisms to escape the host immune response, as is observed in the pathophysiology of some infections. Keratinocytes produce antimicrobial peptides (AMPs), which are a class of small-molecule peptides, usually composed of 12–50 amino acid residues, whose exist widely in nature and are obtained from bacteria, plants, insects, fish, birds, and other animals. They are important effectors in the innate immune system and the first line of defense to protect against pathogen infection⁴⁶. Natural AMPs are produced by the immune system and participate in regulating the immune system against a wide range of invasive pathogens. They are considered to have the potential to replace antibiotics because of their broad-spectrum bactericidal effect⁴⁷. Examples of AMPs include cathelicidin and human β defensin. Lack of these antimicrobial peptides may lead to increased risk of infection or colonization with pathogens such as *Staphylococcus aureus*⁴⁸. Moreover, keratinocytes produce cytokines such as IL-1, IL-6, IL-10, IL-17, IL-18, IL-22, and tumor necrosis factor alpha (TNF- α). In the presence of an infection, IL-17 and IL-22 can activate the production of AMPs by keratinocytes, constituting a form of innate immune response⁴⁵.

2. **Melanocytes:** they derive from the neural crest and can control innate and adaptive local immune responses, promoting pathogen phagocytosis and the production of cytokines such as IL-1 β , IL-6, TNF- α , and chemokines. Similar to keratinocytes and other cells with immune functions in skin, melanocytes may express interferon (IFN) type I and constitute the first line of defense against viruses in the skin⁴⁵.
3. **Endothelial cells:** they play key roles in controlling the flow of immune cells from blood to tissue through the expression of various adhesion molecules, cytokines, and chemokines, which serve as chemo-attractants for leukocyte migration. The endothelial immune response is associated with increased expression of cytokines such as IFN- γ , TNF- α , IL-1 α , and IL-1 β , which increase the expression of adhesion molecules⁴⁹. IFN- γ appears to be one of the most important factors inducing MHC class II expression and is an important agent in the

formation of costimulatory molecules, including adhesion molecules, which modify the processes of cell rolling and tissue transmigration in leukocytes. Cell transmigration through the endothelium is possible only following rupture of the endothelial wall, which is mainly mediated by cell changes induced by proinflammatory cytokines. A cascade of intracellular events leads to changes in the cytoskeleton which allow the extravasation of fluid, chemical mediators, and cells toward the cytokine source. This process results in the formation of perivascular edema and directly combats microbial agents at the site of infection.⁴⁵

- 4. Neutrophils and macrophages:** recruited to the sites of tissue infection or injury by multiple-step processes that are dependent on selectins, integrins, and chemokines. When these cells are recruited to a site of infection, they express receptors that recognize and bind to microorganisms, ingesting and destroying them by phagocytosis and microbicidal molecules present in phagolysosomes⁵⁰. These microbicidal molecules can be grouped into three main classes: reactive oxygen species (ROS), NO, and proteolytic enzymes.⁵⁰

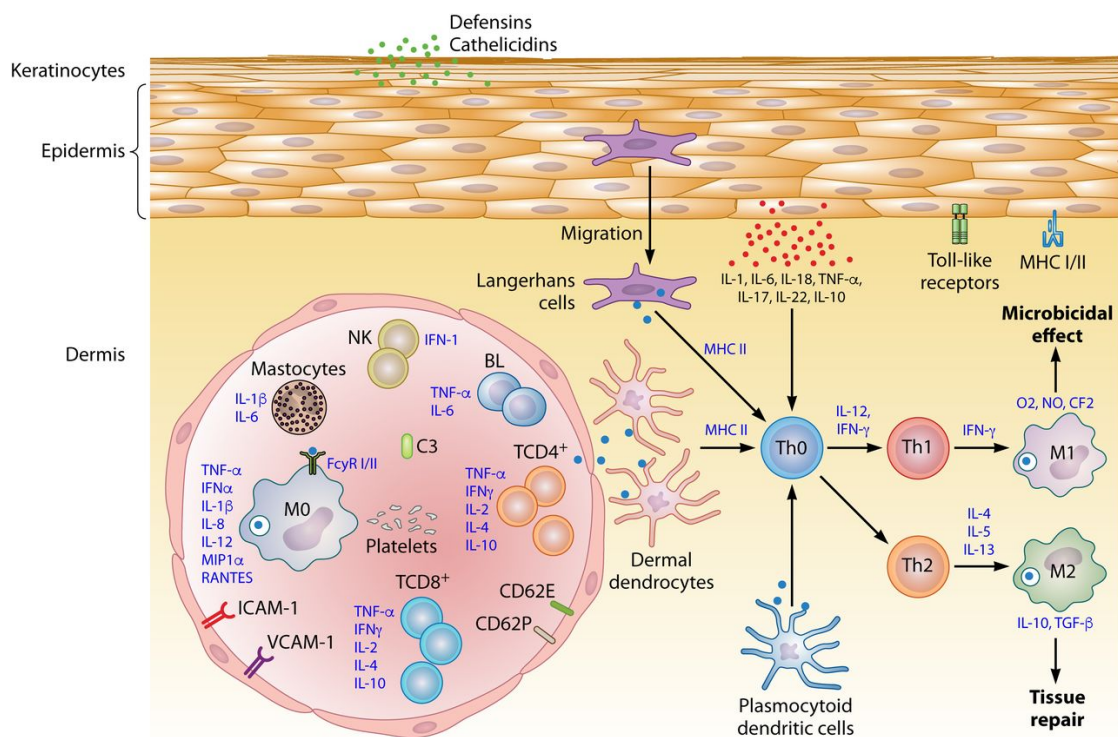


Figure 3: Association between the host cells and infectious agents in the context of the skin's in situ immune response.

1.3 NATURAL ANTIOXIDANTS

An antioxidant is a molecule which can prevent or slow the oxidation of macromolecules. The role of antioxidants is to lower or terminate these chain reactions by removing free radicals or inhibiting other oxidation reactions by being oxidized themselves. Antioxidants can be divided in different groups based on their action mechanism:⁵¹

- Direct antioxidants, which neutralize ROS through direct reaction and exert a classical scavenging activity
- Indirect antioxidants, that activate a particular pathway in which they induce a cellular cytoprotective defense

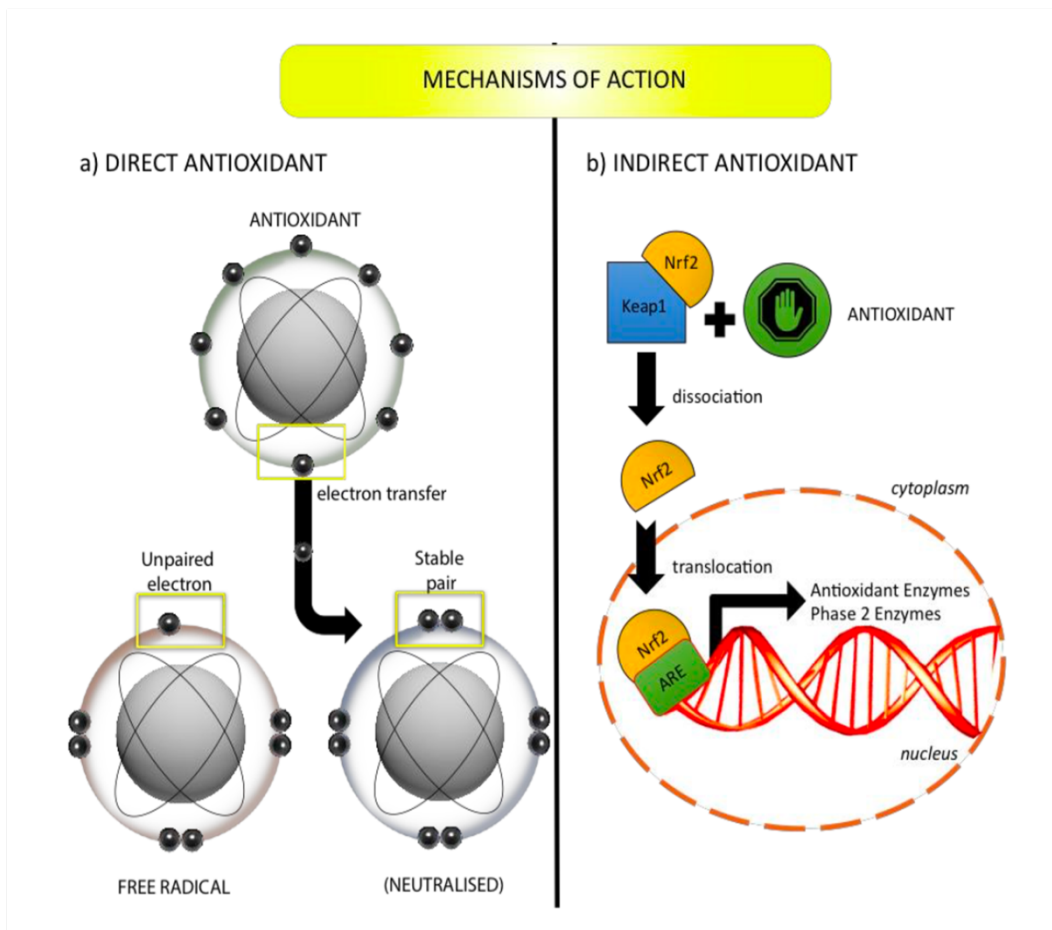


Figure 4: Mechanism of action of direct and indirect antioxidants

Phenolic compounds are a large group of natural antioxidants: the term phenol or polyphenol is characterized by the presence of one or more aromatic nuclei

containing hydroxylated substituents and/or functional derivatives, such as esters, ethers, and glycosides. These compounds can be divided, according to the number and arrangement of carbon atoms present in the main structure of a molecule, into different groups represented in *Table 1*⁵².

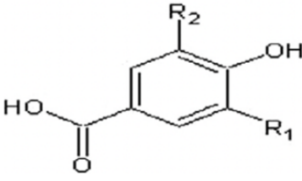
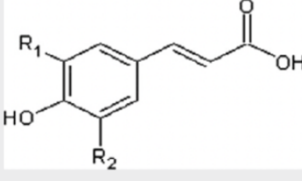
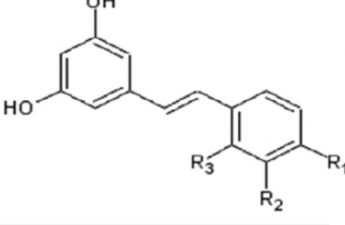
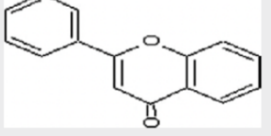
Basic structure	Class of phenolic compounds	Chemical structure
C6-C1	Benzoic acid derivatives	
C6-C3	Cinnamic acid derivatives	
C6-C2-C6	Stilbenes	
C6-C3-C6	Flavonoids	

Table 1: Basic structure of the main phenolic compounds

1. **Phenolic acids:** can be divided into two categories depending on their structure: derivatives of benzoic acid and derivatives of cinnamic acid. These compounds consist of a benzene ring bonded to a carboxylic group (benzoic acids) or to a propenoic acid (cinnamic acids). In many fruits and vegetables, cinnamic acids (especially caffeic acid) is present as ester derivatives (chlorogenic acid, other cinnamoyl quinic acids, phenylethanoic glycosides) which show a high potential as antioxidants. Hydroxybenzoic acids include gallic, p-hydroxy-benzoic, protocatechuic, vanilic and syringic acids, while the most important

hydroxycinnamic acids are caffeic, ferulic, p-coumaric and sinapic acids⁵³

2. **Stilbenes:** they are phenolic compounds displaying two aromatic rings linked by an ethane bridge, and exist in monomeric (resveratrol, oxyresveratrol) and oligomeric form as oligomers of stilbenes (dimers, trimers or polymers of resveratrol) or other stilbenes. They are important because of their health effects, which occur in lower concentrations compared to other phenolic compounds. Resveratrol, an important stilbene, occurs in two isomeric forms, the trans- and cis-configured isomers⁵⁴
3. **Flavonoids:** they are the most important and diversified class of polyphenols, widely distributed in fruits, vegetables, berries, and seeds. The main representative ones of this class have two aromatic rings linked among themselves by an oxygenated heterocycle.⁵² They can be further divided into several subclasses of which the most representative are: flavones, flavanones, flavonols, flavanols (also called flavan-3-ols or catechins), anthocyanidins and isoflavones⁵⁵

The antioxidant activity of phenolic compounds is mainly determined by their chemical structure, especially by the number and position of hydroxyl groups and the presence of an aromatic ring. These compounds work as efficient reactants of ROS, reducing, and chelating ferric ions that catalyze lipid peroxidation, and inactivating free radicals by transferring hydrogen atoms to these molecules or by donating an electron to the radical⁵⁶. The intermediates formed by phenolic antioxidants action are relatively stable due to the resonance of the aromatic ring present in the structure of these substances⁵⁷.

Another important class of compound with antioxidant activity is vitamins (Vitamin C and Vitamin E), which can interfere with oxidative cycles to inhibit or retard the oxidative damage of biomolecules.⁵³

1. Vitamin C (L-ascorbic acid), which is unique among vitamins for several reasons. It is believed to be the most important hydrophilic antioxidant being effective in scavenging superoxide radical anions, hydroxyl

radicals, hydrogen peroxide, reactive nitrogen species and singlet oxygen. Vitamin C can act as a ROS scavenger and inhibits oxidation, however, at low levels, Vitamin C can catalyze oxidation⁵⁵

2. Vitamin E, that refers to a group of chemical compounds (tocopherols and tocotrienols) and is generally accepted to be the primary lipid-soluble antioxidant in humans and acts as an antioxidant via two primary mechanisms: a chain-breaking electron donor (CB- D) mechanism and a chain-breaking acceptor (CB-A) mechanism⁵³

Finally, the last big class of compound with antioxidant property is carotenoids, which are important not only for their provitamin A activity, but also for a spectrum of other actions in biological systems. They are effective singlet oxygen quenchers and free radical (ROS) scavengers.

The singlet oxygen quencher mechanism of carotenes involves the conversion of singlet oxygen into heat: the mechanism involves three different reactions, as follows: electron transfer, adduct formation and hydrogen abstraction. The main categories of carotenoids are:

1. Carotenes, that can be β -carotene, a lipid, soluble, pro-vitamin composed of two retinol groups that can quench singlet oxygen and inhibit lipid oxidation, or lycopene, with many conjugated double bonds which make it a potentially powerful antioxidant
2. Hydroxy carotenoids (xanthophylls), which are oxygenated carotenoids synthesized within the plastids

1.3.1 SEaweEDS

Different species of macroalgae are found in different coastlines of the world which are classified into three taxonomic groups based on pigments⁵⁸:

1. Brown Seaweed (Phaeophyceae). The color of brown seaweeds is due to the presence of the xanthophyll pigment, fucoxanthin⁵⁹. Brown seaweeds are large and measure about 2 to 65 m long and thick and leather-like, and their smaller species is about 30–60 cm long
2. Red Seaweed (Rhodophyta). The color of red seaweeds is due to phycoerythrin, phycoerythrin, chlorophyll a, and xanthophyll pigments⁶⁰. They are small, ranging from few centimeters to about a meter long.
3. Green Seaweed (Chlorophyta). The color of green seaweeds is yellow to green due to the presence of beta-carotene, chlorophyll a, chlorophyll b, and xanthophylls. They are small, like red seaweeds.

Several compounds with potential antioxidant properties are present in seaweed, like phenolic compounds, carotenoids, tocopherols, but also polysaccharides and peptides⁶¹. Particularly, many polysaccharides with antioxidant activity have been discovered from algae such as brown, green, and red. These algal polysaccharides usually have hepatoprotective, neuroprotective, and anti-diabetic activities, which are directly or indirectly related to their antioxidant properties⁶².

1.3.1.1 BROWN ALGAL POLYSACCHARIDES

Mainly found in the form of fucan, and few in the form of alginate and laminarin. Fucans are usually defined as fucoidan for polysaccharides extracted from marine organisms. The dominant polysaccharide, fucoidan, has shown *in vitro* and *in vivo* antioxidant activity, and it also modulates the oxidative stress-mediated diseases by regulating the antioxidant defense systems and the oxidative stress-related signaling pathways.⁶²

Particularly, fucoidan is mainly composed of L-fucose and sulfate groups, and it also consists of other monosaccharides including uronic acid, galactose, xylose, mannose, rhamnose, glucose, arabinose and xylose.

1.3.1.2 RED ALGAL POLYSACCHARIDES

Marine red algae have been extensively studied as a major source of agar: many red algal polysaccharides displayed good *in vitro* and *in vivo* antioxidant activity. Polysaccharides derived from red algae alleviate the damage of the digestive tract organs and liver via the mediation of the oxidative stress, they can prevent the disorder of the antioxidation system by upregulating the antioxidant glutathione activity and can alleviate cell damage and aging⁶³

1.3.1.3 GREEN ALGAL POLYSACCHARIDES

Usually known as ulvan, are mainly composed of α -L-rhamnose, xylose, glucuronic acid, iduronic, and sulfate. Ulvan not only has strong *in vitro* antioxidant activity, but also abrogates the free radical-mediated diseases. Ulvan derived from green algae can alleviate oxidative stress-mediated liver damage by increasing endogenous antioxidant enzyme activity, reducing oxidative stress. In addition, ulvan can also inhibit cell damage and liver cancer cell proliferation by regulating the antioxidant defense system of liver cancer rats induced by diethylnitrosamine⁶⁴.

Furthermore, other antioxidative compounds, such as phlorotannins, carotenoids and tocopherols are found in a wide range of seaweed species. Particularly, phlorotannins are a large and diverse group of naturally occurring polyphenolic compounds and are secondary metabolites restricted to marine algae. They are oligo- or polymers of phloroglucinol (1,3,5-trihydroxybenzene) and they can be classified according to their linkage of phloroglucinol units (PGU)⁶⁵.

Carotenoids play a major role in the protection against photooxidative processes in red, green, and brown algae and among them, fucoxanthin is particularly interesting owing to its health-promoting properties. It is an oxo-

carotenoid (xanthophyll), which carries at least one oxygen atom. It has a unique structure and is known as an efficient quencher of singlet oxygen in photooxidation.⁶¹

Finally, tocopherols are fat-soluble antioxidants widely used due to their efficient radical scavenging activity. They have four isomers, α -, β -, γ -, and δ -tocopherol, and the antioxidant activity order of the four tocopherol isomers in bulk oil is $\delta > \gamma > \beta > \alpha$ ⁶⁶.

1.3.2 EXTRACTION OF ANTIOXIDANTS

Bioactive compounds can be extracted from seaweed using different methods. The extraction yield and composition of the extract are influenced by the conditions under which the extraction process is carried out. Several factors are reported to have an influence on extraction yield, such as type of solvent applied, solid: liquid ratio, extraction time, and temperature⁶¹.

1. **Solid-liquid extraction (SLE):** the driving force for this extraction is the concentration difference of the component between the two phases. An ideal solvent should have a high capacity for the solute being separated into it, it should be selective, dissolving the specific component to a large extent while having a minimum capacity for the other components, it should be chemically stable, it should be regenerable, and it should have low viscosity for easy pumping and transportation. Ethanol is one of the most used solvents for antioxidant extraction, because it is: cheap, reusable, and nontoxic. The extraction yield of antioxidant compounds depends on their solubility in the given solvent or mixture of solvents⁵³
2. **Supercritical fluid extraction (SFE):** it uses fluids in their supercritical state. Supercritical fluids exhibit desirable transport properties that enhance their adaptability as solvents for extraction processes. SFE involving carbon dioxide (Sc-CO₂) uses carbon dioxide, which is readily available, cheap, and environmentally friendly, as a solvent. In addition, it has a relatively low critical temperature (31.1°C) and pressure (73.8

bar). This property of Sc-CO₂ makes it an excellent solvent to extract heat-sensitive bioactive compound⁶⁷

3. **Microwave-assisted extraction (MAE):** has become very popular in the last decade due to the reduction of extraction time and solvent used. This technique involves extraction with controlled pressure and temperature. This method has been applied for the extraction of phenolic compounds from plant material⁶⁸. MAE can be used with or without the addition of any solvent. Solvent-free microwave extraction (SFME) and microwave hydrodiffusion and gravity (MHG) are both types of solvent free MAE performed at atmospheric pressure. SFME is based on a combination of microwave heating and dry, while MHG is a novel, green technology, that requires less energy, combining microwaves and the earth's gravity at atmospheric pressure. Finally, ultrasonics is one of the most used techniques in industry to enhance the mass transfer phenomena, which is increased in ultrasonic extraction by cavitation forces.⁶⁹
4. **High hydrostatic pressure (HHP):** improves mass transfer rates increasing cell permeability as well as increasing secondary metabolite diffusion according to changes in phase transitions⁵³

Methods like SFE are referred to as green extraction techniques owing to their low environmental impact because of the reduction in the use of toxic and hazardous solvents. Besides the reduced organic solvent requirements, the advantages of these techniques include high selectivity, high extraction efficacy, and short extraction time in contrast to traditional SLE⁶¹.

1.4 ANTIOXIDANTS DELIVERY VIA NANOCARRIERS

Nanocarriers have emerged as a promising drug delivery system offering several advantages over conventional passive delivery, such as increased surface area, higher solubility, improved stability, controlled release of active ingredients, reduced skin irritancy, protection from degradation, increased drug loading, and improved permeation of actives into the skin⁷⁰.

There are different types of nanoparticles, such as

1. Liposomes, consisting of spherical self-closed vesicles of colloidal dimensions, in which the phospholipid bilayers sequester part of the solvent in which they freely float into their interior, and the lipid bilayer is mainly composed of natural or synthetic phospholipids
2. Nanocapsules, that consist of vesicular systems that are made up of polymeric membranes in which an inner liquid core is encapsulated at the nanoscale level (10 nm to 1000 nm)
3. Solid lipid nanoparticles, which consist of submicron colloidal carriers composed of physiological lipid dispersed in water or in aqueous solution of surfactant
4. Nanocrystals, which are aggregates composed of several hundreds to thousands of atoms that combine into a cluster (10–400 nm) and are used for the delivery of poorly soluble actives
5. Niosomes, which are nonionic surfactant vesicles devised by using nonionic surfactants and have high entrapment efficiency, improved chemical stability, and enhanced penetration. They have the advantage of accommodating hydrophilic, lipophilic, and amphiphilic drug moieties. They are less toxic and expensive than liposomes but they have disadvantages such as aggregation and leaking of the entrapped drug⁷¹.

Among all the available nanoparticles, inorganic mesoporous silica nanoparticles (MSNs) are the newcomers to the field, contributing with their unique properties⁷². Mesoporous silica nanoparticles, whose attributes include uniform mesopores, easy functionalization and significant biocompatibility, have gained much recent attention for biomedical applications⁷³. MSNs possess many advantages as nanocarriers: it is known that they are biocompatible, it is easier to build multifunctionality in MSNs due to their much higher surface area and uniform internal pores. So, they have been widely used as a carrier for therapeutic applications because of their suitable biological properties⁷⁴.

MSNs possess well-defined structure and high density of surface silanol groups which can be modified with a wide range of organic functional groups⁷⁵. The surface functional groups can play several roles in biomedical applications of MSNs such as controlling the surface charge of MSNs, chemically linking with functional molecules inside or outside the pores; and controlling the size of pore entrance for entrapping molecules in the nanopores⁷⁶.

1.5 LAYER BY LAYER TECHNIQUE (LBL)

Layer-by-layer (LbL) assembly is a rich, versatile, and significantly inexpensive approach by which thin films, particularly of oppositely charged layers, can be prepared. Researchers have been attracted to the fabrication of thin films using LBL for generating advanced coatings and smart surfaces at the molecular level for various biological and material applications. The advantages of the LbL assembly technique include simplicity, universality, and thickness control at the nanoscale level, compared with the other available assembly approaches⁷⁷. Multilayer assembly through the LbL technique involves different types of intermolecular interactions, like electrostatic, charge-transfer, host–guest, hydrophobic interactions, coordination chemistry interactions, and hydrogen and covalent bonding⁷⁸. The electrostatic interaction takes place between molecules and surfaces that are electrically charged. LbL assembly based on electrostatic interactions gives rise to multilayer films with a well-controlled structure, composition, and thickness by alternate deposition of oppositely charged molecules. In this regard, many natural polymers are polyelectrolytes and, therefore, their assembly through the LbL technique occurs through electrostatic interactions between a positively charged polymer (polycation) and a negatively charged polymer (polyanion)⁷⁹. Among different LbL techniques, the most employed are dipping, spraying, and spin coating.

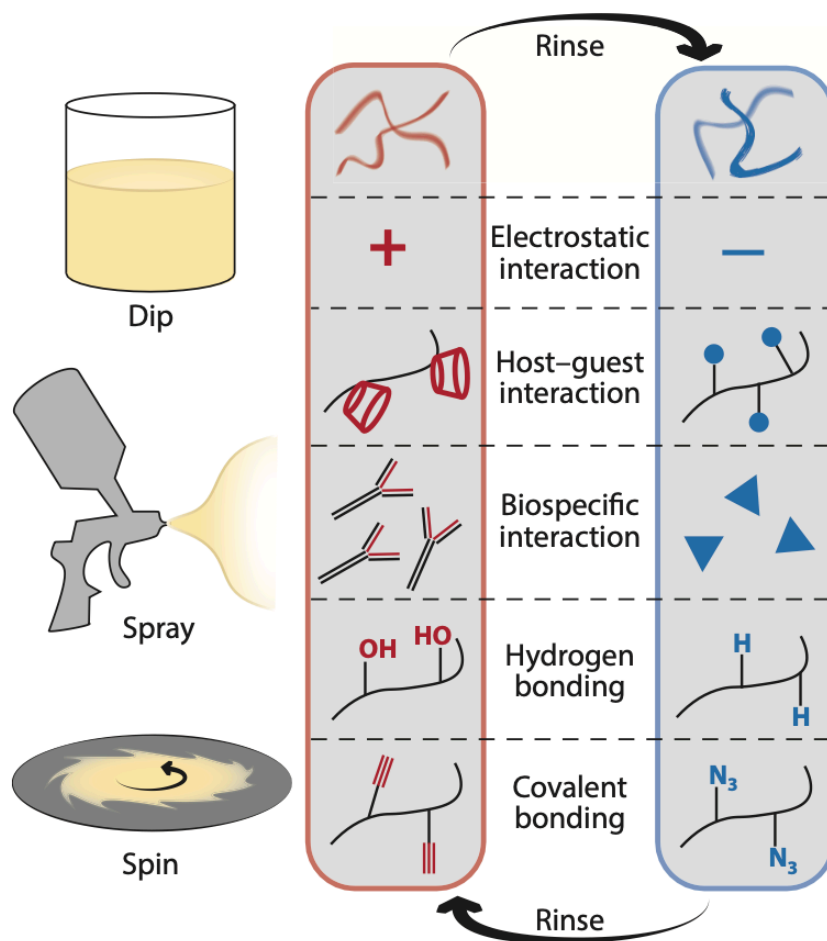


Figure 5: Schematic of common LbL approaches and common interactions exploited in LbL self-assembly

1.5.1 LBL ASSEMBLY WITH NATURAL POLYMERS

Over the last decades, polymers obtained from biomass, known as natural polymers, have been widely employed for a variety of biomedical applications due to their intrinsic properties such as biocompatibility and non-toxicity. They are naturally produced in large quantities because they are present in or created by living organisms such as plants, microorganisms, algae, and animals. Polysaccharides, proteins, and poly-aminoacids are the most employed natural polymers for biomedical applications⁸⁰. Natural polymers are biodegradable under physiological conditions through enzymatic degradation or hydrolytic processes leading to body-friendly degradation products. A strategy to increase the biostability of natural polymers in physiological

conditions without compromising their biocompatibility is the formation of polyelectrolyte complexes (PECs) formed by electrostatic interactions between natural polycations and polyanions. In this regard, LbL assembly, based on the sequential deposition of interacting species onto a substrate, emerged as a versatile, simple, efficient, reproducible, and flexible bottom-up technique, that allows a precise control over the thickness and compositions at the nanoscale⁸¹. Altogether, this makes LbL assembly one of the most useful techniques for building up advanced multilayer polymer structures and implant coatings towards multiple applications in diverse fields such as biomedicine, energy, optics, or coatings⁸². Two polyelectrolytes widely used are chitosan as cationic component and pectin as anionic component.

- Chitosan: polysaccharide derived from deacetylating chitin, which is a major constituent of the exoskeleton of crustaceous water animals. Chitin and chitosan are $\beta(1\rightarrow4)$ glycans whose chains are formed, respectively, by 2-acetamide-2-deoxy-D-glucopyranose and 2-amino-2-deoxy-D-glucopyranose units. Chitosan is known for its unique material and biological properties (e.g., processability, biocompatibility, antimicrobial activity, biological activities, biodegradability) for biomedical applications⁸³.

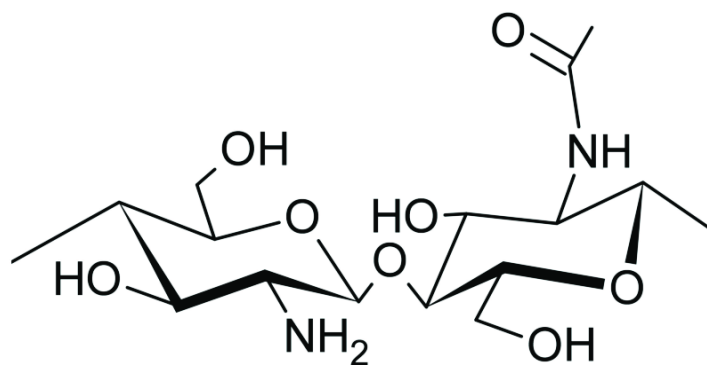


Figure 6: Chitosan structure

- Pectin: complex polysaccharide found in plants and fruits such as apples and berries. It is composed of its sub-domains, rhamnogalacturonan I (RGI), rhamnogalacturonan II (RGII), and xylogalacturonan (XG), attached to the homogalacturonan (HG)

skeleton. The structure of pectin must contain $\geq 65\%$ galacturonic acid (GalA) and the relation between the units of GalA esterified with methyl and the total units of GalA in the HG skeleton represents the degree of esterification (DE). The presence of hydroxyl and carboxyl groups in pectin contribute to their hydrophilicity, biocompatibility, low toxicity, and biodegradability⁸⁴.

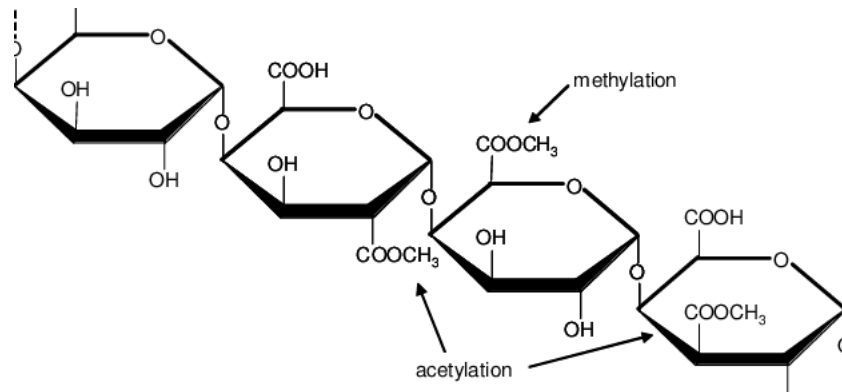


Figure 7: Pectin structure

2 AIM AND OBJECTIVES

The main objective of this study was to enhance an environmentally friendly extraction method for obtaining antioxidant compounds while reducing the usage of harmful solvents, conserving energy, and minimizing waste production. To achieve this goal, six different types of seaweed were selected as natural sources rich in antioxidant compounds. The study employed the Design of Experiments, specifically the Box-Behnken design, to determine the most favourable extraction conditions.

Precisely, using Minitab software, a total of 15 distinct combinations of extraction process parameters were generated. Once all the experiments were conducted, the resulting extracts were examined to determine their total phenolic content. Subsequently, these outcomes were utilized as input data for Response Surface Methodology (RSM) to identify the optimal conditions for the extraction system. More specifically, the combination of extraction time (min), temperature ($^{\circ}\text{C}$), and ratio (mg/mL) was chosen as the parameters to optimize, with the objective of maximizing the total phenolic content in each extract. Seaweed extracts were optimized and then employed to achieve the project's second objective. In the context of addressing PTSD and skin infection, the Layer-by-Layer assembly coating technique was used to modify silica mesoporous nanoparticles, imbuing them with antioxidant properties. To accomplish this, chitosan and pectin were used as the polycation and polyanion solutions, respectively, and loaded the antioxidant extract into the negative solution based on their ζ -potential measurement. Once the control over the layer deposition process was established, six distinct systems, two for the Bladder Wrack seaweed, two for the Knotted Wrack seaweed and two for the Toothed Wrack seaweed were obtained. *Figure 8* provides a schematic representation of each deposited layer and the resulting functionalization of the mesoporous silica nanoparticles (MNPs). Experiments with the extracts on fibroblast cells were conducted using a two-dimensional cell culture model. Cell viability, metabolic activity, and cell morphology were assessed before and after treatment with the free extracts. The final step involved a bacterial test of the antioxidant extracts to evaluate two parameters, the MBC, the

minimal bactericidal concentration, and the MIC, the minimal inhibitory concentration.

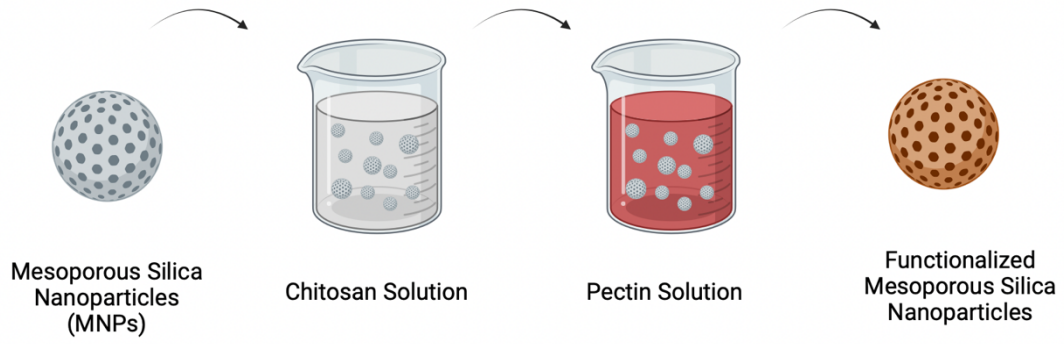


Figure 8: Functionalization process with Layer-by-Layer technique

3 MATERIALS AND METHODS

3.1 MATERIALS

Seaweeds were obtained from Shore Seaweed Ltd, company located in Scotland. The extraction process was carried out using Distilled water (Milli-Q® water system) and Ethanol (99.8%, Sigma-Aldrich) as solvents. For layer-by-layer deposition silica mesoporous nanoparticles (200 nm particle size, pore size 4nm), Chitosan (Low Mw, Deacetylation Degree 75%) and Acetic acid (glacial, ReagentPlus®, ≥99%) were purchased by sigma Aldrich. Antioxidant characterization was performed on extracts using Folin & Ciocalteu's phenol reagent and sodium carbonate (Na₂CO₃), purchased by sigma Aldrich, and Invitrogen™ assay kit (Thermo Fisher Scientific, Inc.). Other materials used included Hydrochloric acid (HCl) (reagent grade 37%), (Sigma-Aldrich, UK), Gallic Acid (97.5-102.5% (titration)), (Sigma-Aldrich, UK). For cell culture tests, Fetal Bovine Serum (FBS, ThermoFisher Scientific, Inc), penicillin/streptomycin (P/S, Sigma-Aldrich), Human Fibroblast Growth Factor (hFGF-2, Sigma-Aldrich), L-Glutamine (LG, 5 mM, Sigma-Aldrich), Phosphate Buffered Saline (PBS Sigma-Aldrich), Trypsin/EDTA (Sigma-Aldrich), Dulbecco's Modified Eagles Medium (DMEM, Sigma-Aldrich, Gibco high glucose 4500 mg/L) were used.

3.2 METHODS

3.2.1 ULTRASOUND ASSISTED EXTRACTION TECHNIQUE

Six different types of seaweed were used:

1. Organic Dried Bladder Wrack BW (*Fucus vesiculosus*)
2. Organic Dried Spiral Wrack SW (*Fucus spiralis*)
3. Organic Dried Knotted Wrack KW (*Ascophyllum nodosum*)
4. Organic Dried Sea Spaghetti SS (*Himanthalia elongata*)
5. Organic Dried Kelp KE (*Laminaria digitata*)
6. Organic Dried Toothed Wrack TW (*Fucus serratus*)

The samples were prepared using powdered seaweed mixed with 150 mL of a 50% ethanol solution. As shown in *Figure 9*, the samples were incubated in a VWR ultrasonic cleaner bath at 45 kHz, then centrifuge at 4400 rpm for 40 minutes into the Thermo Scientific™ Megafuge 16R TX-200 Centrifuge and finally after the centrifuge, the supernatant was collected for ethanol evaporation performed in a rotary evaporator RV- 8-Flex (IKA) at 130 rpm and 48 °C until the initial volume was half reduced.

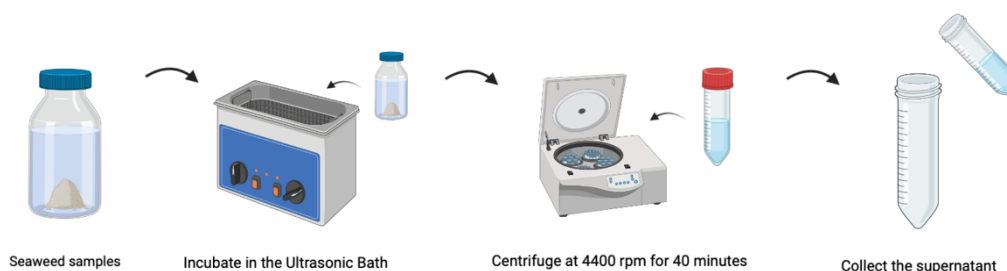


Figure 9: Ultrasound assisted extraction technique.

The extraction process was carried out according to the Design of Experiments, through Box-Behnken design, to evaluate the effect of Temperature (°C), Extraction Time (min) and Liquid/Solid Ratio (mL/g) on the total phenolic content of coffee and cocoa samples. Minitab Statistical software was used to generate 15 combinations of extraction variables for each seaweed, reported in *Table 2*, in which is shown that the temperature was set

from 10 to 30°C, the time of incubation between 15 and 40 minutes and finally, the ratio between 5 and 20 mg/mL.

Table 2: Extraction Parameters

<i>RUN ORDER</i>	<i>TEMP (°C)</i>	<i>TIME (min)</i>	<i>RATIO (mg/mL)</i>
1	20	15	20
2	20	40	20
3	20	15	5
4	30	27.5	20
5	10	27.5	5
6	10	15	12.5
7	20	40	5
8	30	40	12.5
9	20	27.5	12.5
10	30	27.5	5
11	10	27.5	20
12	30	15	12.5
13	20	27.5	12.5
14	10	40	12.5
15	20	27.5	12.5

3.2.2 CHARACTERIZATION OF ANTIOXIDANTS EXTRACT

3.2.2.1 METABOLITES EVALUATION - METABOLOMICS

The samples processing comprised two different phases, the metabolite extraction, and the resuspension. To perform the metabolite extraction, 10 mg of material was immersed in 1 mL of analytical grade methanol. The samples were then sonicated in ice water bath for 15 minutes, and afterward the

samples were centrifuged at 15k rpm for 15 minutes at 4°C. Finally, the supernatant was collected and dried down at 45°C for 2 hours.

To perform the resuspension, the metabolite extracts were resuspended in 100µL of LC/MS grade water and sonicated for 15 minutes at 15k rpm at 4°C. Then, it was filtered via 0.22 µm Costar spin column at 10k rpm for 5 minutes and transferred into a 1.5 mL autosampler vial with a 200 µL microinsert, capped and labelled accordingly. Finally, it was submitted for LC/MS analysis. For the mass spectrometry (MS) acquisition, the MS data were acquired using the AcqvieX acquisition workflow (data dependent analysis). The MS operating parameters were as follows: MS1 mass resolution 15K, for MS2 15K stepped energy (HCD) 20, 35, 50 scan range 100-1000, RF len (%) 35, AGC gain, intensity threshold 2⁴ 50% custom injection mode with an injection time of 25 ms. An extraction blank was used to create a background exclusion list and a pooled QC were used to create the inclusion list.

For the reverse phase C18 chromatographic separation it was used the Waters Acquity UPLC HSS T3 column (2.1 x 150 mm with particle size of 1.8 µm) operating at 45°C with a flow rate of 200µL/min. The LC gradient consist of a binary buffer system: buffer A: LC/MS grade water/ACN v/v (95/5) and buffer B: LC/MS grade ACN/water (95/5).

For the polyphenol, positive mode buffer (acidic) was used, and the data was acquired in the negative mode. The LC gradient was the same for both polarity: 5% B at T0, held for 1.5 min and linearly decreased to 95% B at 11 min held for 4 mins, then returned to starting condition and held for further 4.5 min (column stabilization). The voltage applied for positive mode and negative mode was 3.5 kV and 2.5 kV respectively, while the autosampler temperature was maintained for 4°C.

The negative data sets were processed via compound discoverer 3.3 for peak table generation: untargeted metabolomic workflow matching to m/z cloud online database. MS2 ID to 70% or higher. Annotation m/z 10 ppm or less and signal processing via QC (25% or less is retained)

The detected polyphenols were: catechin, catechol, chlorogenic acid, kaempferol-3-glucuronide, kaempferol-7-O-neohesperidoside, lariciresinol 4-O-glucoside, neochlorogenic acid, procyanidin B1, quercetin-3β-D-glucoside.

3.2.2.2 FOLIN-CIOCALTEU METHOD TO EVALUATE THE TOTAL PHENOLIC CONTENT

The total phenolic content (TPC) of the extracts was determined using the Folin-Ciocalteu method of a UV-vis spectrophotometer (FLUOstar Omega, BMG Labtech, Germany). In this method, the Folin-Ciocalteu reagent reacts with the phenolic compounds present in the extract, forming a blue color whose intensity is directly proportional to the number of phenolic compounds.

To perform the analysis, 50 μL of the extract was mixed with 430 μL of distilled water and 20 μL of the Folin-Ciocalteu reagent. After thorough mixing, 50 μL of Na_2CO_3 solution was added, and the mixture was left to rest for 10 minutes. Subsequently, the mixture was diluted with 450 μL of distilled water, and its absorbance was measured at a wavelength of 680 nm, using ultrapure water as the blank. To quantify the phenolic content, a calibration curve was constructed (*Figure 10*) using known concentrations (ranging from 0.05 mg/mL to 5 mg/mL) of gallic acid dissolved in distilled water. The calibration curve exhibited a good linear relationship ($R^2=0.997$) between the concentration of gallic acid and the absorbance at 680 nm.

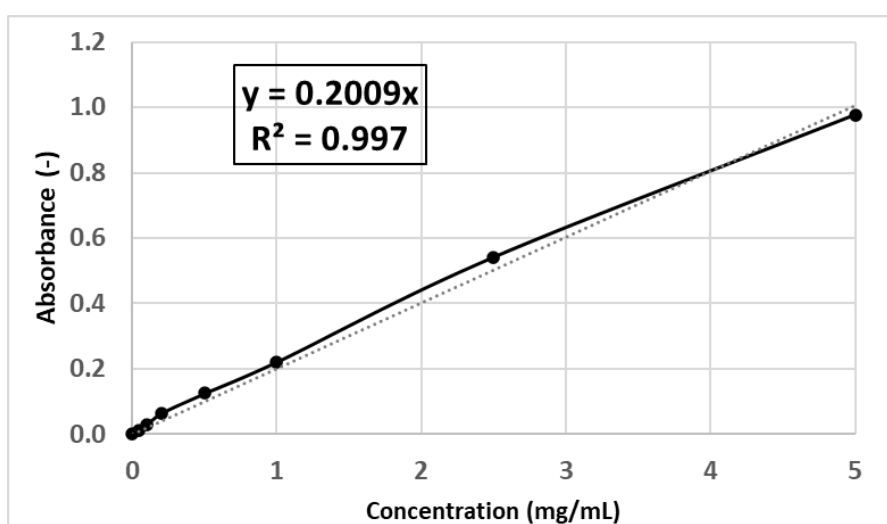


Figure 10: Calibration curve to quantify TPC

The TPC of the extracts was expressed as grams equivalent of gallic acid per mL of sample (GAE (mg/mL)). All measurements were performed in triplicate and the mean values were calculated to ensure accuracy and reliability.

3.2.2.3 FERRIC REDUCING ANTIOXIDANT POWER METHOD TO EVALUATE THE ANTIOXIDANT ACTIVITY

The Ferric Reducing Antioxidant Power (FRAP) test was performed to assess the overall antioxidant effectiveness of the seaweed extract. For this purpose, an Invitrogen™ assay kit from Thermo Fisher Scientific, Inc. was used. Following a 30 minutes incubation at room temperature, the absorbance of the resultant colored substance was gauged at 560 nm wavelength using a UV-vis spectrophotometer, specifically the FLUOstar Omega model from BMG Labtech in Germany. The findings were presented as an equivalent amount of ascorbic acid (AAE μM), serving as the positive benchmark. Every measurement was taken three times, and the average values were computed.

3.2.2.4 FOURIER-TRANSFORM INFRARED SPECTROSCOPY (FTIR-ATR) TO DETERMINE SURFACE FUNCTIONAL GROUPS

The surface functional groups present in seaweed extracts were identified using the Fourier Transform Attenuated Total Reflectance (FTIR-ATR) technique. This analysis was carried out using a Spectrum Two PE instrument shown in *Figure 11* that was equipped with a horizontal attenuated total reflectance crystal made of ZnSe, manufactured by PerkinElmer Inc, in the United States.



Figure 11: FTIR-ATR instrument

Before the analysis, the seaweed samples were freeze-dried to obtain powders, which were then placed directly onto the ATR crystal. The FTIR spectra were collected in absorbance mode, covering a wavelength range from 4000 to 500 cm^{-1} . To improve data quality, each spectrum was generated by averaging 16 scans, with a resolution of 2 cm^{-1} .

3.2.3 PREPARATION OF NANOPARTICLES

3.2.3.1 POLYELECTROLYTES PREPARATION

The two polyelectrolytes used in the Layer by Layer were chitosan (CH) and pectin (PEC). The solution of chitosan was prepared mixing 2 mg of chitosan for each mL of distilled water, to obtain a 2 mg/mL chitosan solution, adding 1% V/V of glacial acetic acid to make the chitosan dissolve, while the 1 mg/mL pectin solution was prepared mixing 1 mg of pectin for each mL of distilled

water. The pectin for the control samples was used as it was, but for the samples containing the antioxidants, six different solutions were prepared at two different ratios (4:1 and 10:1 antioxidants:pectin ratio), respectively containing antioxidants extracted from the Bladder Wrack, the Knotted Wrack and the Toothed Wrack seaweed. Each solution was then titrated, using HCl and NaOH solutions, to reach pH=6. The same titration process was used for the buffer solution of distilled water.

3.2.3.2 LAYER BY LAYER FUNCTIONALIZATION

The process of deposition, represented in *Figure 12*, started with the preparation of the samples, adding 20 mg of mesoporous silica nanoparticle (MNPs) for each sample. Then, 10 mL of the first polyelectrolyte, were added (the first layer was the Chitosan) and the samples were put on a magnetic stirrer for 15 minutes at 95 rpm to mix. The first layer was chitosan, because the MNPs have a negative superficial charge. After this step, the samples were centrifuged at 4400 rpm for 5 minutes, the supernatant was then collected, and the washing step started: 10 mL of buffer solution were added to the samples and, after 5 minute shake on the magnetic stirrer, the samples were again centrifuged at 4400 rpm for 5 minutes and the supernatant removed. Afterwards, other 2 mL of buffer solution were added, the MNPs were shaken again and before the last centrifuge, 100 μ L of the solution were taken to test their ζ -potential. Finally, after the last centrifuge, the supernatant was collected one last time and the whole process was repeated with the opposite charged polyelectrolyte, the pectin, and so on for 5 layers, terminating with a layer of chitosan.

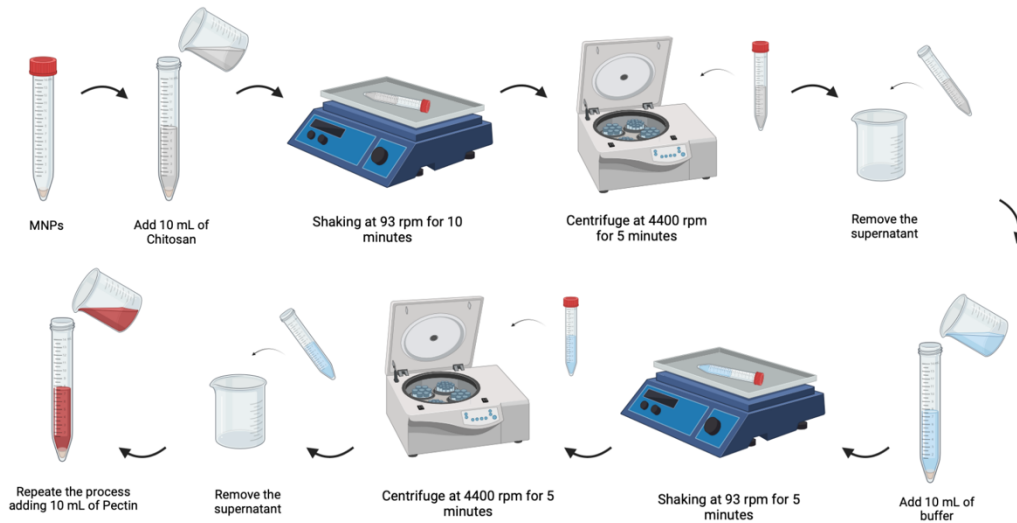


Figure 12: Layer by Layer process

3.2.4 CHARACTERIZATION OF NANOPARTICLES

All the samples prepared were characterized using different measurement.

3.2.4.1 DYNAMIC LIGHT SCATTERING TO MEASURE THE ζ -POTENTIAL

The ζ -potential analysis was carried out using a Zetasizer Nano-S90 (Malvern Instruments, Malvern, UK). After the deposition of each layer of polyelectrolytes on MNPs, 100 μL of the solution were taken and mixed with 900 μL of distilled water. Then, 750 μL were taken and put into a Zetasizer cuvette. All measurements were recorded in triplicate and the mean values were calculated and results were expressed then as the mean \pm standard deviation.

3.2.4.2 TRANSMISSION ELECTRON MICROSCOPE (TEM) FOR THE MORPHOLOGY CHARACTERIZATION

A Transmission Electron Microscope (TEM) was employed to examine the morphology of the MNPs. Specifically, a Philips CM 100 Compustage FEI TEM operating at 100 keV was used. To prepare samples for TEM imaging, a 10 μL

portion of the supernatant, taken out prior to the final centrifugation step was directly deposited onto a TEM grid. This grid was then positioned within the designated chamber of the microscope. Upon capturing high-magnification images, the exact diameters of the nanoparticles were measured with precision using ImageJ software.

3.2.4.3 X-RAY PHOTOELECTRON SPECTROSCOPY (XPS) ANALYSIS

Freeze-dried nanoparticles were subjected to X-ray Photoelectron Spectroscopy (XPS) to precisely determine the elemental composition on the surface of the biomaterials. The analysis was conducted using a scanning microprobe Kratos Axis UltraDLD XPS spectrometer, available through the EPSRC Harwell XPS Service in Cardiff, UK. This spectrometer was equipped with a monochromatized X-ray radiation source emitting AlK α X-rays. The vacuum conditions in the analysis chamber were maintained at a base pressure of 10⁻⁹ mbar. During the analysis, the samples were examined in High Power mode using an X-ray take-off angle of 45°, resulting in a scanned area of about 1400 × 200 μ m. For each specimen, two types of data were collected: survey scans and high-resolution spectra. The survey scans were obtained using Fixed Analyser Transmission (FAT) mode within a binding energy (BE) range of 0–1200 eV, with a pass energy of 117.4 eV. Additionally, high-resolution spectra were gathered using FAT mode and a pass energy of 29.35 eV for C1s and O1s elements.

To quantify the atomic concentration (At.%) from the survey scans, the CasaXPS software package built into the system was utilized. For the purpose of identifying the specific chemical binding states of the elements within the films, XPS spectra were subjected to peak deconvolution using the same CasaXPS software. This process allowed the determination of the Binding Energy (BE) values associated with various chemical elements detected within the films.

3.2.4.1 FOLIN-CIOCALTEU METHOD

It was used the same process described in par. 3.2.2.2

3.2.4.2 FTIR ANALYSIS

It was used the same process described in par. 3.2.2.4

3.2.5 CELL CULTURE

Fibroblasts cells were grown in Dulbecco's Modified Eagle's Medium (DMEM), with 10% fetal bovine serum (FBS) and 5000 U/mL penicillin/streptomycin and maintained at 37 °C with 5 % CO₂ in a humidified incubator. All culture materials were purchased from Sigma Life Science.

To assess how these cells behave following exposure to artificially produced nanoparticles, CELLSTAR® 96 well-plates were utilized, with each well containing 10000 cells.

3.2.6 CITOTOXICITY EVALUATION

3.2.6.1 PRESTO BLUE ASSAY

To assess the metabolic activity of fibroblasts, the PrestoBlue assay was conducted using PrestoBlue™ Cell Viability Reagent from Thermo Scientific, USA (Figure 14).



Figure 13: PrestoBlue assay kit

Here's a summary of the procedure:

1. Cells were initially seeded in a 96-well plate, with each well containing 8000 cells. Different concentrations of antioxidant extracts (2, 5, 12.5, 25, 50, 100 mg/mL) to be tested were added to the wells
2. After a 48-hour incubation period, the culture medium was removed, and the samples were washed with pre-warmed PBS at 37°C
3. To assess cell metabolic activity, PrestoBlue solution was employed. This solution was prepared by diluting PrestoBlue™ reagent (Thermo Scientific, USA) in DMEM at a 1:10 ratio. The reagent vial was covered with aluminium to protect it from light

4. Next, 200 μL of the reagent solution was added to each well, and the samples were incubated for 1 hour at 37°C with 5% CO_2
5. Following the incubation, 100 μL of the solution from each well was transferred to a white-bottom 96-well plate
6. A FLUOstar Omega MicroPlate Reader from BMG Labtech was used to measure the fluorescence, with excitation at 544 nm and emission at 590 nm.
7. To obtain accurate results, it was subtracted the average fluorescence value of control wells containing only PrestoBlue solution.
8. The results are presented as viability percentages, which were calculated by comparing the fluorescence values of each sample with the average fluorescence value of the control cells that were incubated with only DMEM.

3.2.6.2 LIVE/DEAD ASSAY

To assess cell viability, a two-colour fluorescence test known as the Live/Dead assay (utilizing the LIVE/DEAD® Cell Imaging Kit from Life Technologies, Thermo Fisher Scientific, UK) was employed (*Figure 13*).

This method enables the simultaneous determination of two cell populations: live cells (stained blue) and dead cells (stained green).

Various samples were prepared by dissolving different amounts of seaweed antioxidant extracts into DMEM. This was done to investigate the effects of different concentrations ranging from 1 mg/mL to 100 mg/mL. Subsequently, the Live/Dead assay was conducted following the manufacturer's instructions. Briefly, a Live/Dead staining solution was created by mixing 2 drops of each blue and red staining in 1 mL of PBS. Cells were then exposed to antioxidants



Figure 14: LIVE/DEAD assay kit

at different concentrations for 48 hours. After the incubation period, all wells were washed twice with PBS and subsequently incubated with 100 μ L of the Live/Dead staining solution for 30 minutes at 37°C. Finally, the samples were imaged using the EVOS M5000 fluorescence microscope from Thermo Fisher Scientific.

3.2.7 BACTERIAL TESTS

To evaluate the antibacterial properties of the antioxidant extract, a bacterial test was performed. The bacteria used in this test were *Staphylococcus Aureus* (Gram positive) and *Klebsiella Pneumonia* (Gram negative), which were contained into the Muller Hilton Broth (MHB).

The first thing done at day one was to set up an overnight culture taking a colony from the specific bacteria, putting it into a sterile tube containing 10 mL of MHB and incubate the tube at 37 °C for 24 h. Afterwards, at day two, the bacterial suspension the pectin and the antioxidant extracts samples were prepared:

1. For the bacterial suspension, 1 ml of the activated culture was taken and put into a sterile 1.5 tube, and it was then centrifugate at 5G for 5 minutes. Then, the supernatant was removed, and it was resuspended in 1 ml of MHB. Finally, a serial dilution was prepared and 100 μ L of each dilution (10^{-5} , 10^{-6} , 10^{-7}) were spread onto BHIA (duplicate plates), incubated at 37°C for 24 hours and then enumerated the survivors.
2. For the antioxidant extract samples preparation, 10 mg of each seaweed extract were mixed with different amount of MHB to reach different concentrations (*Table 3*).

Table 3: Sample parameters

CONCENTRATION (mg/mL)	COMPOUND (μ L)	MHB (μL)	CELLS (μL)	TOTAL (μL)
0	0	135	15	150
4	6	129	15	150
8	12	123	15	150
16	24	111	15	150
32	48	87	15	150
64	96	39	15	150
90	135	0	15	150

Next, the multiwell was prepared putting a volume of 150 μ L per well at different concentration adding the corresponding volume of pectin and antioxidant extracts in each well, the corresponding volume of MHB and 15 μ L of 10^{-3} dilution of overnight culture of bacteria and the tube was incubate at 37°C for 24 hours.

Finally, at day three, the multiwell was observed and a spread plate was prepared: first, each well in the plate was studied and the concentration at which low or no bacterial growth is not observed (resulting in a clear liquid) was determined, then, 100 μ L of each net well solution (low or no bacterial) were spread onto BHIA plate and 100 μ L of a diluted solution (10 μ L well: 90 μ L of MHB) (low or no bacterial) were spread onto a BHIA plate. The tube was then incubated at 37°C for 24 hours and the survivors were enumerated. At the end, 11650 cells were inoculated for the Klebsiella Pneumonia strain, while for the Staphylococcus Aureus they were 8,300.

4 RESULTS AND DISCUSSION

4.1 ULTRASOUND-ASSISTED EXTRACTION TECHNIQUE

4.1.1 EFFECT OF TEMPERATURE, TIME, AND RATIO ON TOTAL PHENOLIC CONTENT (TPC)

Table 4 summarizes the total phenolic content (TPC) of each seaweed extract. Thanks to the Design of Experiments, the ultrasound assisted extraction conditions were optimized to evaluate how the extraction parameters influenced the TPC. In this regard, 15 different combinations of extraction parameters were created through Minitab and they were tested and analysed.

Table 4: Combination of extraction parameters and system responses expressed through total phenolic content (TPC)

RUN ORDER	TEMP (°C)	TIME (min)	RATIO (mg/mL)	SS TPC (mg/mL)	BW TPC (mg/mL)	KW TPC (mg/mL)	SW TPC (mg/mL)	KE TPC (mg/mL)	TW TPC (mg/mL)
1	20	15	20	0.74	6.93	4	6.08	0.32	5.11
2	20	40	20	0.76	5.56	5.68	4.61	0.38	4.42
3	20	15	5	0.31	4.37	3.56	1.81	0.21	2.01
4	30	27.5	20	0.53	6.52	4.76	3	0.25	3.76
5	10	27.5	5	0.28	2.86	2.21	1.16	0.18	1.54
6	10	15	12.5	0.6	5.49	1.92	2.3	0.22	3.54
7	20	40	5	0.3	4.15	3.8	2.18	0.29	1.42
8	30	40	12.5	0.42	4.27	3.2	2.35	0.35	3.69
9	20	27.5	12.5	0.49	7.82	6.43	3.02	0.21	2.64
10	30	27.5	5	0.31	3.03	1.88	1.07	0.18	1.77
11	10	27.5	20	0.78	5.5	6.03	3.3	0.25	3.84

12	30	15	12.5	0.36	3.51	2.89	2.73	0.24	3.84
13	20	27.5	12.5	0.41	7.43	6.99	4.45	0.26	3.26
14	10	40	12.5	0.46	4.7	3.61	2.79	0.18	3.44
15	20	27.5	12.5	2.29	16.21	6.06	4.82	0.21	3.27

Response surface methodology (RSM) was used to express TPC for each seaweed, as a function of the independent variables exploiting a second-order polynomial equation, expressed in *Table 5*. Together with the equations the R-squared (R sq) value and the Adjusted R-squared (R sq(adj)) value were also calculated for each type of seaweed. The R squared values are all around 90% with the exception of the KE which is lower, while the R square adjusted values goes from 70% to 98% also with the exception of the KE, which has a R squared adjusted value of 1.54%, which is very low.

Table 5: Minitab equations

VARIABLES	FITTED MODEL EQUATIONS	R SQ (%)	R SQ (ADJ) (%)
BW	$\text{TPC} = -7.95 + 0.670 \text{ Temp } (^{\circ}\text{C}) + 0.088 \text{ Time (min)} + 0.513 \text{ Ratio (mg/mL)} - 0.01546 \text{ Temp } (^{\circ}\text{C}) * \text{Temp } (^{\circ}\text{C}) - 0.00003 \text{ Time (min)} * \text{Time (min)} - 0.00738 \text{ Ratio (mg/mL)} * \text{Ratio (mg/mL)} - 0.00174 \text{ Temp } (^{\circ}\text{C}) * \text{Time (min)} - 0.00068 \text{ Temp } (^{\circ}\text{C}) * \text{Ratio (mg/mL)} - 0.00491 \text{ Time (min)} *$	89.61	70.9
SW	$\text{TPC} = -0.027 + 0.0214 \text{ Temp } (^{\circ}\text{C}) + 0.0333 \text{ Ratio (mg/mL)} - 0.000400 \text{ Temp } (^{\circ}\text{C}) * \text{Temp } (^{\circ}\text{C}) - 0.000490 \text{ Ratio (mg/mL)} * \text{Ratio (mg/mL)} - 0.000946 \text{ Temp } (^{\circ}\text{C}) * \text{Ratio (mg/mL)}$	93.29	98.55
KW	$\text{TPC} = -14.85 + 0.924 \text{ Temp } (^{\circ}\text{C}) - 0.589 \text{ Time (min)} + 0.427 \text{ Ratio (mg/mL)} - 0.02043 \text{ Temp } (^{\circ}\text{C}) * \text{Temp } (^{\circ}\text{C}) - 0.00986 \text{ Time (min)} * \text{Time (min)} - 0.01227 \text{ Ratio (mg/mL)} * \text{Ratio (mg/mL)} - 0.00275 \text{ Temp } (^{\circ}\text{C}) * \text{Time (min)} - 0.00364 \text{ Temp } (^{\circ}\text{C}) * \text{Ratio (mg/mL)} + 0.00383 \text{ Time (min)} * \text{Ratio}$	91	74.80
SS	$\text{TPC} = 0.283 + 0.0092 \text{ Temp } (^{\circ}\text{C}) - 0.0048 \text{ Time (min)} + 0.0140 \text{ Ratio (mg/mL)} - 0.000391 \text{ Temp } (^{\circ}\text{C}) * \text{Temp } (^{\circ}\text{C}) + 0.000076 \text{ Time (min)} * \text{Time (min)} + 0.000506 \text{ Ratio (mg/mL)} * \text{Ratio (mg/mL)}$	88.62	80.09
KE	$\text{TPC} = 0.192 + 0.0147 \text{ Temp } (^{\circ}\text{C}) - 0.0150 \text{ Time (min)} + 0.0083 \text{ Ratio (mg/mL)} - 0.000522 \text{ Temp } (^{\circ}\text{C}) * \text{Temp } (^{\circ}\text{C}) + 0.000215 \text{ Time (min)} * \text{Time (min)} - 0.000065 \text{ Ratio (mg/mL)} * \text{Ratio (mg/mL)} + 0.000299 \text{ Temp } (^{\circ}\text{C}) * \text{Time (min)} + 0.000033 \text{ Temp } (^{\circ}\text{C}) * \text{Ratio (mg/mL)} - 0.000058 \text{ Time (min)} * \text{Ratio}$	64.94	1.84
TW	$\text{TPC} = 2.48 + 0.012 \text{ Temp } (^{\circ}\text{C}) - 0.2010 \text{ Time (min)} + 0.361 \text{ Ratio (mg/mL)} + 0.00030 \text{ Temp } (^{\circ}\text{C}) * \text{Temp } (^{\circ}\text{C}) - 0.00347 \text{ Time (min)} * \text{Time (min)} - 0.00641 \text{ Ratio (mg/mL)} * \text{Ratio (mg/mL)} - 0.00011 \text{ Temp } (^{\circ}\text{C}) * \text{Time (min)} - 0.00101 \text{ Temp } (^{\circ}\text{C}) * \text{Ratio (mg/mL)} - 0.00027 \text{ Time (min)} * \text{Ratio (mg/mL)}$	94.94	85.84

4.1.2 METABOLOMICS

In *Figure 15* it is possible to see the results of the metabolomics, and it's immediately clear the main difference in colour between four of the six seaweed, TW, BW, SW and KW, and the other two, the KE and the SS. Those two categories seem to have a very opposite behaviour expressing the same metabolites: as it's possible to see from the colour code legend, SS and KE have a higher abundance of Nicotinate and Betaine, which in the other four extract are the least present. Particularly, nicotinate is a conjugate base of nicotinic acid, which exerts anti-inflammatory actions that may be beneficial to patients with inflammatory skin diseases⁸⁵, while betaine is a native compound widely studied as an antioxidant in agriculture and human health which mechanism remains unclear⁸⁶. Moreover, in those two seaweed extracts, all the other metabolites analyzed are less abundant.

In the list of the analyzed metabolites it is possible to find some very crucial ones such as phenylalanine, which is a precursor of flavonoids, one of the main class of phenolic compounds present in antioxidants, nicotinamide, which is hydro soluble vitamin from group B, threonic acid, whose L-isomer is a metabolite of ascorbic acid (vitamin C), citric acid, which has antioxidant properties, and so on. The presence of these metabolites is mostly preponderant in BW, KW, SW and TW, and almost absent in KE and SS.

The same behavior is possessed by one the most important metabolite that needs to be analyzed, which is gallic acid, an hydroxybenzoic acids whose content will be further investigated using Folin-Ciocalteu method to evaluate the total phenolic content (TPC). The presence of gallic acid is a little more preponderant in BW, but really similar to SW, TW and KW, and very different from KE and SS, in which the levels of the gallic acid seems to be really low.

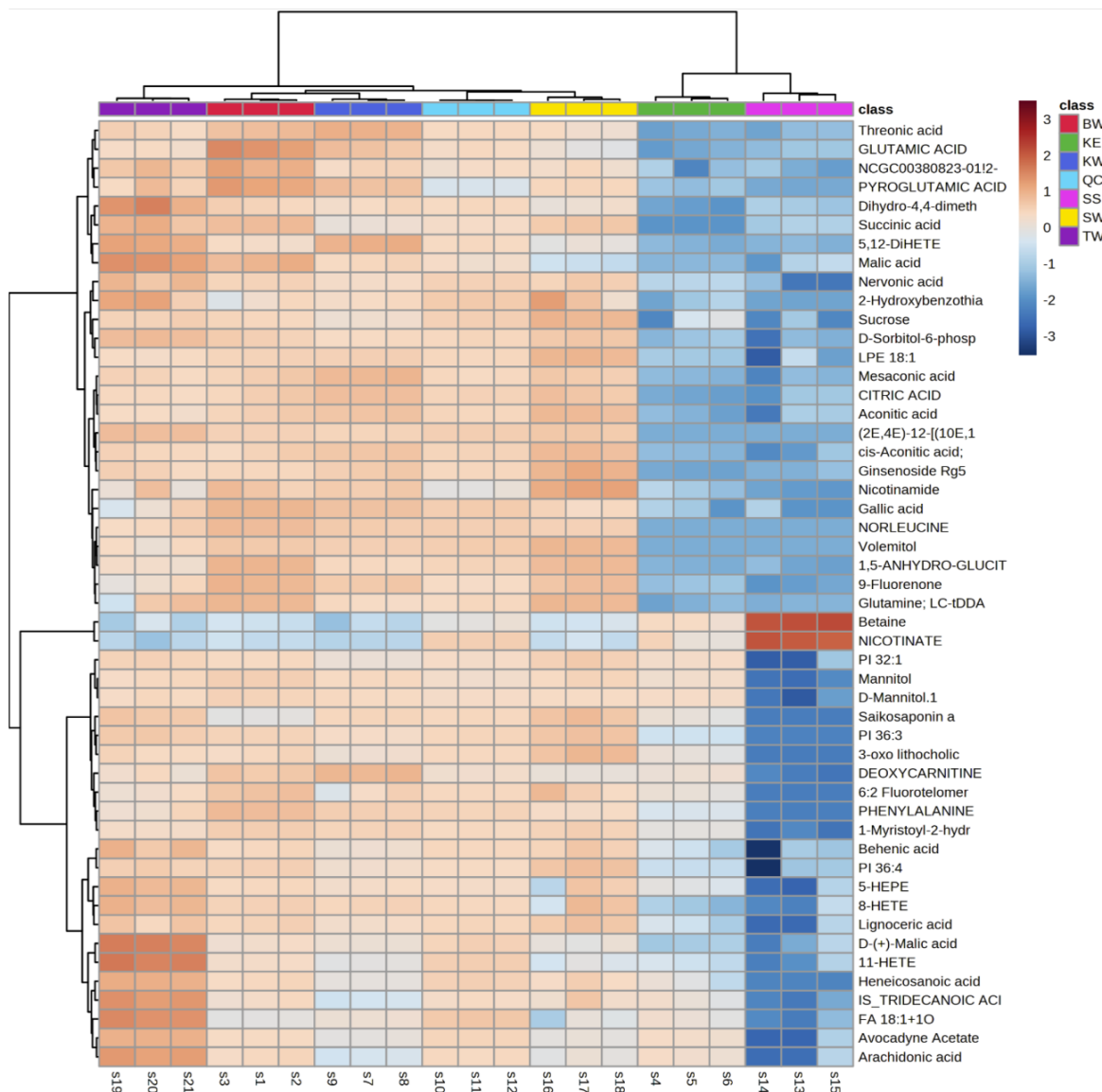


Figure 15: Metabolomic of seaweed antioxidant extract

From this first analysis of the metabolites, three of the six seaweed extract were preliminary selected as the best ones for the purpose of the project, the BW, KW, TW.

4.1.3 EVALUATION OF RELIABILITY OF THE FITTED MODELS

Using Minitab, a statistical analysis was performed to evaluate whether each parameter was statistically significant influencing the TPC content (mg/mL) of each of the three selected seaweed extracts. To this purpose, Pareto Charts, Contour Plots and Surface Plots of the results against parameters were evaluated.

From *Figure 16* it's possible to see the Pareto Chart for BW TPC (mg/mL) showing that the two most statistically significant parameters are the ratio (mg/mL) and the temperature (°C), exceeding the threshold value and therefore influencing the TPC of the BW seaweed extract.

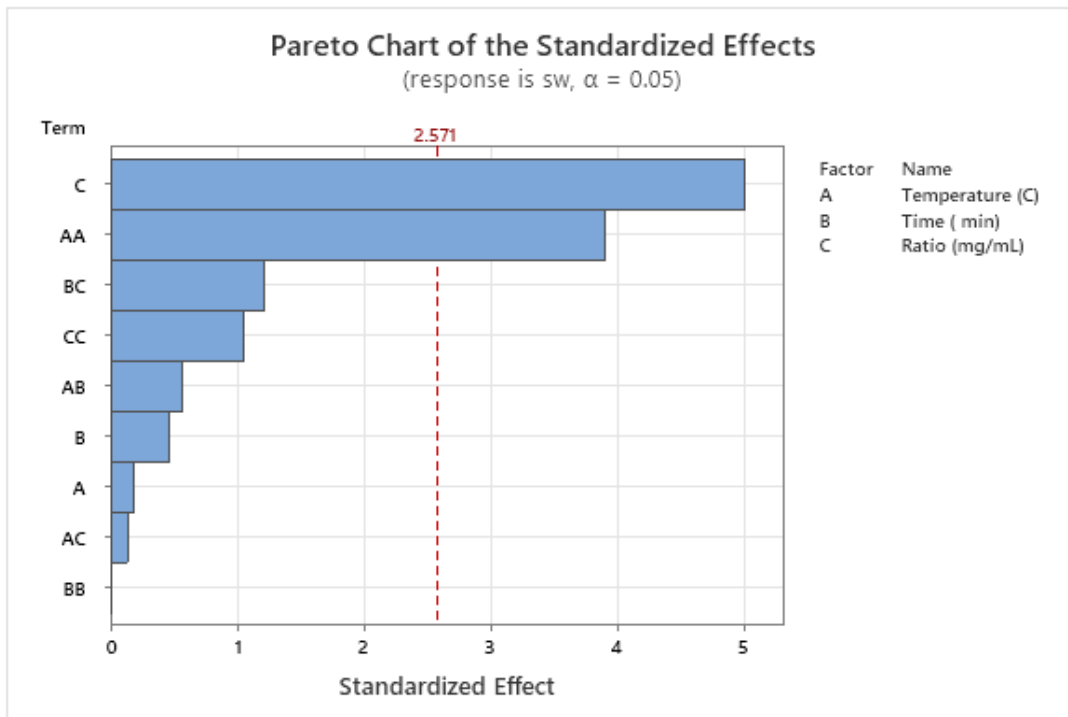


Figure 16: BW Pareto Chart for TPC (mg/mL) showing the alpha value and the standardized effect of each parameter on the resulting TPC content in the seaweed extract

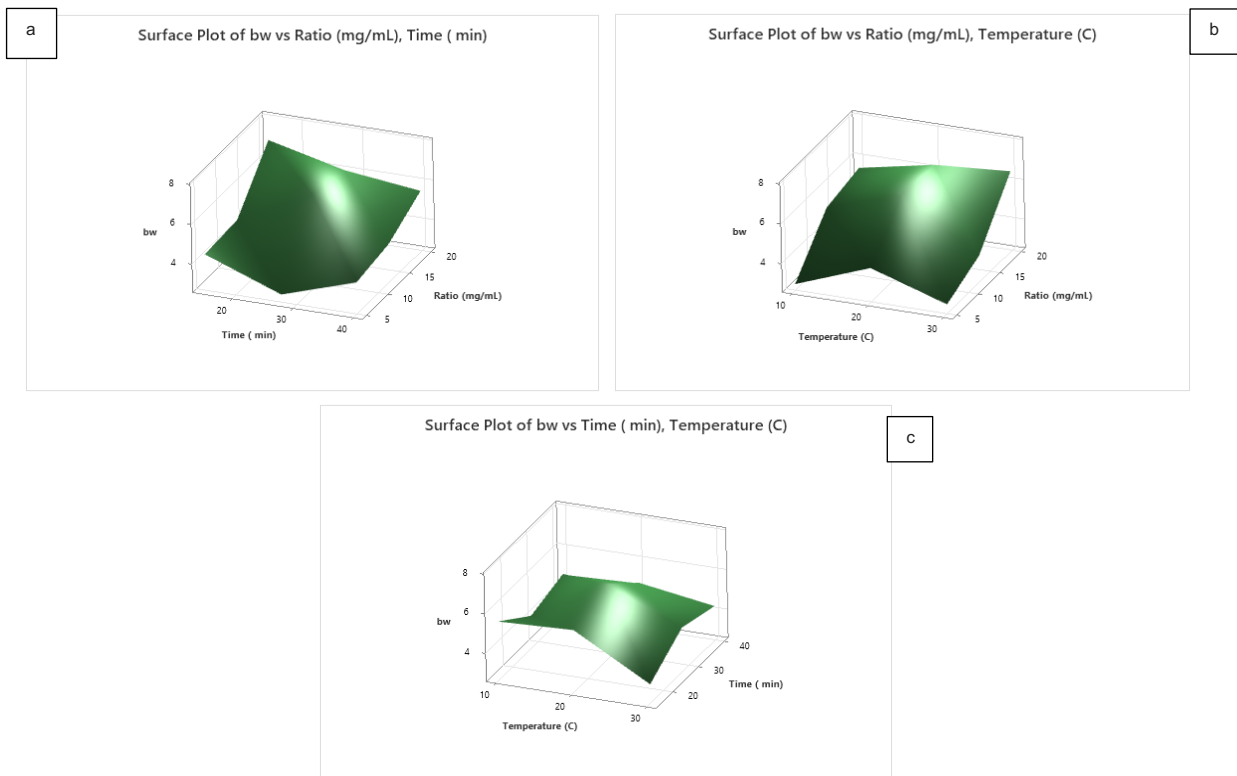


Figure 17: **a)** Surface Plot of BW TPC (mg/mL) against Time (min) and Ratio (mg/mL), **b)** Surface Plot of BW TPC (mg/mL) against Temperature (°C) and Ratio (mg/mL), **c)** Surface Plot of BW TPC (mg/mL) against Temperature (°C) and Time (min).

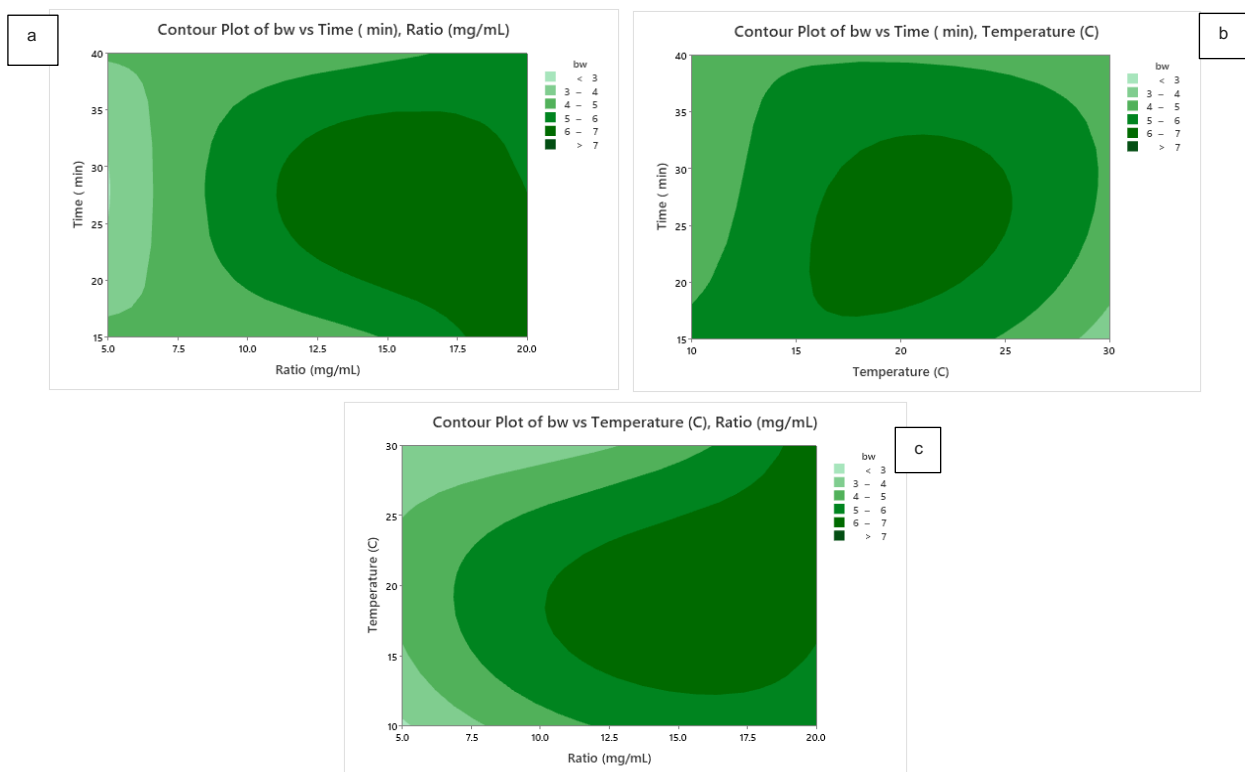


Figure 18: **a)** Contour Plot of BW TPC (mg/mL) against Time (min) and Ratio (mg/mL), **b)** Contour Plot of BW TPC (mg/mL) against Time (min) and Temperature (°C), **c)** Contour Plot of BW TPC (mg/mL) against Temperature (°C) and Ratio (mg/mL).

Looking at the Surface and Contour Plots in *Figure 17* and *Figure 18*, it's possible to see how the relationship between the different parameters influence the TPC in BW seaweed extract. The highest TPC could be reached in a time range from 15 to 30 minutes with a ratio between 12.5 and 20 mg/mL (a), or in a smallest time range between 20 and 30 minutes with a temperature of 20/25 °C (b), or moreover between 15 and 25 °C with a ratio from 12.5 to 20 mg/mL (c).

As well as for the BW seaweed extract, from *Figure 19* it's possible to see the Pareto Chart for KW TPC (mg/mL), and in this case the parameters that overcome the threshold are temperature (°C), ratio (mg/mL) and time (min).

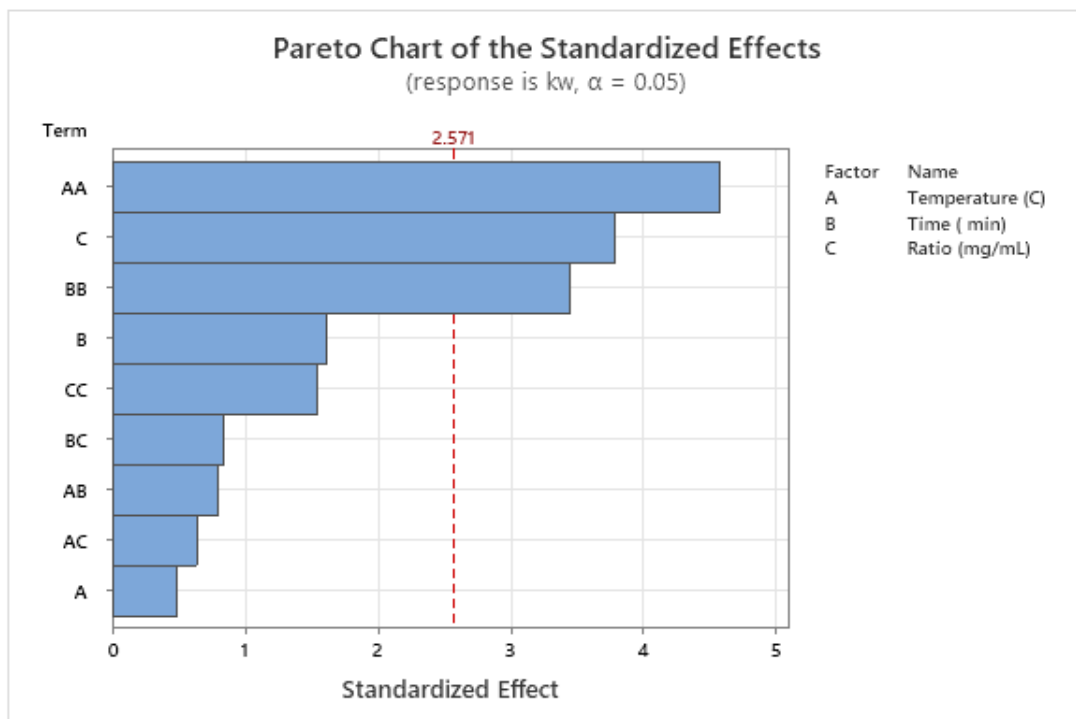


Figure 19: KW Pareto Chart for TPC (mg/mL) showing the alpha value and the standardized effect of each parameter on the resulting TPC content in the seaweed extract

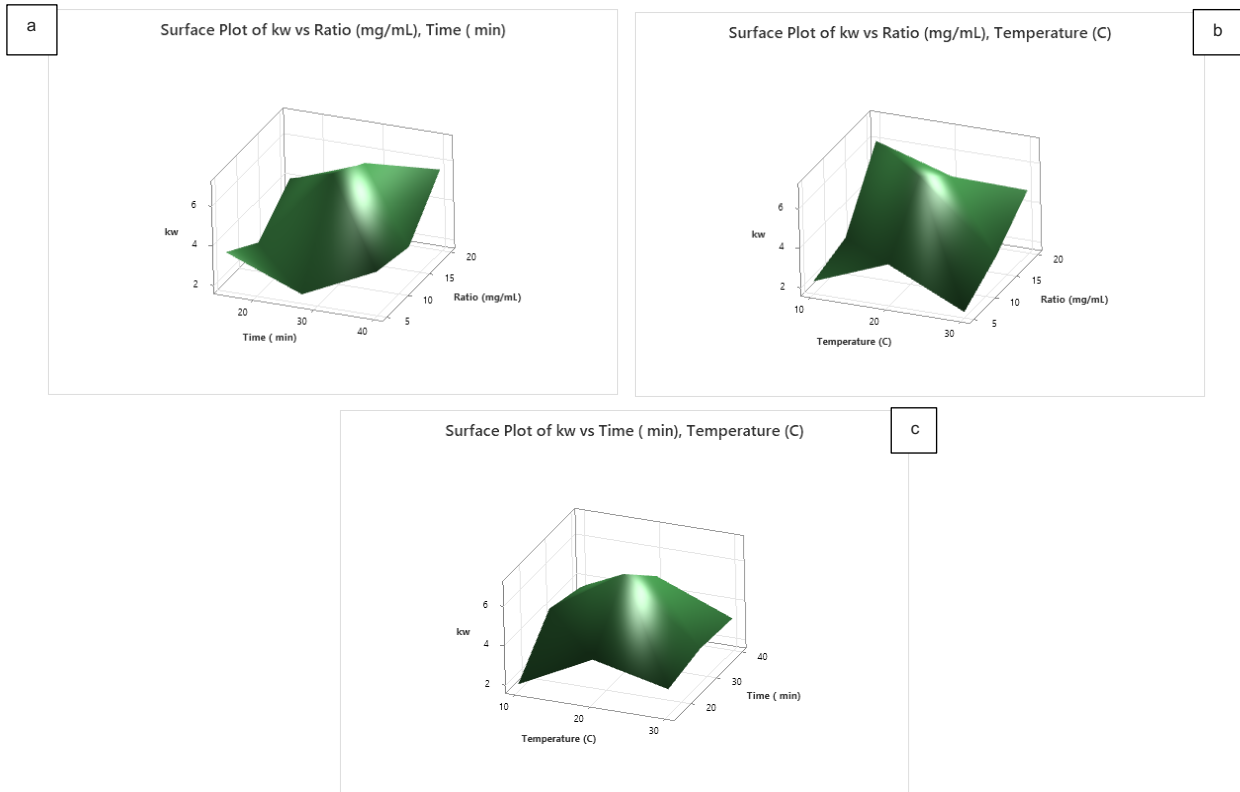


Figure 20: **a)** Surface Plot of KW TPC (mg/mL) against Time (min) and Ratio (mg/mL), **b)** Surface Plot of KW TPC (mg/mL) against Temperature (°C) and Ratio (mg/mL), **c)** Surface Plot of KW TPC (mg/mL) against Temperature (°C) and Time (min).

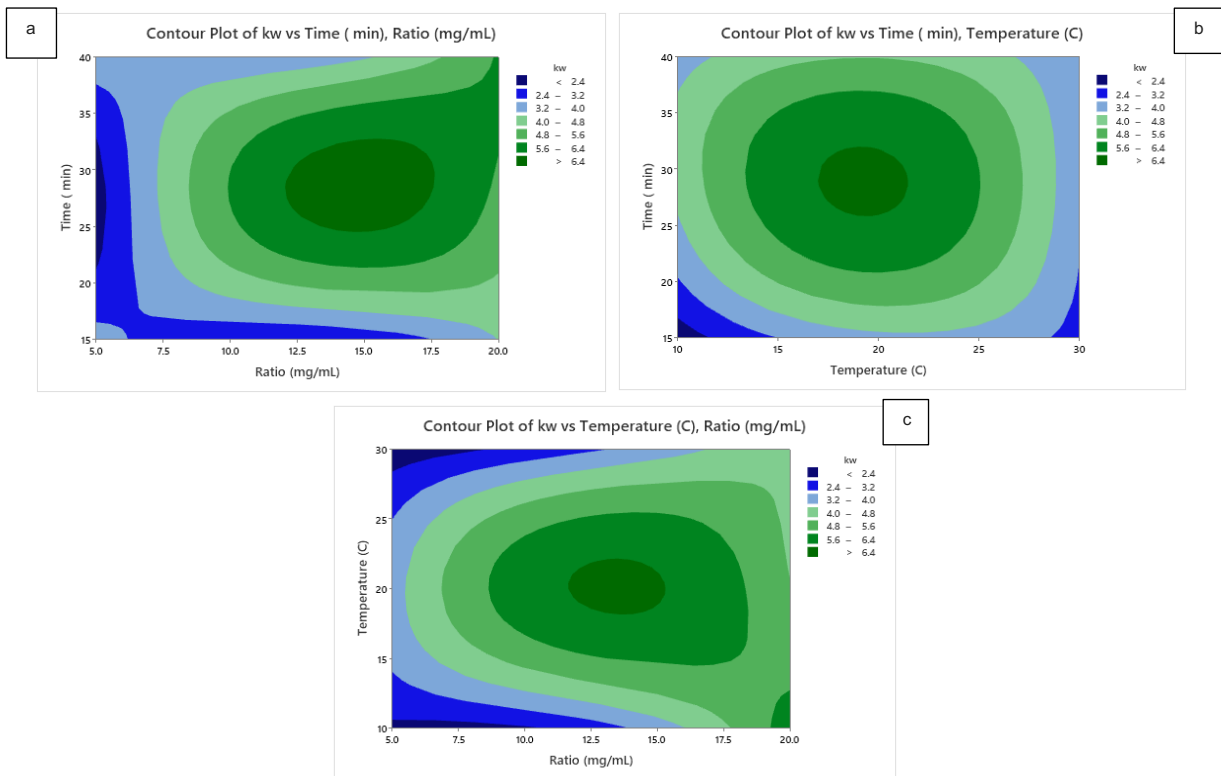


Figure 21: **a)** Contour Plot of KW TPC (mg/mL) against Time (min) and Ratio (mg/mL), **b)** Contour Plot of KW TPC (mg/mL) against Temperature (°C) and Ratio (mg/mL), **c)** Contour Plot of KW TPC (mg/mL) against Temperature (°C) and Time (min).

Looking at the Surface and Contour Plots in *Figure 20* and *Figure 21*, it's possible to see that in this case the highest TPC could be reached in a time range from 25 to 30 minutes with a ratio between 12.5 and 17.5 mg/mL (a), or around 30 minutes with a temperature of 20 °C (b), or moreover between at 20 °C with a ratio of 12.5/15 mg/mL (c).

Finally, in *Figure 22* it is possible to see the Pareto Chart for the last seaweed extract selected, the TW TPC (mg/mL), and in this case the main parameter that is actually relevant is the ratio (mg/mL), but it is also possible to consider the time (min), being on the threshold line.

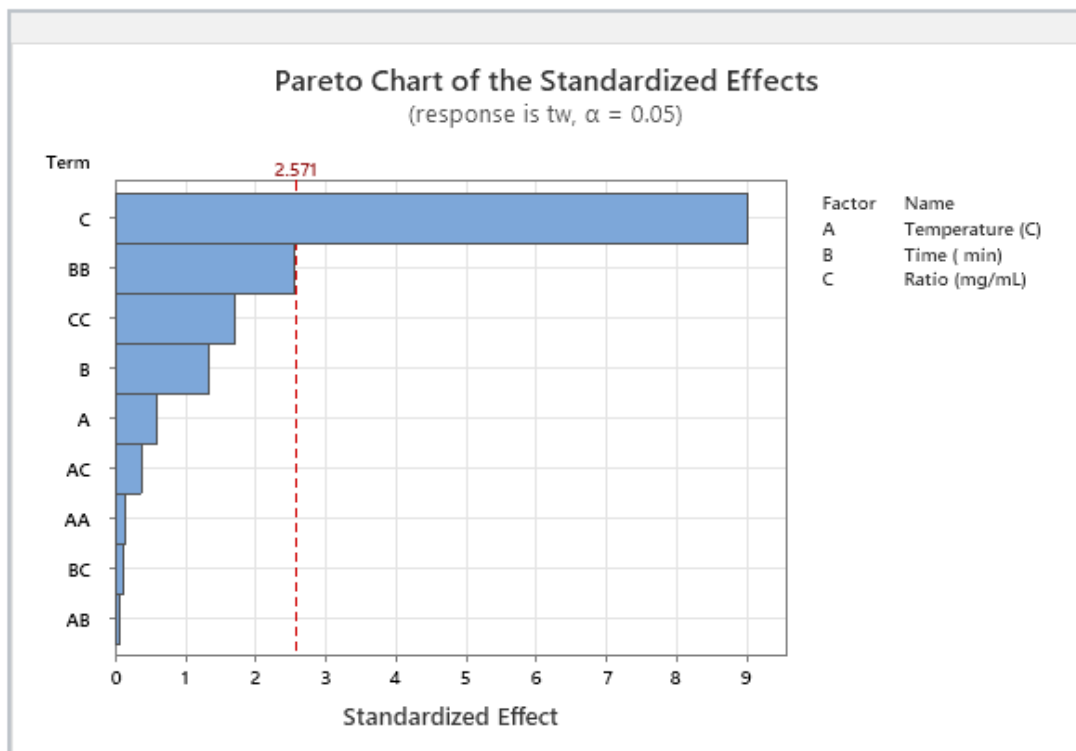


Figure 22: TW Pareto Chart for TPC (mg/mL) showing the alpha value and the standardized effect of each parameter on the resulting TPC content in the seaweed extract

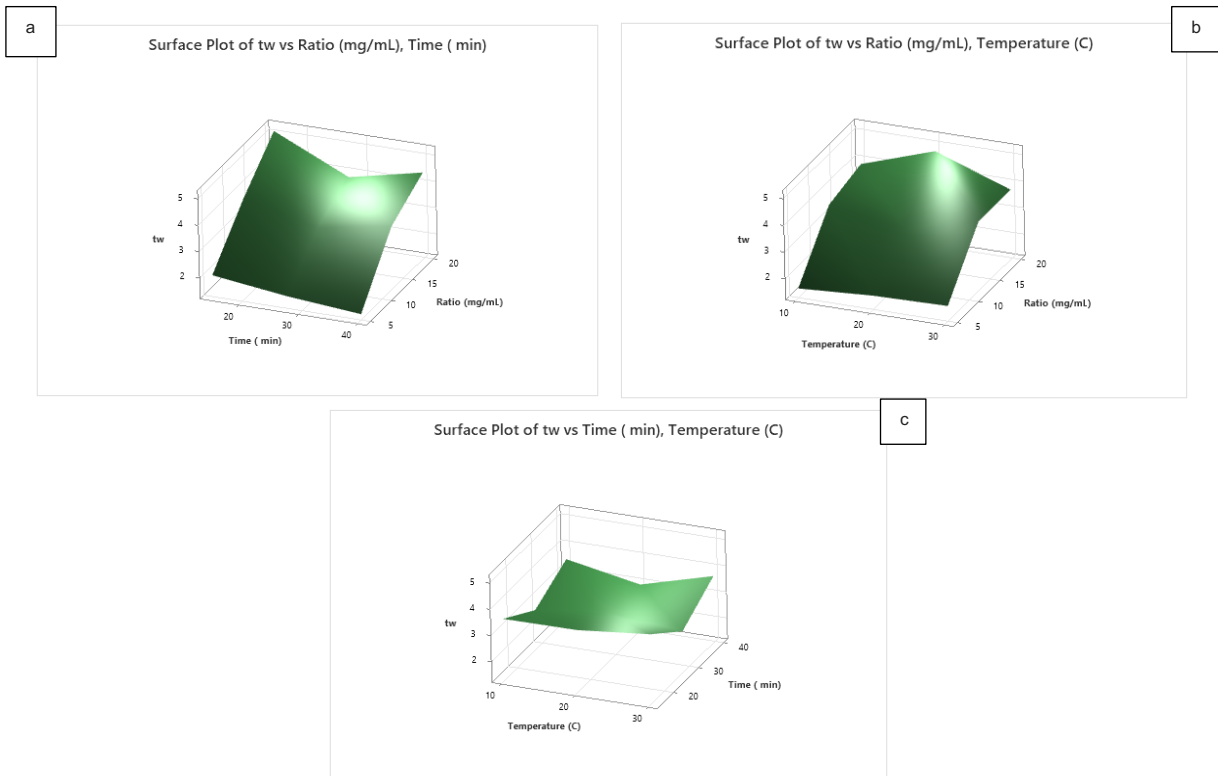


Figure 24: **a)** Surface Plot of TW TPC (mg/mL) against Time (min) and Ratio (mg/mL), **b)** Surface Plot of TW TPC (mg/mL) against Temperature (°C) and Ratio (mg/mL), **c)** Surface Plot of TW TPC (mg/mL) against Temperature (°C) and Time (min).

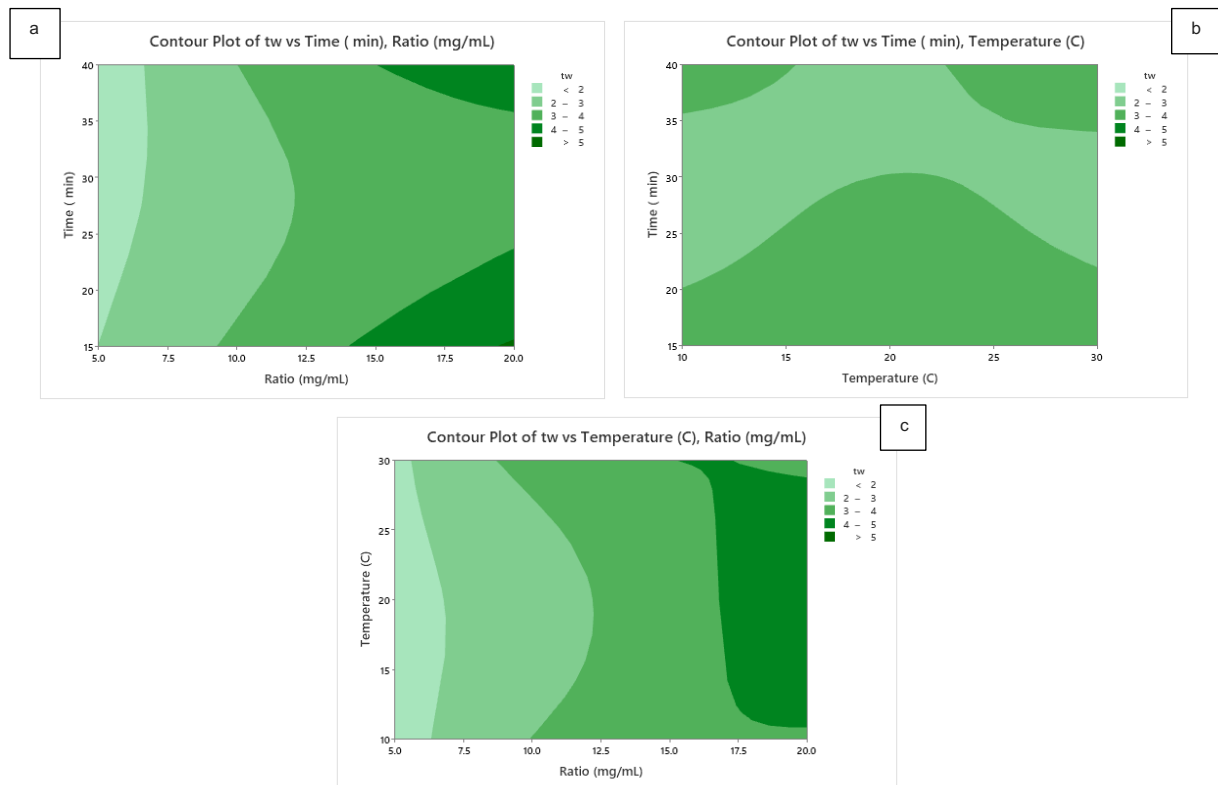


Figure 23: **a)** Contour Plot of TW TPC (mg/mL) against Time (min) and Ratio (mg/mL), **b)** Contour Plot of TW TPC (mg/mL) against Temperature (°C) and Ratio (mg/mL), **c)** Contour Plot of TW TPC (mg/mL) against Temperature (°C) and Time (min).

Looking at the last Surface and Contour Plots in *Figure 23* and *Figure 24*, it is possible to see that for this seaweed extract, the highest TPC could be reached in a time range from 15 to 20 or close to 40 minutes with a ratio over 15 mg/mL (a), or less than 20 minutes (b), or still with a ratio over 17.5 mg/mL (c). In this case, as confirmed from the Pareto Chart, the temperature is not an influencing parameter, so each scenario could be carried on at a casual temperature.

The final step included the Response Optimization of extraction process using Response Optimizer on Minitab. Response Optimization was performed to determine the optime combination of extraction parameters able to maximize the final TPC. The results are shown in *Table 6*.

Table 6: Response optimization of extraction process

RESPONSE OPTIMIZATION	TPC (target)	TEMPERATURE (°C)	TIME	RATIO
BW	7.82	19.36	15	20
KW	6.99	19.69	29.45	18.48
TW	5.11	30	15	20

Response prediction of TPC in BW antioxidants extract should reach the maximum value (TPC= 7.82 (mg/mL)) with a ratio of 20 mg/mL when the extraction is performed at 19.36 °C for 15 min. for the KW extraction, the highest total phenolic content (TPC= 6.99 (mg/mL)) should be obtained when the process is carried out at 19.68°C for 29.45 min and the ratio is 18.48 mg/mL. Finally, the TW optimized extraction (TPC= 5.11 (mg/mL)) should be carried out at 30°C for 15 minutes with a ratio of 20 mg/mL.

The following extraction performed with optimized parameters confirmed the model prediction.

In the *Appendix* it is possible to find all the remaining results of the non-selected seaweeds, with Pareto Charts, Contour and Surface Plots.

4.2 CHARACTERIZATION OF ANTIOXIDANT EXTRACT

4.2.1 FTIR-ATR CHARACTERIZATION

The seaweed extract samples were freeze-dried and then analysed to a FTIR-ATR for investigating the chemical composition. From *Figure 25* it is possible to see that all the six spectra are mainly characterized by the presence of the same peaks:

- The 3200-3600 cm^{-1} range, which indicates the presence of the hydroxyl groups (-OH)
- The 2800-3000 cm^{-1} range that correspond to the C-H stretching vibration of polysaccharides CH_2 groups
- The 1500-1600 cm^{-1} range, which indicates the C=C stretching vibration of aromatic rings, that identifies the presence of the phenolic compound through their characteristic absorption band⁸⁷
- The 1200–1450 cm^{-1} range is annotated to the C–O–H bending and C–O stretching vibrations
- The 1000-1200 cm^{-1} range identifies the carbohydrates component present in the seaweed extract and it corresponds to the C=O stretching vibration⁸⁸
- Finally, the 900-600 cm^{-1} range is attributed to the stretching vibration of the anhydroglucose ring

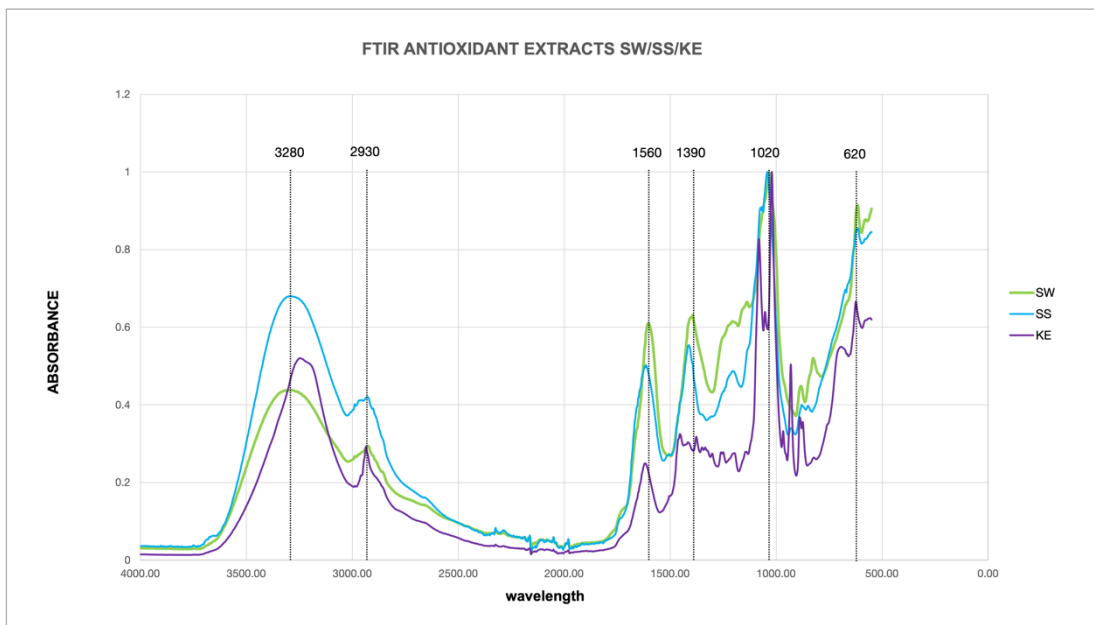
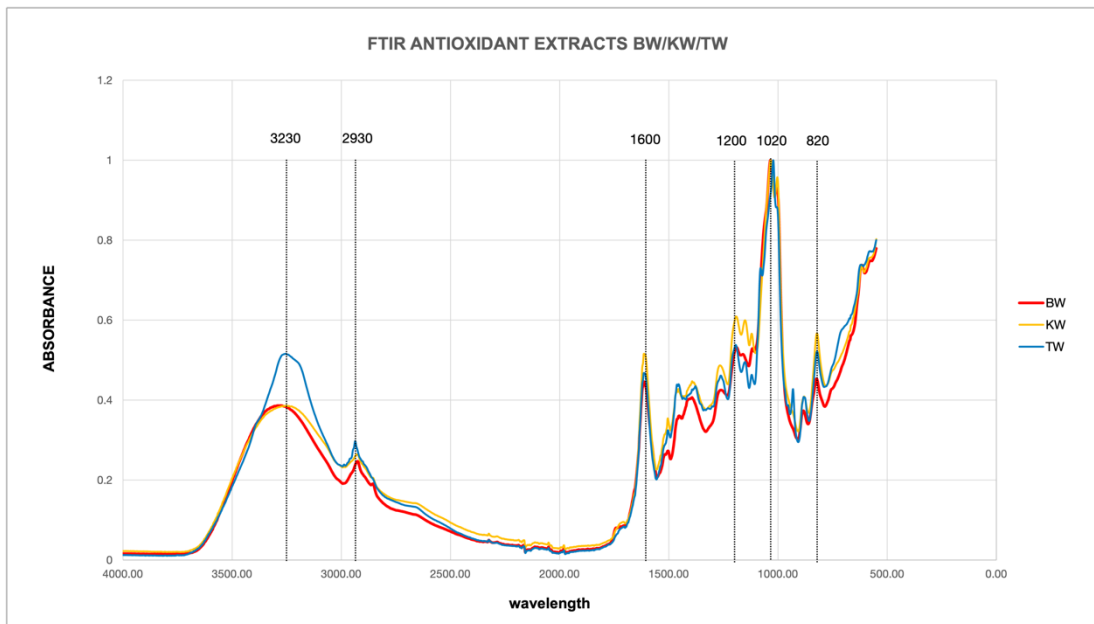


Figure 25: FTIR analysis of antioxidant extract from seaweed

These minimal differences in chemical composition of extracts could be ascribed to the algal species and to the different locations where the seaweeds were collected⁸⁹.

4.2.2 TOTAL PHENOLIC CONTENT (TPC) AND ANTIOXIDANT ACTIVITY EVALUATION

4.2.2.1 FOLIN-CIOCALTEU METHOD

The total phenolic content was measured as the equivalent of gallic acid (GAE) in milligrams per milliliter (mg/mL) present in the sample. The analysis was conducted on all the six seaweed extract using the 15 different combinations of the extraction parameters.

Table 7: Folin-Ciocalteu results with corresponding extraction parameters

SEAWEED	TEMPERATURE (°C)	TIME (min)	RATIO (mg/mL)	GAE (mg/mL)
SS	20	27.5	12.5	2.29
BW	20	27.5	12.5	16.21
KW	20	27.5	12.5	6.99
SW	20	15	20	6.08
KE	20	40	20	0.38
TW	20	15	20	5.11

In *Table 7* it is possible to see the highest value of each sample and the corresponding temperature, time of incubation and solid/liquid ratio. From this measurement, confirming the metabolomic results, three of the six seaweed extract with the highest TPC were chosen to be put into the pectin solution which was used to functionalize the mesoporous silica nanoparticles with the layer-by-layer technique: the Organic Dried Bladder Wrack (BW), the Organic Dried Knotted Wrack (KW) and the Organic Dried Toothed Wrack (TW).

Some studies, for example the one carried on by Sasadara et al. which examined the effect of extraction solvent on total phenolic content of *Gracilaria* sp. demonstrated that the TPC of the extracts changed with the solvent used. For example, in this study, the lowest TPC level produced by the usage of water as the extraction solvent, while the highest was obtained using 100% of acetone. These results could indicate that the polarity of the solvent has an

impact on the TPC of the extracts⁹⁰, so the use of a 50% ethanol solution could have been a good choice to enhance the total phenolic content of the extracts.

4.2.2.2 FERRIC REDUCING ANTIOXIDANT POWER METHOD (FRAP)

After the optimization of the extraction parameters, the total antioxidant activity of the seaweed extracts was evaluated through FRAP method, analysing the ascorbic acid equivalent (AAE (mg/mL)) present in the sample. The results are shown in *Table 8*:

Table 8: FRAP assay results in AAE

SS	BW	KW	SW	KE	TW
38.46	187.56	121.67	51.41	80.89	171.28
AAE	AAE	AAE	AAE	AAE	AAE
(mg/mL)	(mg/mL)	(mg/mL)	(mg/mL)	(mg/mL)	(mg/mL)

These results showed that the greater antioxidant properties were held by the three seaweed that presented the highest TPC (BW, KW and TW) and that were previously chosen to be used in the MNPs.

4.3 CHARACTERIZATION OF NANOPARTICLES

4.3.1 ζ -POTENTIAL ANALYSIS

Dynamic light scattering (DLS) analysis were performed on the mesoporous silica nanoparticles, on the two polyelectrolytes solution of chitosan and pectin and on the antioxidant solution to evaluate the correct deposition for the layer by layer.

4.3.1.1 MESOPOROUS SILICA NANOPARTICLES (MNPs)

From *Figure 26* it is possible to see that the MNPs show a quite strong negative charge (-26.3 mV), which means that the first deposited layer should be a cationic polyelectrolyte.

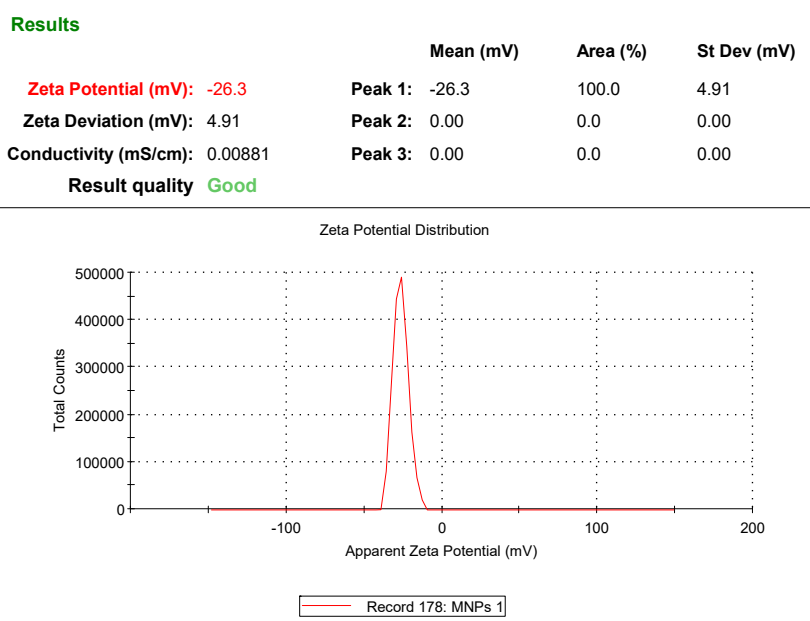


Figure 26: ζ -potential evaluation of MNPs

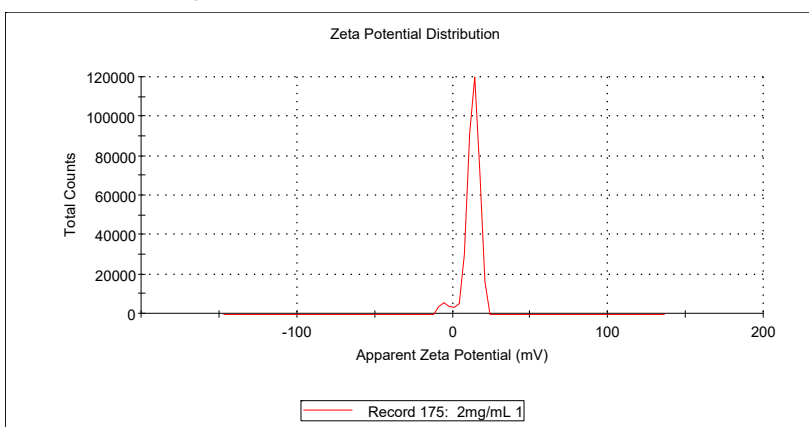
4.3.1.2 POLYELECTROLYTES SOLUTION

As expected, the DLS results confirmed the positive charge of the chitosan (12.7 mV) and the negative charge of the pectin (-48.8 mV), as it shown in *Figure 27*. For this reason, chitosan was used for the first layer.

Results

	Mean (mV)	Area (%)	St Dev (mV)
Zeta Potential (mV): 12.7	Peak 1: 13.4	95.1	3.75
Zeta Deviation (mV): 5.24	Peak 2: -4.23	4.9	3.47
Conductivity (mS/cm): 1.28	Peak 3: 0.00	0.0	0.00

Result quality Good



Results

	Mean (mV)	Area (%)	St Dev (mV)
Zeta Potential (mV): -48.8	Peak 1: -48.8	100.0	5.54
Zeta Deviation (mV): 5.54	Peak 2: 0.00	0.0	0.00
Conductivity (mS/cm): 0.0532	Peak 3: 0.00	0.0	0.00

Result quality Good

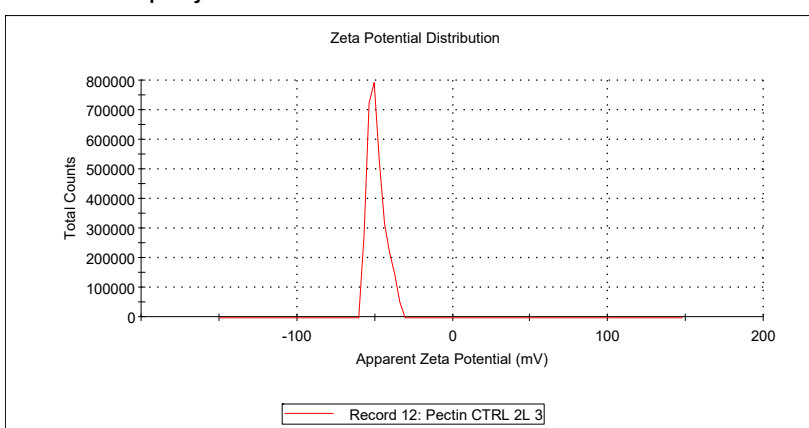


Figure 27: ζ -potential evaluation of chitosan and pectin

4.3.1.3 ANTIOXIDANT SOLUTIONS

Finally, the DLS analysis performed on the antioxidant solution show for all of the three chosen seaweeds extract a negative charge, as shown in *Figure 28*, *Figure 29* and *Figure 30*:

- Organic dried Bladder Wrack (-27.3 mV)
- Organic dried Knotted Wrack (-28 mV)
- Organic dried Toothed Wrack (-33.3 mV)

For that reason, it was chosen to put the antioxidant extract into the pectin solution, and particularly, two different concentration ratios were chosen: 4:1 antioxidant:pectin ratio, and 10:1 antioxidant:pectin ratio.

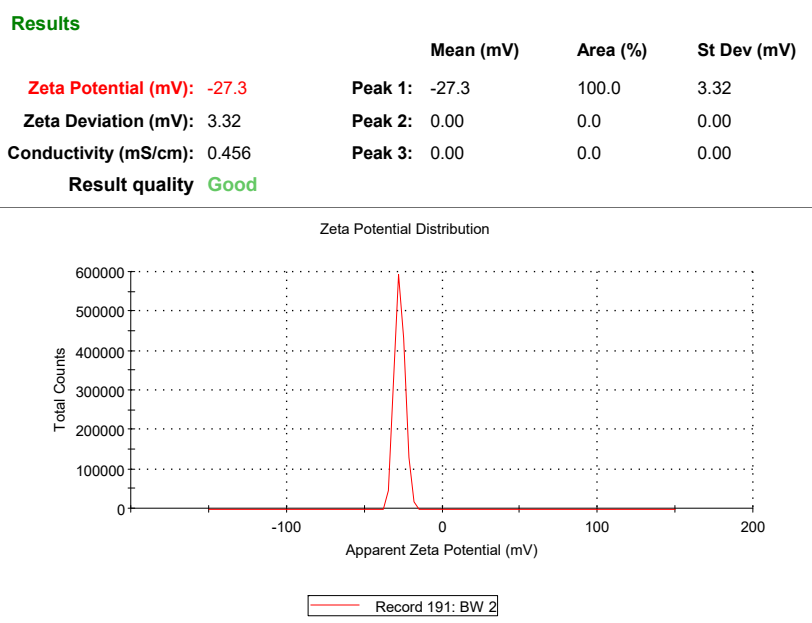


Figure 28: -potential evaluation of Bladder Wrack (BW) antioxidant extract

Results

	Mean (mV)	Area (%)	St Dev (mV)
Zeta Potential (mV): -33.3	Peak 1: -33.3	100.0	4.39
Zeta Deviation (mV): 4.39	Peak 2: 0.00	0.0	0.00
Conductivity (mS/cm): 2.25	Peak 3: 0.00	0.0	0.00

Result quality Good

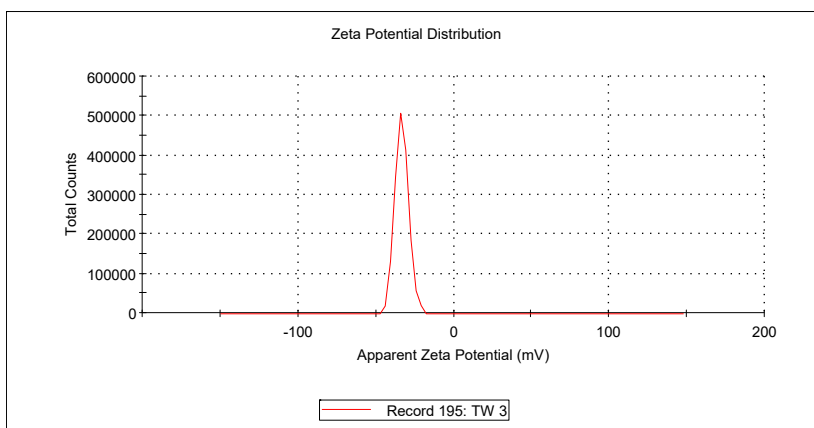


Figure 29: ζ -potential evaluation of Toothed Wrack (TW) antioxidant extract

Results

	Mean (mV)	Area (%)	St Dev (mV)
Zeta Potential (mV): -28.0	Peak 1: -28.0	100.0	5.60
Zeta Deviation (mV): 5.60	Peak 2: 0.00	0.0	0.00
Conductivity (mS/cm): 0.719	Peak 3: 0.00	0.0	0.00

Result quality Good

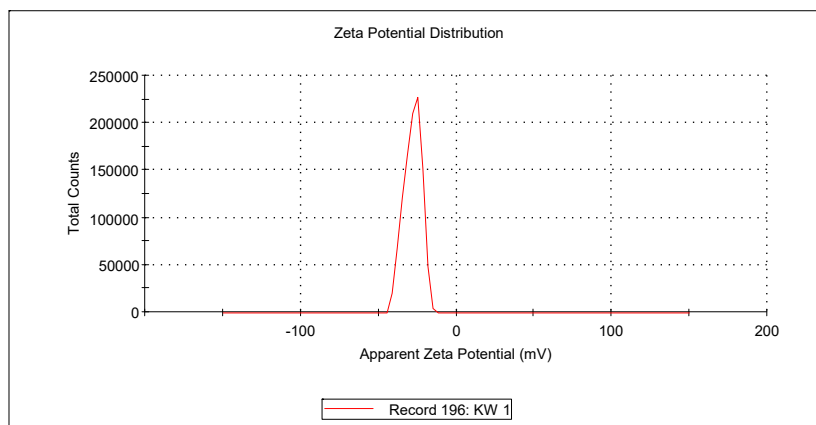


Figure 30: ζ -potential evaluation of Knotted Wrack (KW) antioxidant extract

4.3.1.4 LAYER-BY-LAYER

For both concentrations, as shown in *Figure 31* and *Figure 32* it was possible to confirm the right charge of each deposited layer, with three positive layers of chitosan and two negative layers of pectin with antioxidant extract.

For the first tested concentration (antioxidant 4:1 pectin) the zeta-potential values of each layer were:

1. Layer-by-Layer with Bladder Wrack (BW) antioxidant extract:

- I. 33.35 mV \pm 5.44 mV
- II. -26.87 mV \pm 3.40 mV
- III. 29.47 mV \pm 0.70 mV
- IV. -33.80 mV \pm 0.28 mV
- V. 18.17 mV \pm 4.88 mV

2. Layer-by-Layer with Knotted Wrack (KW) antioxidant extract

- I. 25.53 mV \pm 2.93 mV
- II. -48.30 mV \pm 2.31 mV
- III. 13.83 mV \pm 3 mV
- IV. -34.27 mV \pm 0.91 mV
- V. 29.03 mV \pm 0.80 mV

3. Layer-by-Layer with Toothed Wrack (TW) antioxidant extract

- I. 30.30 mV \pm 2.10 mV
- II. -44.90 mV \pm 1.84 mV
- III. 12.04 mV \pm 2.3 mV
- IV. -41.83 mV \pm 1.89 mV
- V. 24.65 mV \pm 1.65 mV

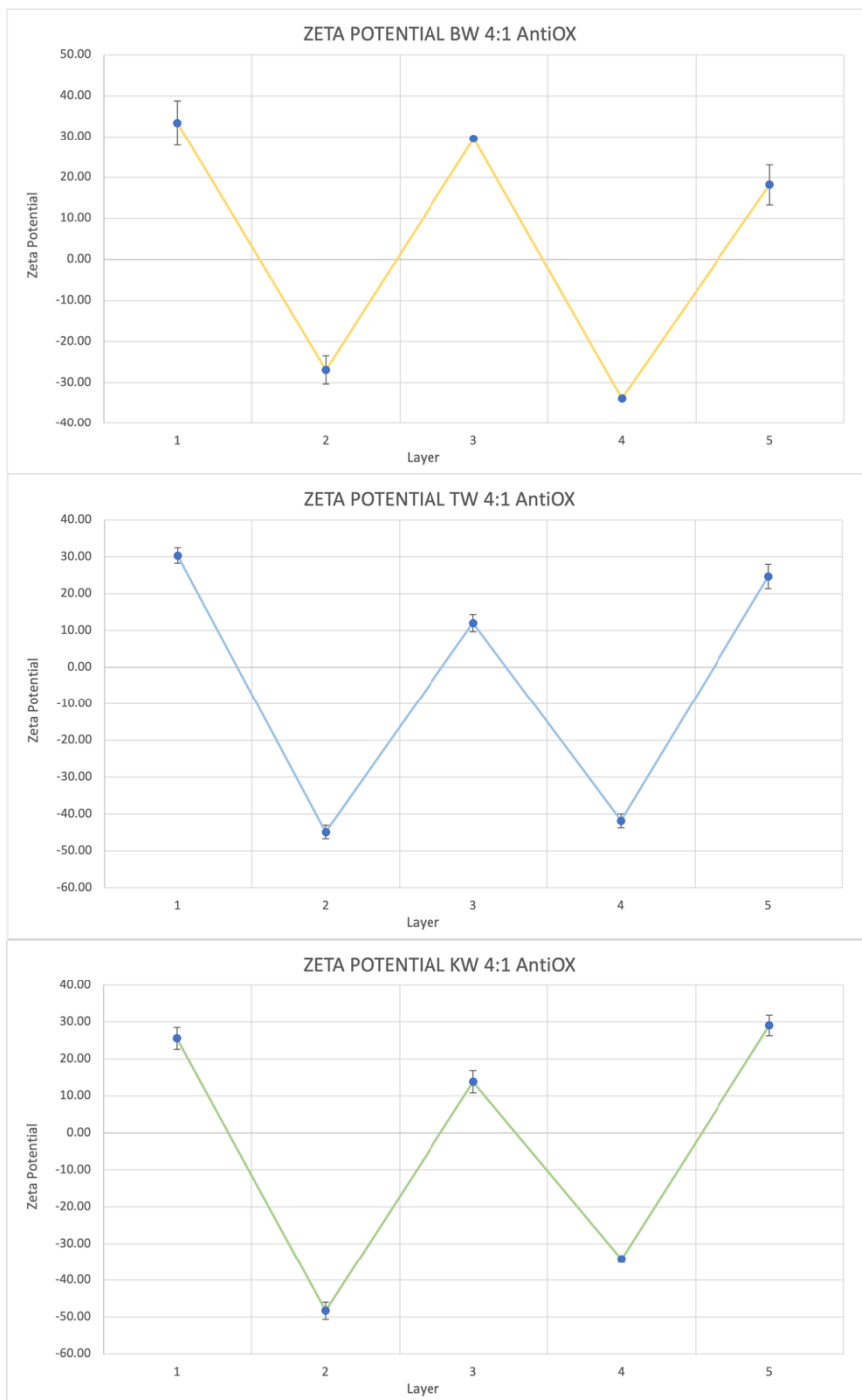


Figure 31: ζ -potential evaluation of LbL Chitosan/Pectin-AntiOX (4:1 concentration)

For the second tested concentration (antioxidant 10:1 pectin) the zeta-potential values of each layer were:

1. Layer-by-Layer with Bladder Wrack (BW) antioxidant extract:

- I. 32 mV \pm 12.59 mV
- II. -54.50 mV \pm 5.55 mV
- III. 9.78 mV \pm 3.96mV
- IV. -35.27 mV \pm 2.97 mV
- V. 22.85 mV \pm 2.78 mV

2. Layer-by-Layer with Knotted Wrack (KW) antioxidant extract

- I. 34.10 mV \pm 3.82 mV
- II. -36.77 mV \pm 4.20 mV
- III. 13.40 mV \pm 0.61 mV
- IV. -34.27 mV \pm 0.91 mV
- V. 7.14 mV \pm 1.80 mV

3. Layer-by-Layer with Toothed Wrack (TW) antioxidant extract

- I. 35.83 mV \pm 2.80 mV
- II. -51.87 mV \pm 10.46 mV
- III. 12.06 mV \pm 4.95 mV
- IV. -36.50 mV \pm 4.91 mV
- V. 4.83 mV \pm 4.04 mV

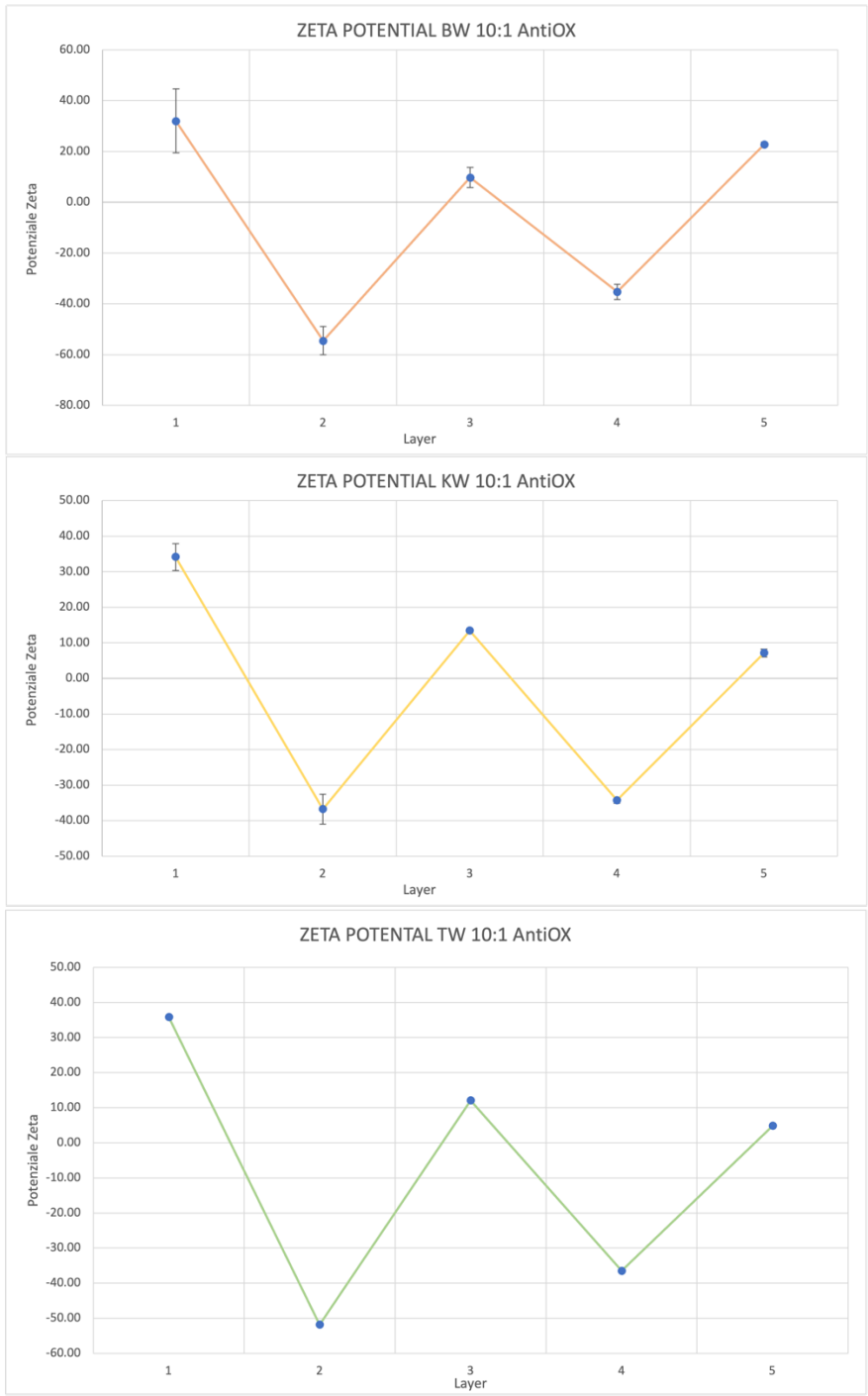


Figure 32: ζ -potential evaluation LbL Chitosan/Pectin-AntiOX (10:1 concentration)

4.3.1 FTIR-ATR

FTIR-ATR analyses were performed on MNPs at different stages of layer deposition to ensure the proper execution of the LbL technique. Moreover, one analysis on a control system where the antioxidant was not added to the pectin solution was conducted.

For the MNPs spectrum, the most prominent peaks are strongly dependent from the synthesis method, the size, and the shape of the nanoparticle, and in this case the most relevant, as it is possible to see in *Figure 33*, were:

- The stretching vibration of the Si-O bond in the region of 1000 -1200 cm^{-1}
- The peaks at 3000 cm^{-1} were assigned to the stretching and bending vibration of hydroxyl and water.
- Additional peaks in the range of 500-800 cm^{-1} corresponding to the bending and stretching modes of the Si-OH bonds on the surface of the mesoporous silica nanoparticles, in particular symmetric stretching and bending vibration of Si-O-Si.
- The bond in the range of 950-1100 cm^{-1} corresponding to asymmetric stretching of Si-O-Si and symmetric stretching of Si-OH.
- The two peaks between 1300-1600 cm^{-1} could be assigned to the C-H bending vibrations

From this figure it is possible to see how the functionalization of the MNPs with alternating layers of chitosan and pectin changes the IR spectrum, making the two peaks at 1554 and 1394 cm^{-1} almost disappear, smoothing the peak at 641 cm^{-1} and creating a new peak around 3000 and 3600 cm^{-1} which could be attributed to the O-H vibration and C-H stretching of the chitosan and the pectin. Moreover, the peak around 1620 cm^{-1} is related to C=O stretching vibration of the chitosan amide carbonyl group, and to the stretching of the pectin C-O bond.

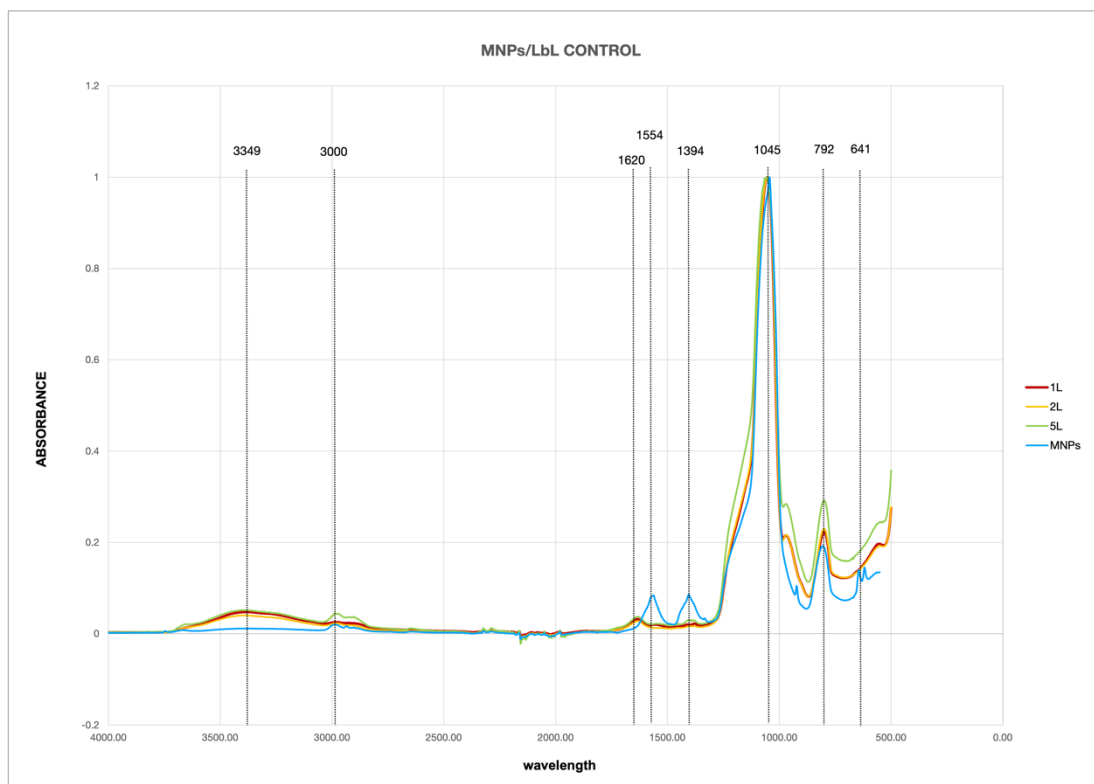


Figure 33: FTIR spectrum of MNPs and LbL control (1, 2 and 5 layers)

The FTIR-ATR analysis was conducted on the MNPs systems obtained adding the antioxidant extract from the seaweeds and the results are shown in Figure 34. MNPs seaweed spectra shows a peak around 1200 cm^{-1} and between $900\text{-}600\text{ cm}^{-1}$ which confirm the presence of seaweed extract.

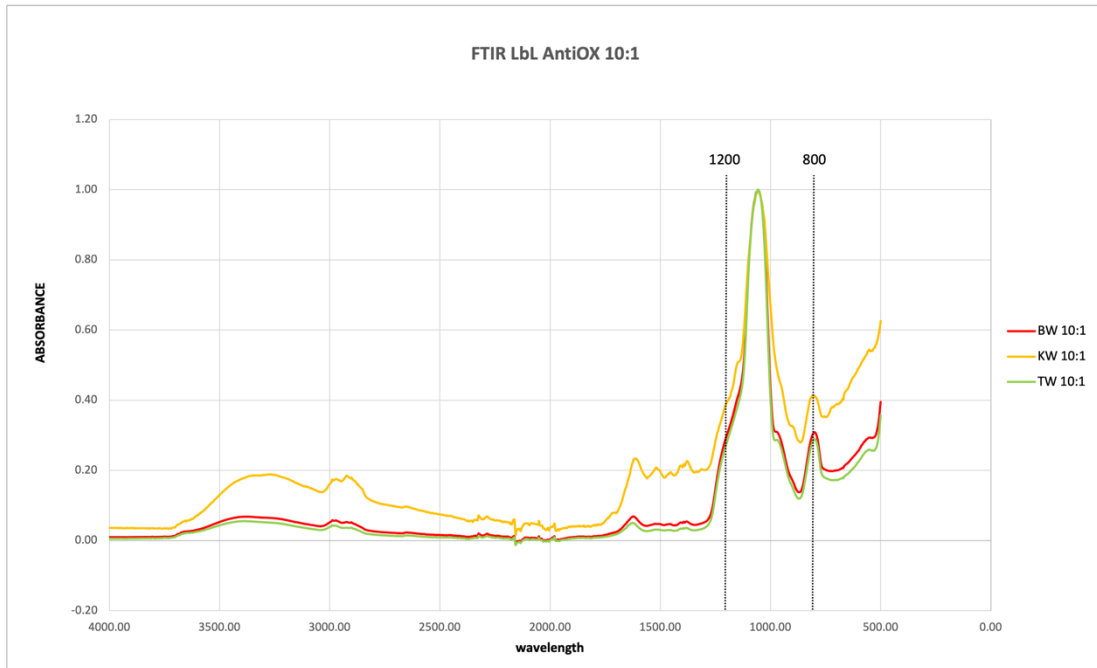
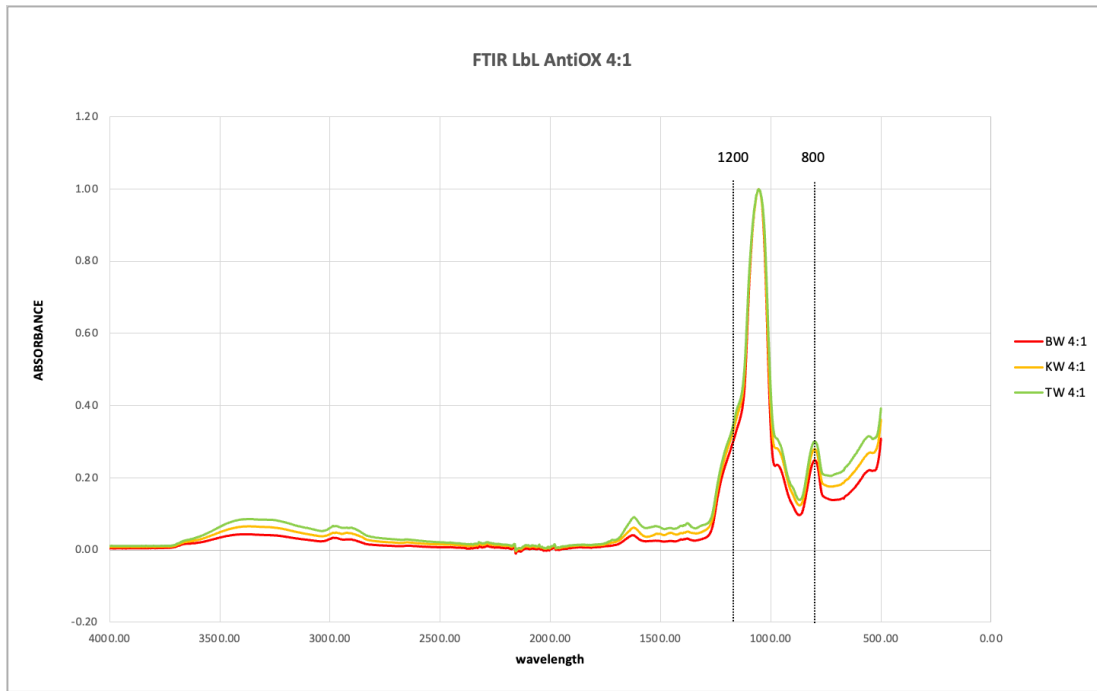


Figure 34: FTIR spectrum of LbL with antioxidant extracts of both concentration of BW, KW and TW

4.3.2 XPS

The X-ray Photoelectron Spectroscopy (XPS) analysis was performed to precisely determine the elemental composition on the surface of the biomaterials. Various samples were analysed and compared with XPS readings to validate the composition of these structures obtained by FTIR-ATR. In *Figure 35* it is represented the MNPs control sample XPS reading which reveals a prominent signal at approximately 103 electron volts (eV), which can be attributed to the Si2p signal, providing strong evidence of the existence of silica in the system. Additionally, there are distinct peaks at around 285 eV and 533 eV in both samples, which correspond to carbon and oxygen, respectively.

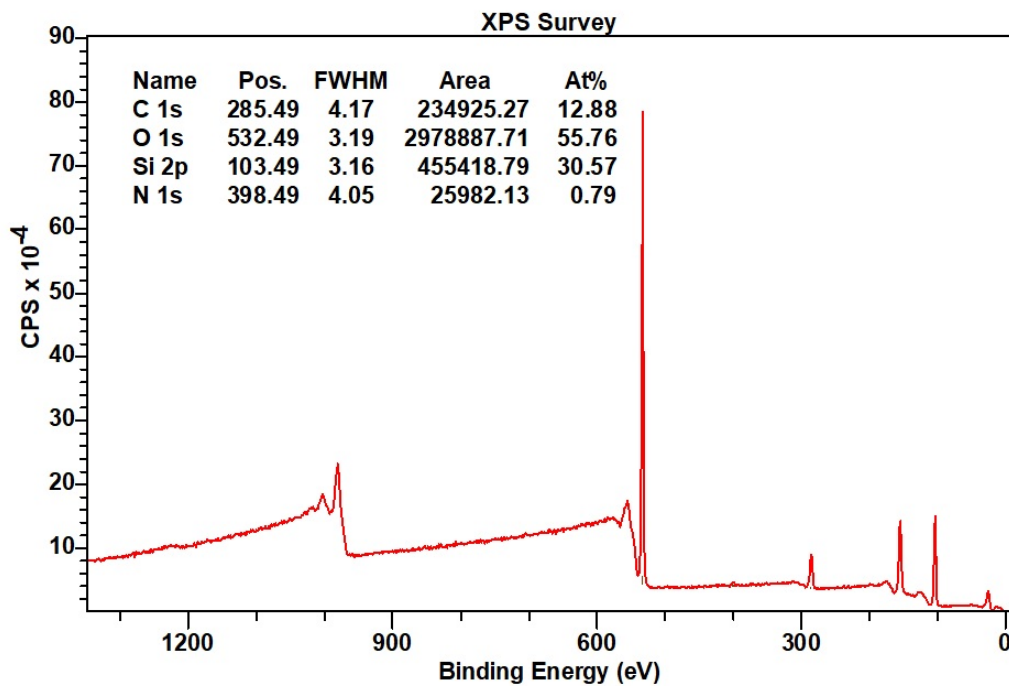


Figure 35: XPS spectra of MNPs control system

In this case, as shown in *Figure 36*, when analyzing the C1s peak, the presence of both C-C and C-O peaks further substantiates the presence of pectin in the functionalized system. Furthermore, in the XPS spectra of the MNPs control system, a noticeable N1s peak emerges at approximately 400 eV, affirming the presence of chitosan.

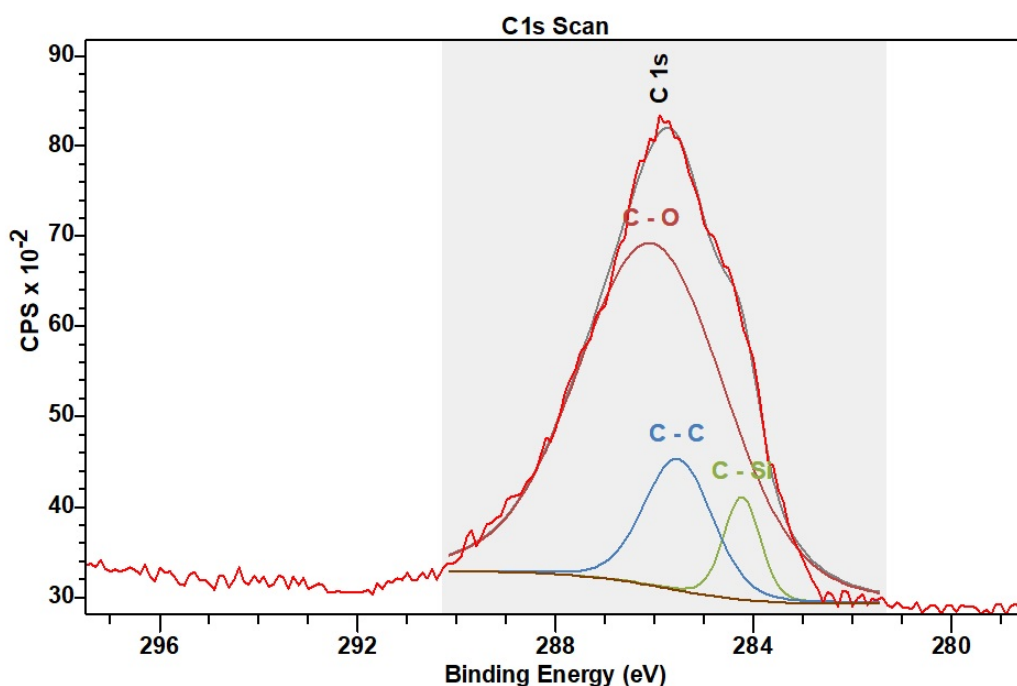


Figure 36: XPS spectra of deconvoluted C1s peak of MNPs control system

Moreover, XPS was employed to analyze MNPs derived from seaweed extracts: two different samples with two different concentration of antioxidant extracts were analysed (4:1 concentration and 10:1 concentration). The results, presented in *Figure 37*, reveal almost identical spectra for both samples. Specifically, peaks corresponding to O1s, C1s, N1s, and Si2p are observed at approximately 533 eV, 286 eV, 400 eV, and 103 eV, respectively, which corroborates the findings obtained from Fourier-Transform Infrared Attenuated Total Reflectance (FTIR-ATR) analysis.

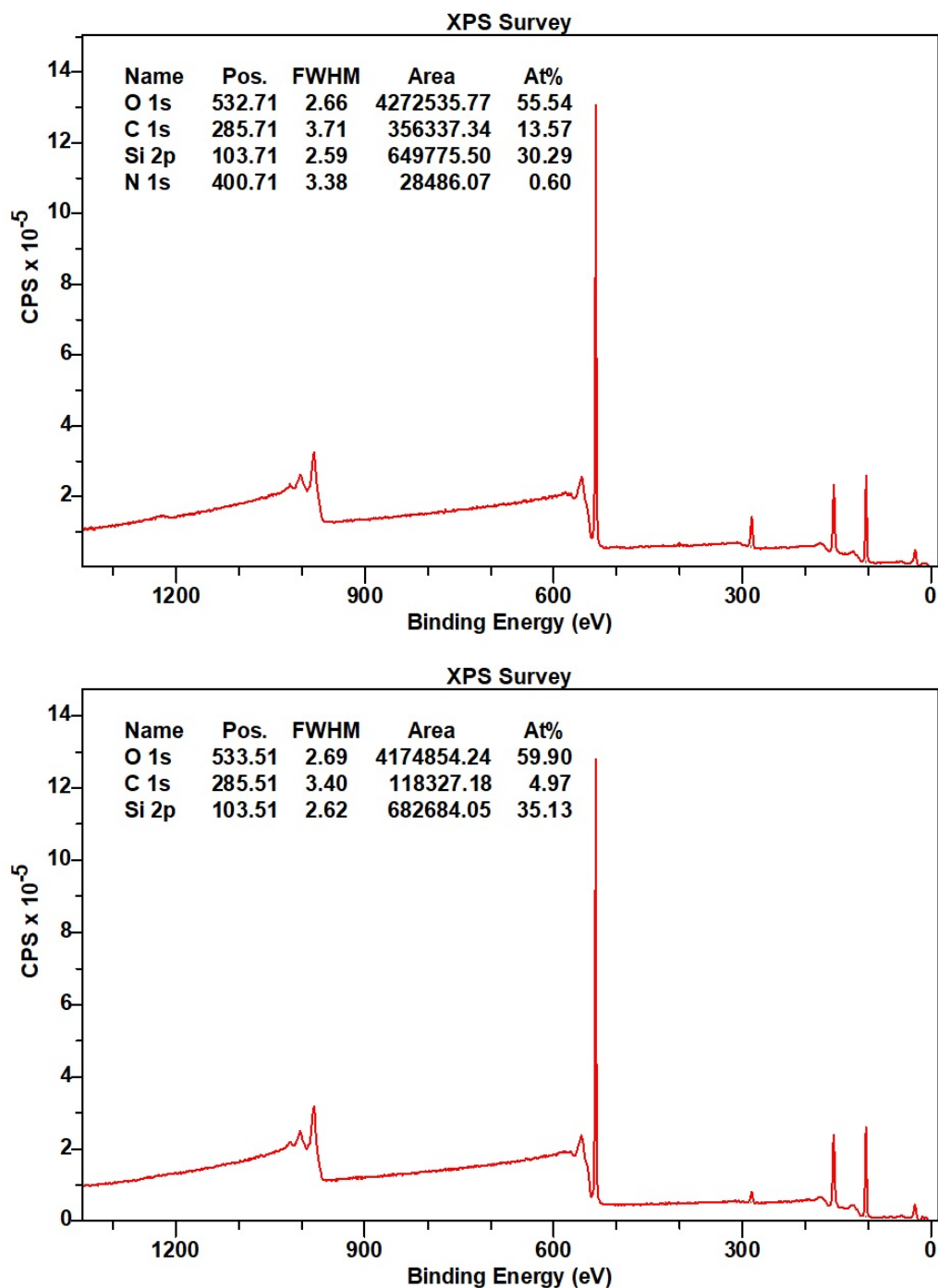


Figure 37: XPS spectra of functionalized MNPs with TW seaweed extract: a) 4:1 concentration b) 10:1 concentration

With a particular focus on the C1s peak, in both samples, the presence of C-C and C-O peaks further validates the presence of both pectin and antioxidant extracts within the functionalized system, as presented in *Figure 38*.

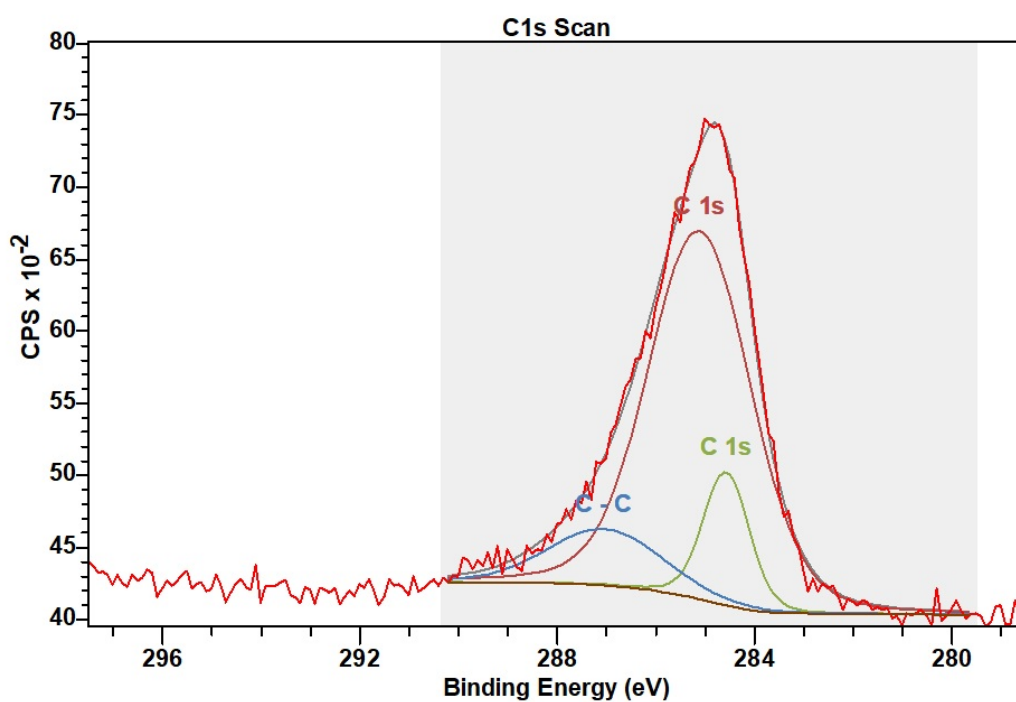
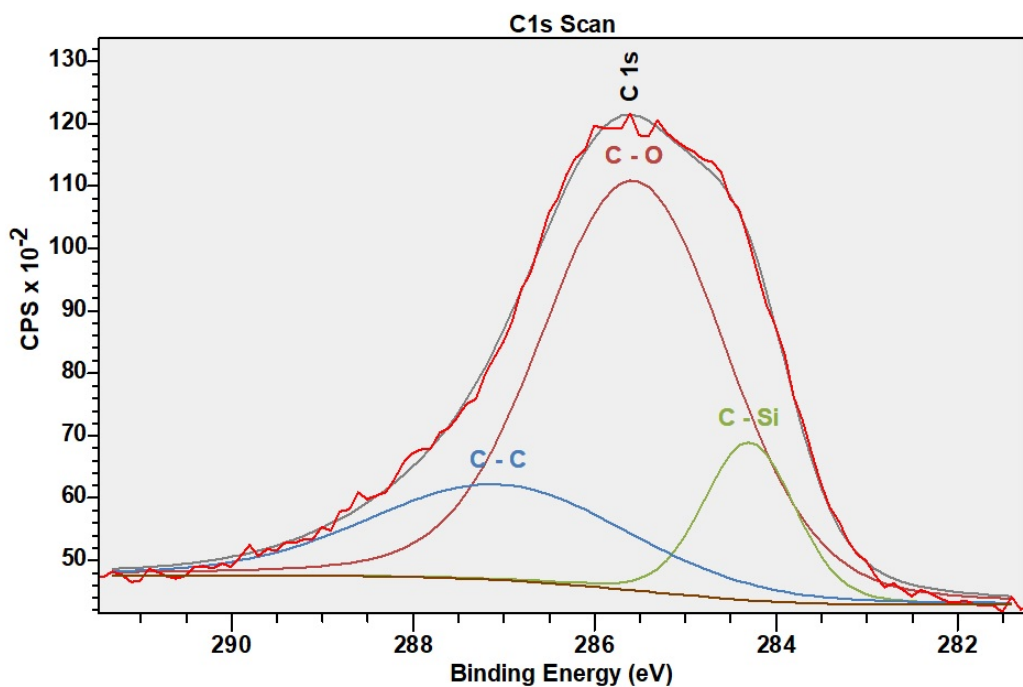


Figure 38: XPS spectra of deconvoluted C1s peak of functionalized MNPs

From these images it is possible to see the atom percentage for all samples, which is basically the same both for the control and the functionalized system. There is a slight difference in the percentage of the C1s atom between the functionalized MNPs system with 4:1 concentration of seaweed extract and

the 10:1 concentrated system, in which this percentage is a bit lower, compensated by the percentage of O 1s atom which is slightly higher. The percentage of the 4:1 concentrated system is more similar to the control system than to the 10:1 concentrated system, due probably to the fact that the lower concentration of antioxidant extract into the system has a little influence on the properties of the MNPs.

4.3.3 FOLIN-CIOCALTEU METHOD

In *Table 9* it is possible to see the total phenolic content evaluation of the MNPs. The results show that the MNPs encapsulating the BW seaweed antioxidant extract have the highest total phenolic content, while the other two samples show a similar value of TPC. It is also possible to evaluate the difference between the two concentrations of antioxidant extract put into the MNPs (4:1 concentration and 10:1 concentration): as expected, in all samples the total phenolic content is higher for the most concentrated solution.

Table 9: TPC content

CONC	BW	KW	TW
4:1	0.556 GAE	0.184 GAE	0.189 GAE
10:1	0.768 GAE	0.589 GAE	0.469 GAE

4.3.4 TRANSMISSION ELECTRON MICROSCOPE (TEM)

High-resolution TEM images performed on nanoparticles purchased from sigma and functionalized MNPs after five layer deposition for both concentration of antioxidant extracts are reported in *Figure 35* and *Figure 36*. Results confirm that spherical shape is preserved after LbL deposition and show an increase in functionalized nanoparticles average diameter compared to silica one. The average diameter before the functionalization was around 254.25 nm, while after the functionalization it increased around 270.2 nm, as expected considering the five layers added to the nanoparticles.

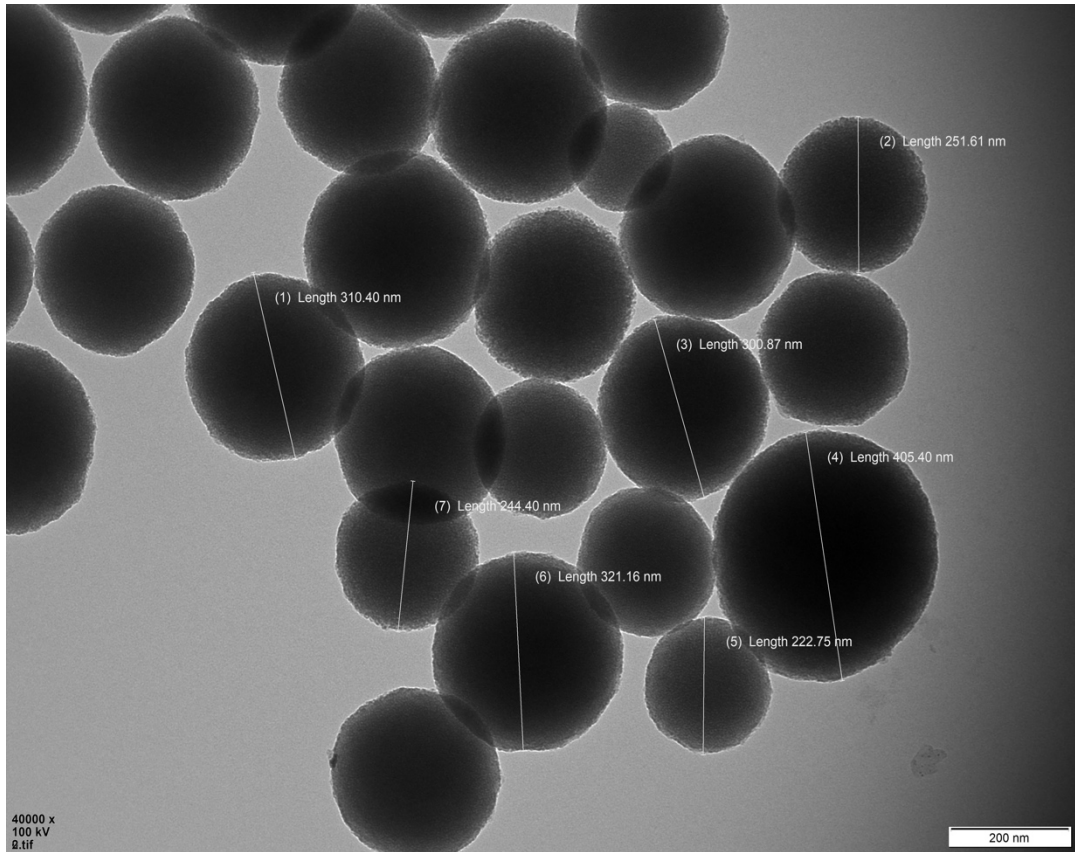


Figure 39: TEM analysis for morphological characterization of MNPs

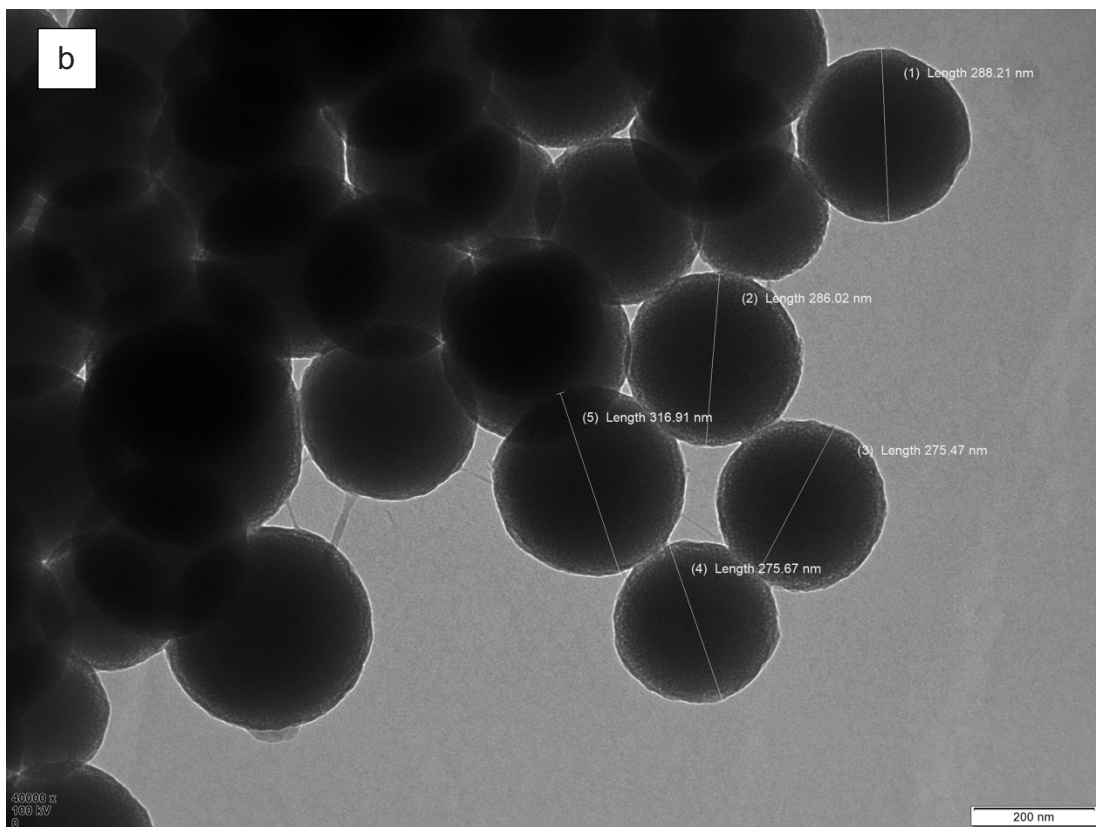
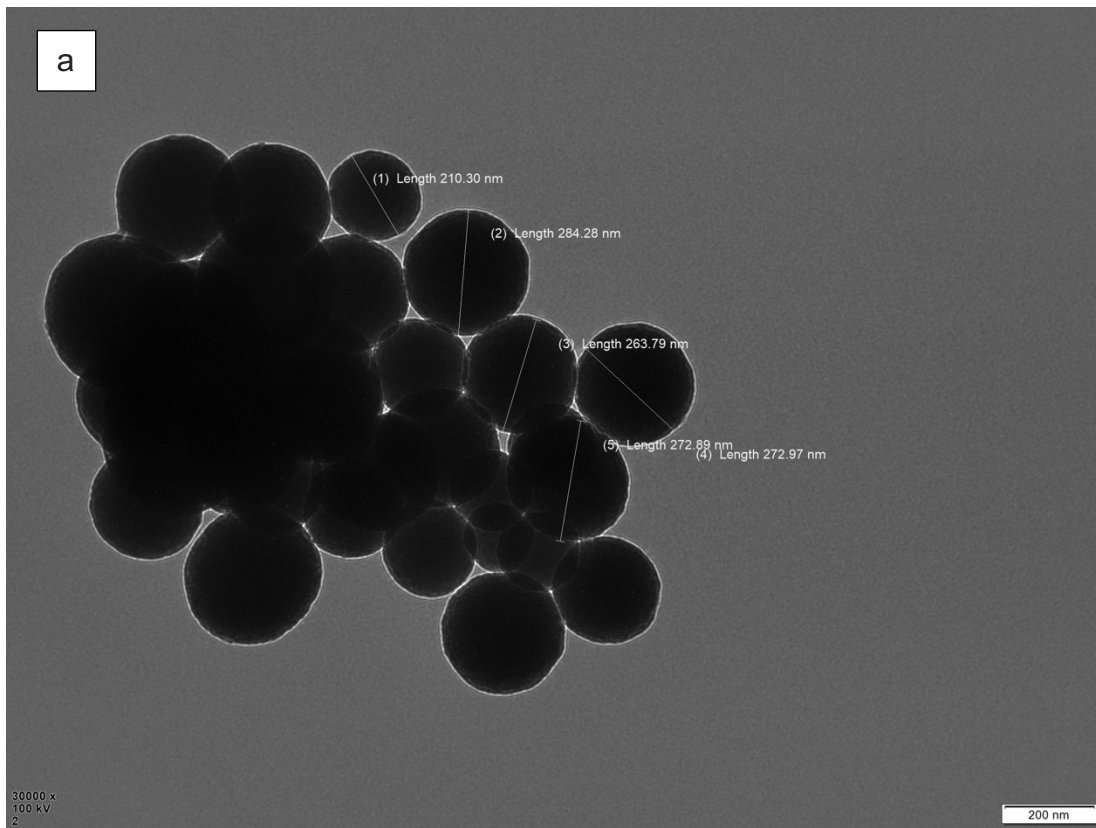


Figure 40: TEM analysis for characterization of functionalized MNPs with LbL for both concentration:
 a) 4:1 concentration b) 10:1 concentration

4.4 CELL CULTURE

4.4.1 PRESTO BLUE ASSAY

PrestoBlue assay was performed to assess the metabolic activity of cells following treatment with various concentrations of antioxidant extracts (2, 5, 12.5, 25, 50, 100 mg/mL). After 48 hours of incubation, metabolic activity was measured by recording the fluorescence values of the PrestoBlue solution and then normalized these values by comparing them to the negative control, which consisted of fibroblasts cultured in DMEM. The results of this experiment are presented in *Figure 41*. The findings indicate that, generally, lower sample concentrations led to greater fibroblast viability, regardless of the specific engineered systems being examined. The only sample that has a different behavior is the Sea Spaghetti (SS) which shows the lowest cell viability for all concentrations except for the 25 mg/mL that has a viability so much higher than the control. Except for this one, all other samples show a viability around 100% for the two lowest concentrations (2 and 5 mg/mL) that decrease a little bit increasing the concentration of antioxidant extracts. Particularly, exposing fibroblast cells to the highest concentrated antioxidant extracts solutions led to the lowest cell metabolic activity, hovering at around 80%.

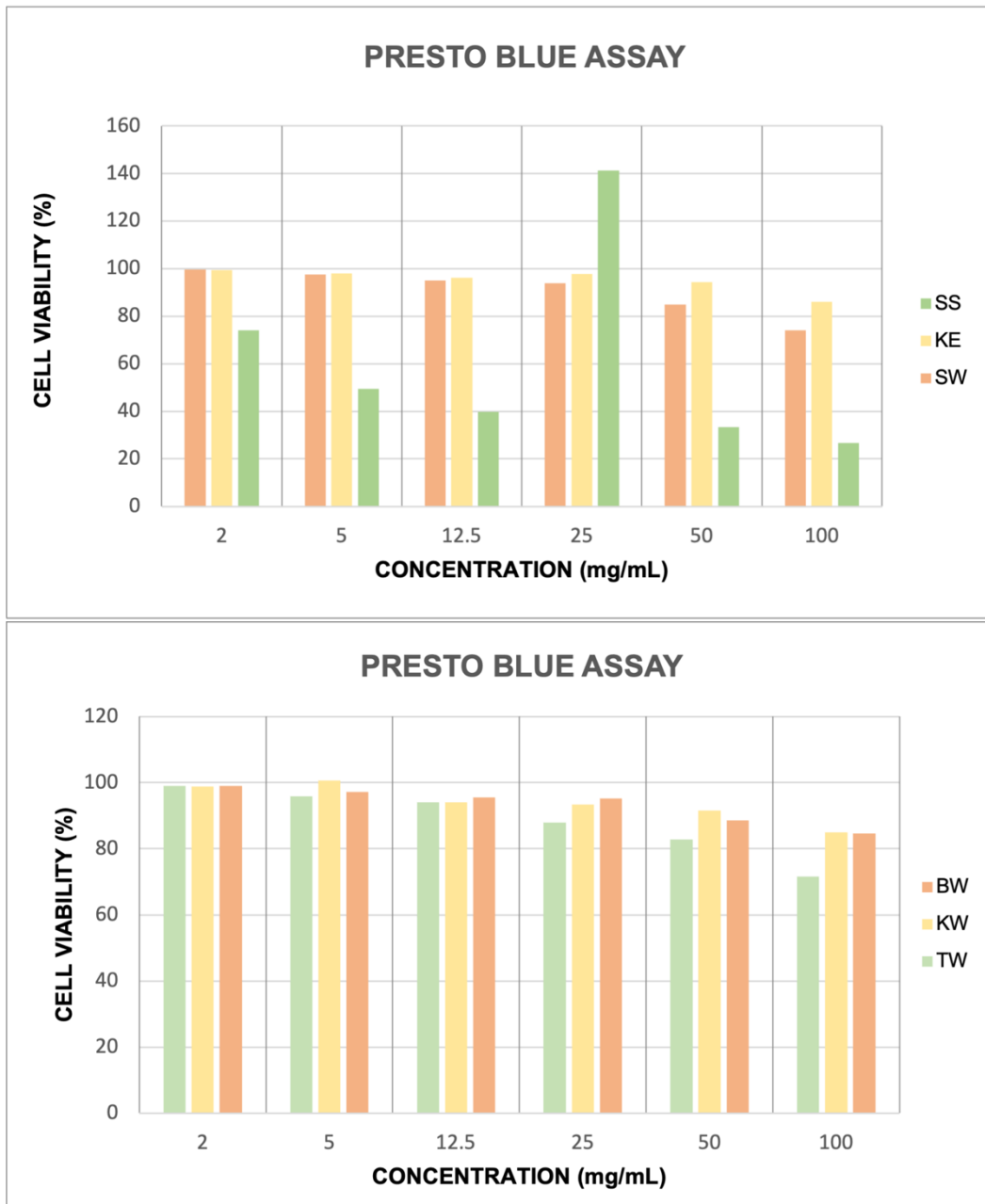


Figure 41: Cell viability results obtained incubating fibroblasts with different concentrations of antioxidant extracts: a) SS, KE, SW b) BW, KW, TW

Numerous studies have confirmed that after the treatment with the antioxidant, the cell viability remains mostly untouched. Serena Mirata et al. analysed the cell viability of L929 fibroblasts after being incubated with four different *E. amantacea* extracts resulting in a good perspective on their biocompatibility given that neither of the four extracts showed significant cytotoxicity on this cell line⁹¹. This could be considered in line with the results obtained especially with

the three seaweed extracts that have been encapsulated into the layer-by-layer, the BW, the KW and the TW.

4.4.2 LIVE/DEAD ASSAY

The LIVE/DEAD assay on cells was conducted within a two-dimensional model to assess cell viability at various concentrations of antioxidant extract (2, 5, 12.5, 25, 50, 100 mg/mL). The fibroblasts that received no treatment were used as the control group. All samples were incubated for a period of 48 hours of time. The results of this experiment are depicted in *Figure 42*. In this figure it is possible to see live and dead images of fibroblast cells after 48 hours of incubation without any treatment, showing that the cells have proliferated during this time.

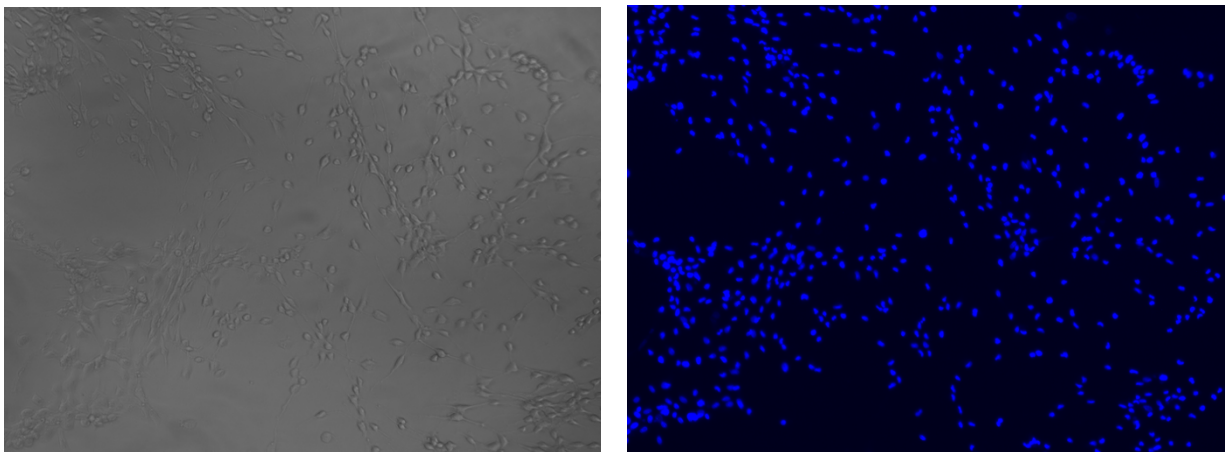


Figure 42: LIVE/DEAD assay conducted on fibroblasts without any treatment

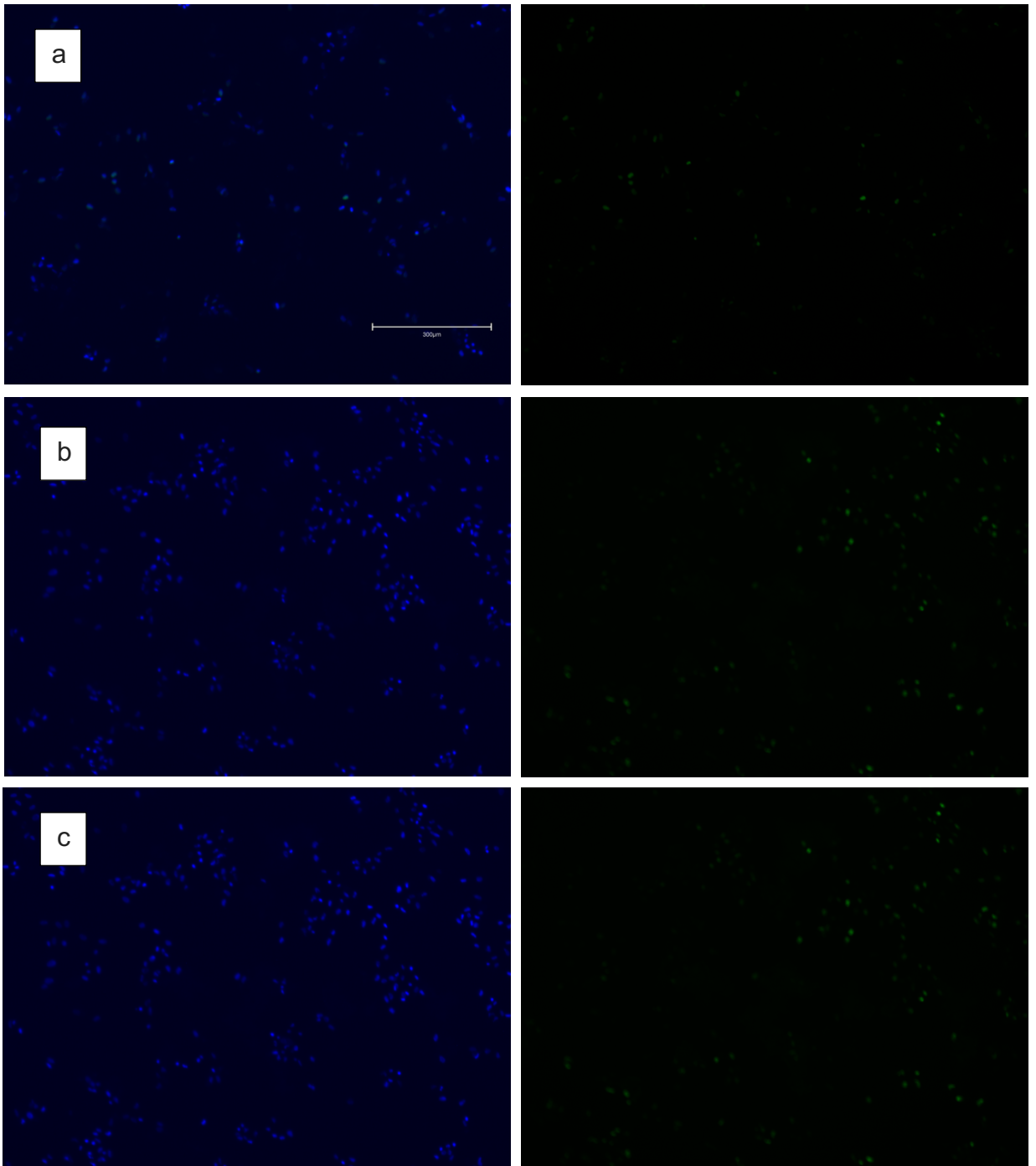
The three different type of seaweed extract were incubated at various concentration, and the results are shown in *Figure 43*, *Figure 44* and *Figure 45*, comparing living cells (stained blue) and dead cells (stained green).

Cell death was observed in all samples, but the numbers were inconsistent, particularly when compared to the number of viable cells. This inconsistency suggests that the apoptotic activity of all of the three seaweed extract was low. Considering the cell count, it appeared that they remained relatively stable across all tested concentrations, with only minor variations in the highest

concentration sample. Specifically, the highest concentration of antioxidant extract resulted in a slightly lower number of cells.

Comparing the three different seaweed it is possible to see that the Bladder Wrack and the Knotted Wrack have a more similar trend than the Toothed Wrack, which shows a higher apoptotic activity already at 25 mg/mL that increases with the concentration.

1. Bladder Wrack (BW):



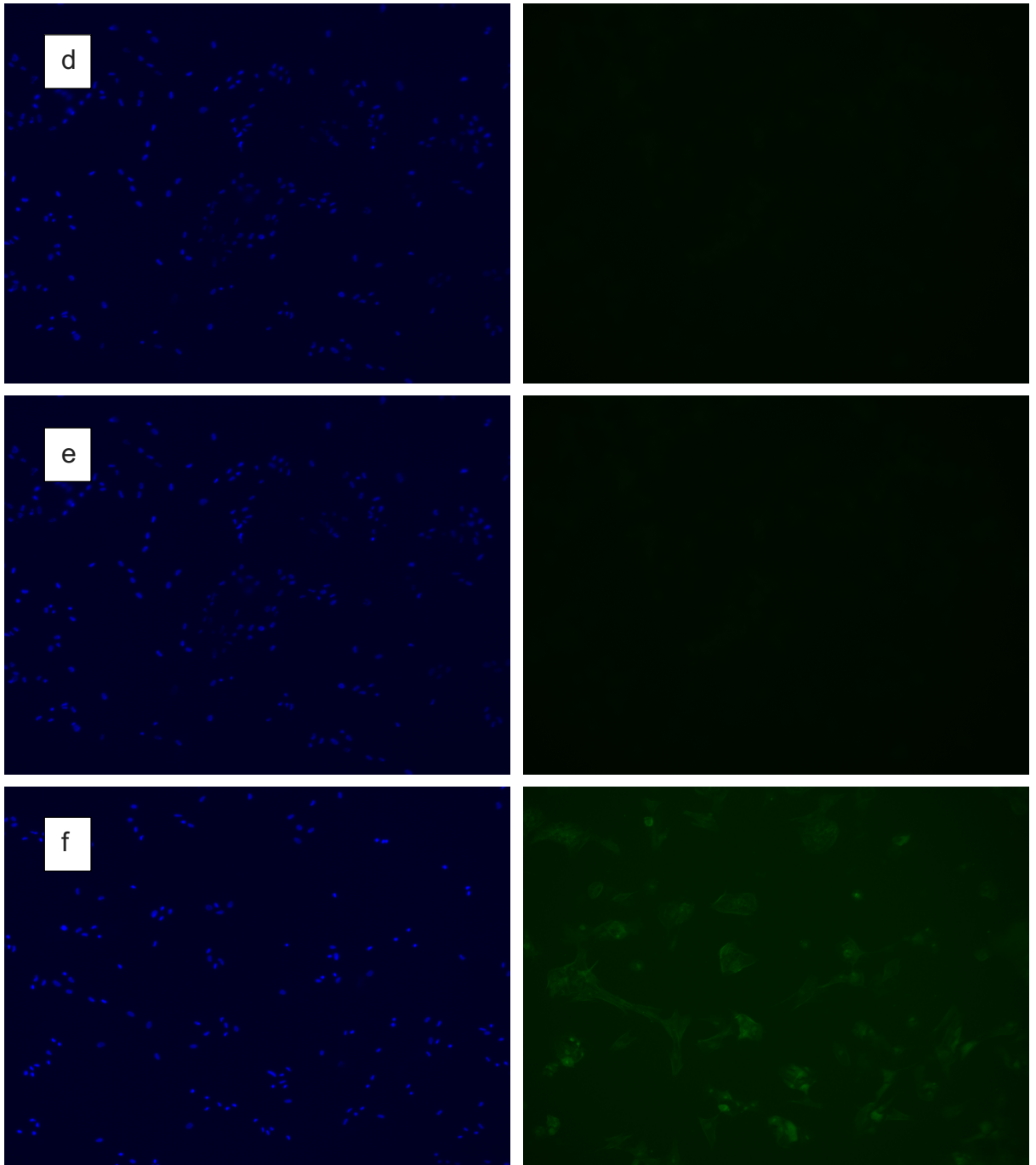
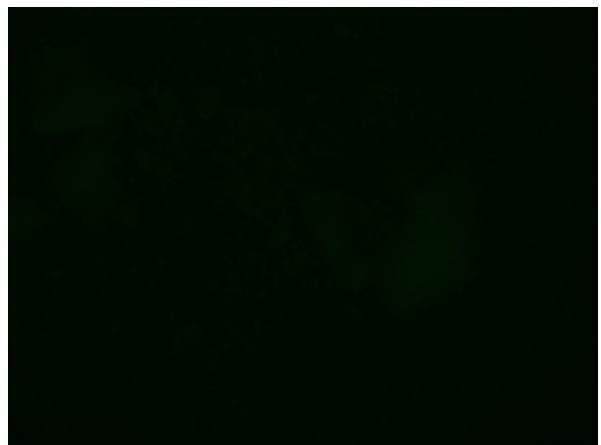
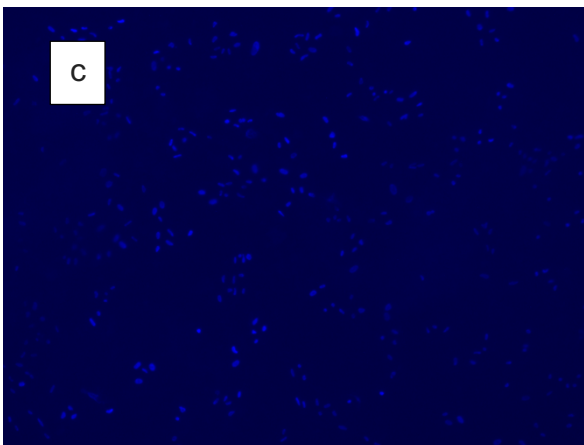
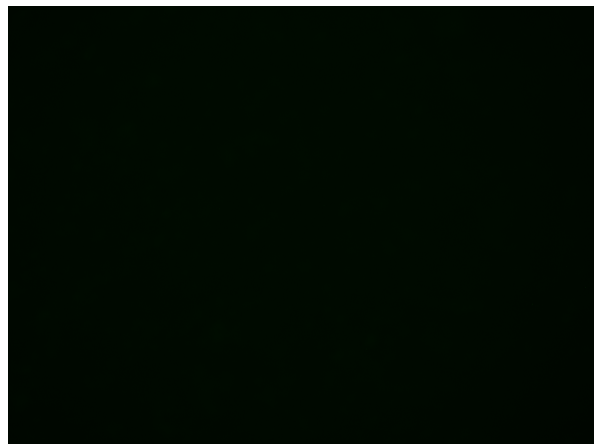
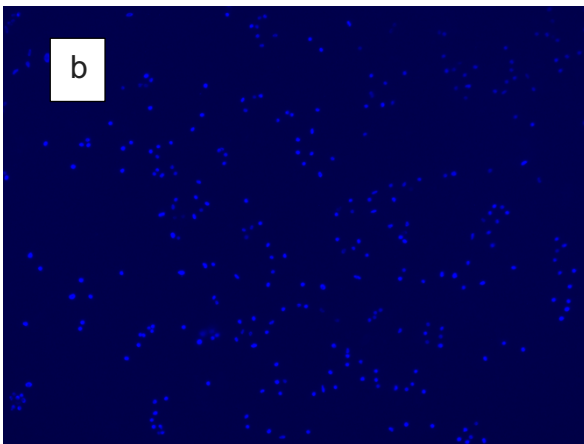
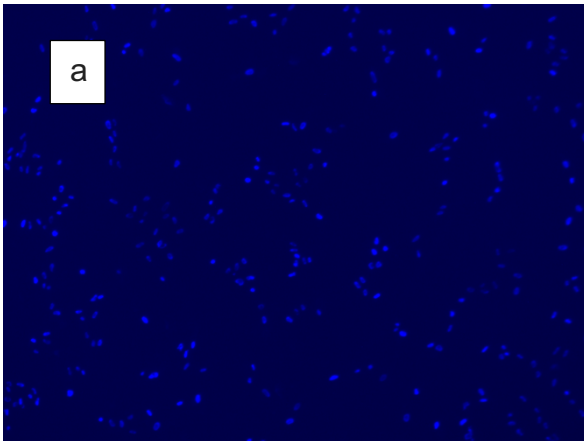


Figure 43: Live/Dead assay results obtained incubating fibroblasts with Bladder Wrack (BW) antioxidant extracts at different concentrations: a) 2mg/mL b) 5 mg/mL c) 12.5 mg/mL d) 25 mg/mL e) 50 mg/mL f) 100 mg/mL.

2. Knotted Wrack (KW):



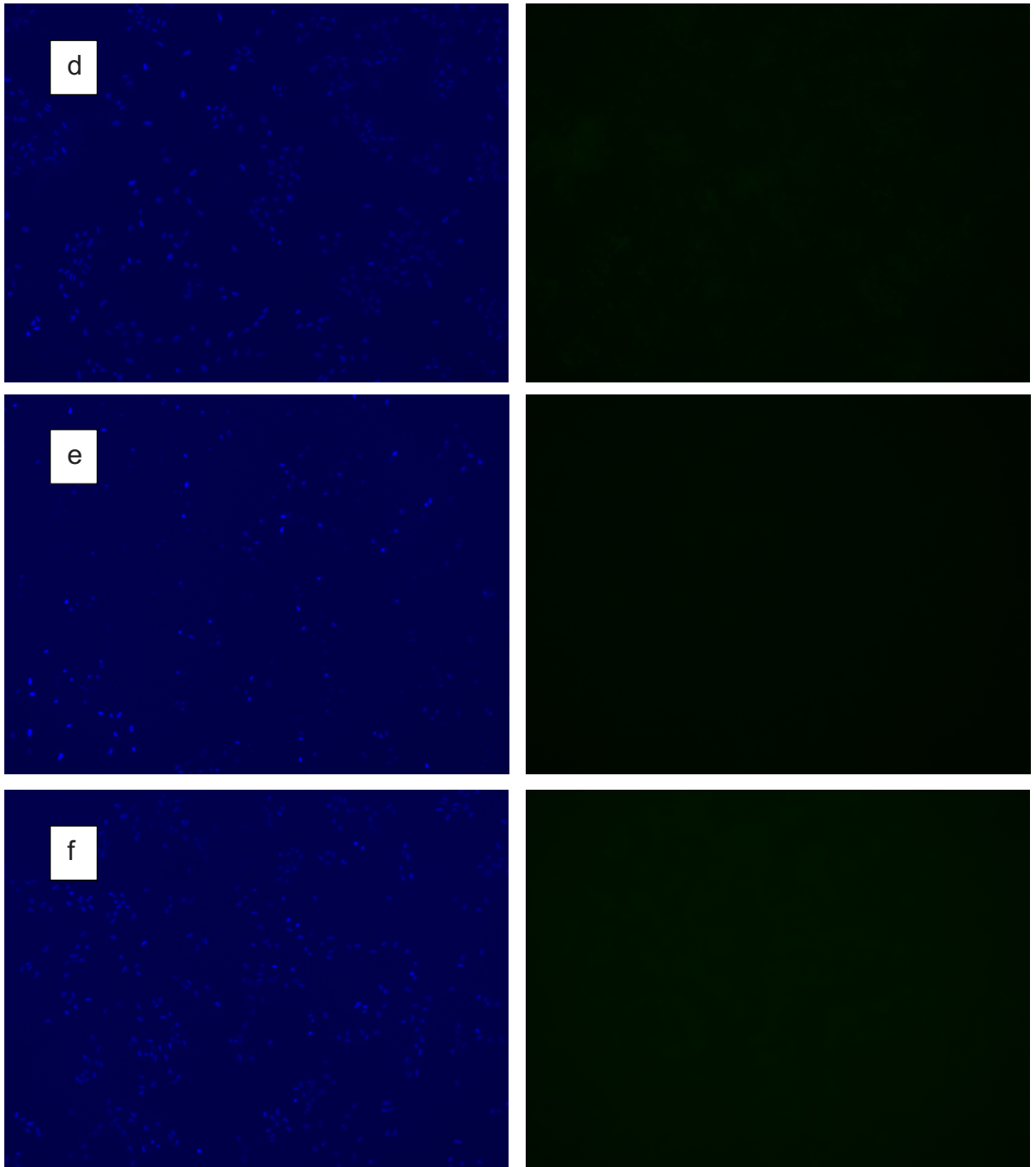
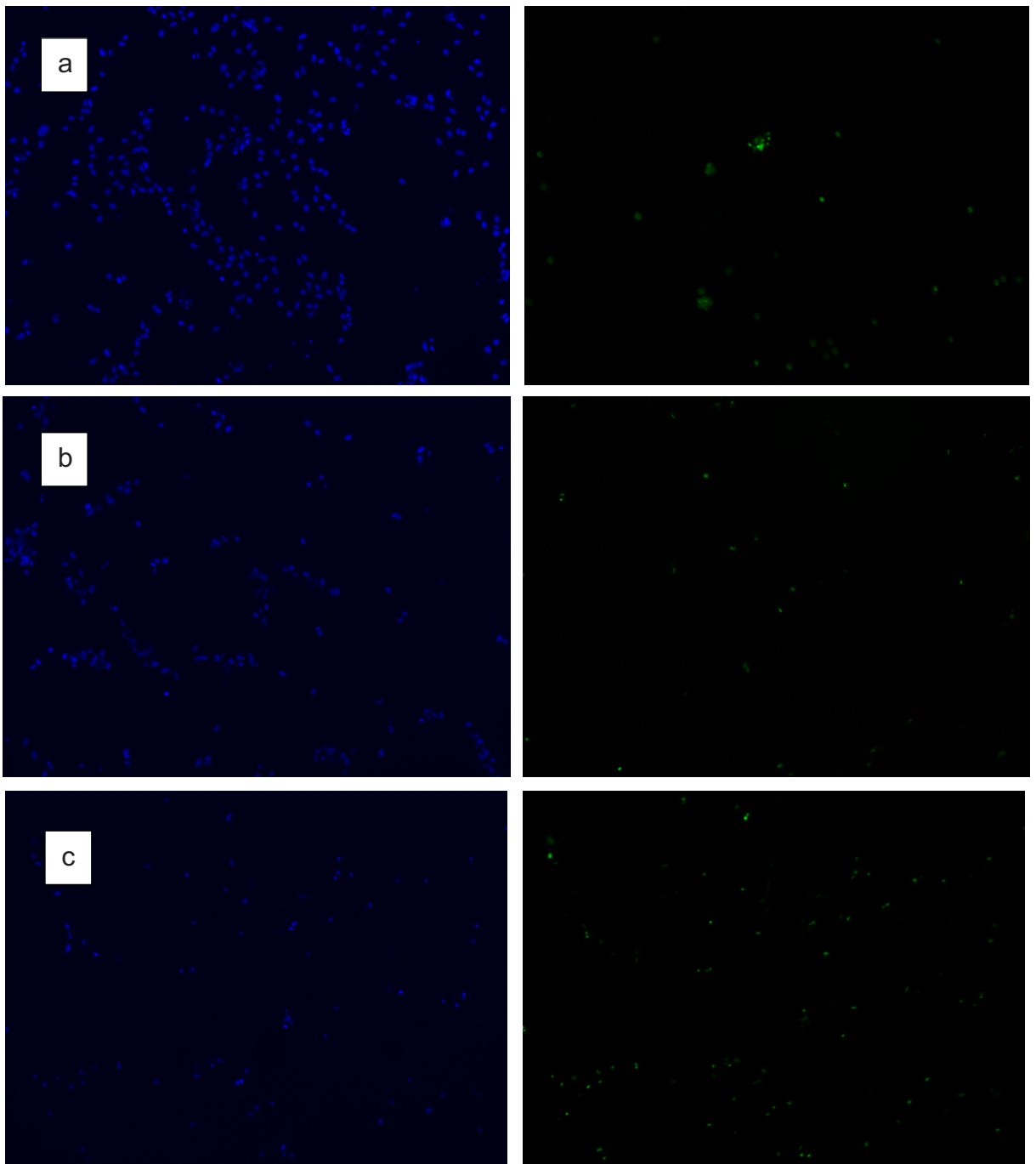


Figure 44: Live/Dead assay results obtained incubating fibroblasts with Knotted Wrack (KW) antioxidant extracts at different concentrations: a) 2mg/mL b) 5 mg/mL c) 12.5 mg/mL d) 25 mg/mL e) 50 mg/mL f) 100 mg/mL.

3. Toothed Wrack (TW)



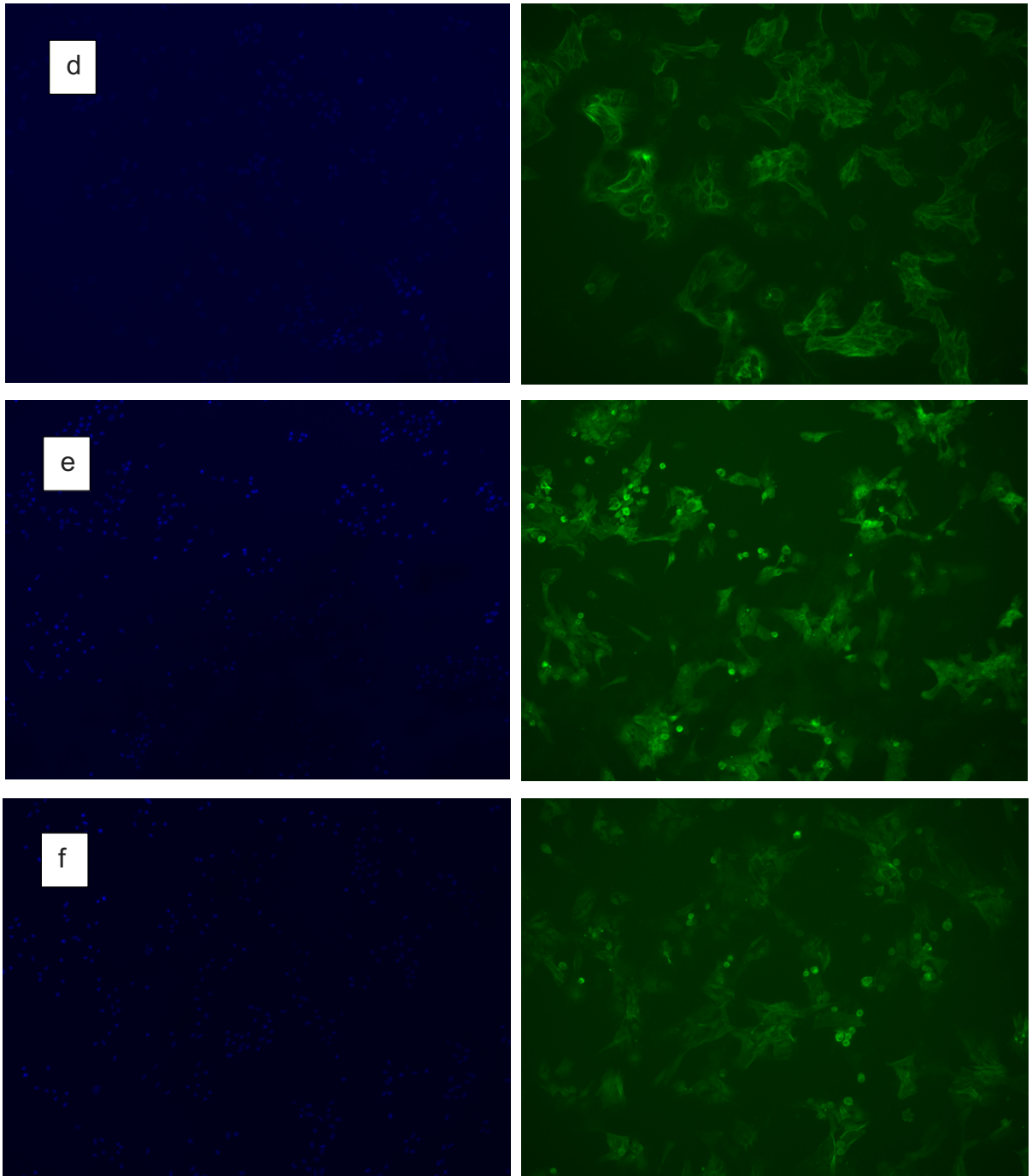


Figure 45: Live/Dead assay results obtained incubating fibroblasts with Toothed Wrack (TW) antioxidant extracts at different concentrations: a) 2mg/mL b) 5 mg/mL c) 12.5 mg/mL d) 25 mg/mL e) 50 mg/mL f) 100 mg/mL

These results can be considered reliable, according to Dina Rodrigues et al. which evaluated the cytotoxicity of the extract of *Sargassum muticum* and *Osmundea pinnatifida* on fibroblasts, observing no cytotoxicity against these cells, making these seaweed extracts very interesting functional ingredients, which could be explored as a food ingredient (salt replacer, nutrient vector) or nutraceutical supplement⁹². Another study carried on by Gina de La Fuente et

al. confirmed that the brown alga *Cystoseira amentacea* antioxidant extract wasn't cytotoxic for the fibroblasts. Particularly, the results showed that the ethanolic extract never affected the cell viability at all concentrations tested. The ethanolic extract also showed a slight cell number increase at 10 and 50 µg/mL concentration indicating that this extract may be safely used in humans⁹³.

The other three seaweed extract Live/Dead results are shown in the *Appendix*.

4.5 BACTERIAL TEST

4.5.1 KLEBSIELLA PNEUMONIA

From *Table 10*, it is possible to evaluate the Minimum Inhibitory Concentration (MIC) and the Minimum Bactericidal Concentration (MBC) for each type of seaweed antioxidant extract for the *Klebsiella Pneumonia* bacteria strain. The results show that for the BW and the KW the MIC is obtained at the lowest concentration of 12.5 mg/mL, for the TW, the SS and the SW at 25 mg/mL, while for the KE it is obtained at the highest concentration of 100 mg/mL. On the other hand, the MBC is obtained at 12.5 mg/mL for the BW antioxidant extract, at 25 mg/mL for the KW, the SW and the TW, at 50 mg/mL for the SS and again at the highest concentration of 100 mg/mL for the KE, showing that this seaweed has the lowest antibacterial power.

SEAWEED	[MIC]	[MBC]
BW	12.5	12.5
KW	12.5	25
TW	25	25
KE	100	100
SS	25	50
SW	25	25

Table 10: MIC and MBC evaluation for each seaweed type for Klebsiella Pneumonia

4.5.2 STAPHYLOCOCCUS AUREUS

For this *Staphylococcus Aureus* strain the results are a little bit different: from *Table 11*, it is possible to see that both the MIC and the MBC are obtained at a lower concentration than for the *Klebsiella Pneumonia*: particularly the MIC is obtained at 1.25 mg/mL for the BW, at 2.5 mg/mL for the KW, at 5 mg/mL for the TW and the KE, at 12.5 mg/mL for the SW and at 25 mg/mL for the SS, while the MBC is obtained at the same concentrations except for the KE which is higher at 12.5 mg/mL. This shows a slightly stronger antibacterial effect of the studied antioxidant extracts on the *Staphylococcus Aureus* than on the *Klebsiella Pneumonia*.

SEAWEED	[MIC]	[MBC]
BW	1.25	1.25
KW	2.5	2.5
TW	5	5
KE	5	12.5
SS	25	25
SW	12.5	12.5

Table 11: MIC and MBC evaluation for each seaweed type for Staphylococcus Aureus

Some researchers, who have examined the chemical composition of antioxidant extracts have found that, depending on the solvent used, they are rich in flavonoids; terpenes; terpenoids; phenols; bibenzyls; and sterols. These compounds are known to exert an antibacterial activity⁹⁴. Another study shows that the ethanol extract of *Sargassum* sp. possesses a strong antimicrobial activity against both gram-positive, as well as gram-negative, bacteria when compared with Ampicillin as standard⁹⁵. Moreover, Natália Cmíková, Lucia Galovicová et al. demonstrated that the seaweed kombu extract exhibited high antimicrobial activity on Gram- positive G+ bacteria, *Enterococcus faecalis*, producing an inhibition zone of 8 ± 1 mm, which can be considered as a strong

antimicrobial activity. On another G+ bacteria, *Bacillus subtilis*, the kombu extract had a moderate effect (5.33 ± 0.58 mm). On all bacteria-, the extract had weak activity where inhibition zones were formed from 2.67 ± 0.58 to 4.00 ± 1.00 mm⁹⁶. These findings confirmed the results previously obtained, showing the antibacterial properties of the seaweed extract.

5 CONCLUSIONS

In this work it is validated the already existing ultrasound-assisted extraction method to recover antioxidant compounds from seaweeds, which can serve as valuable reservoirs of natural antioxidants with the potential for extraction using different solvents, leading to a more environmentally friendly process.

The ultrasound-assisted process was fine-tuned, yielding well-established predictive extraction model for all the different type of seaweed.

The optimal combination of extraction parameters for the three chosen seaweed type included a temperature around 19°C for the BW and the KW and of 30°C for the TW, an extraction time of 15 minutes for the BW and the TW with a ratio of 20 mg/mL for both, whereas for the KW it involved an extraction time around 29 minutes with a ratio of 18,48 mg/mL.

The TPC was the highest for BW (16.21 mg/mL), decreasing for the KW (6.99 mg/mL) and for the TW (5.11 mg/mL), affirming the overall high quality of the extracts. The BW extract showed also superior antioxidant activity in the FRAP assay (187.56 mg/mL) follow by the TW extract (171.28 mg/mL) and the KW extract (121.67 mg/mL). finally, all the three seaweed extract displayed a strong negative charge, respectively of -27.3 mV, -28 mV and -33.3 mV for the BW, KW and TW when subjected to Dynamic Light Scattering (DLS) analysis. Furthermore, the extracted compounds from seaweed were incorporated into the Layer-by-Layer technique to produce silica mesoporous nanoparticles with antioxidant properties. Based on the ζ -potential values of the extracts, the seaweed extract solutions were integrated into the pectin polyanion solution, which was then combined with chitosan in the layering process. Transmission electron microscopy (TEM) images verified that the initial spherical shape of the nanoparticles remained unchanged throughout the deposition process, with a slight increase in the diameter of functionalized nanoparticles compared to pure silica nanoparticles. The seaweed antioxidant extracts showed a high biocompatibility with fibroblasts, especially at low concentration, and also a good antibacterial property both for *Staphylococcus Aureus* and *Klebsiella Pneumonia* already at low concentration.

6 FUTURE DEVELOPMENTS

To further characterize the manufactured functionalized silica nanoparticles, all cellular tests should be conducted also with the nanoparticles encapsulating the antioxidant extract, and it would also be interesting to perform a deeper study of their behaviour in the PTSD context, using a neuronal cell line.

Another possibility could be using micro-RNA to better target and inhibit the expression of some pro-inflammatory markers. Particularly, for the PTSD, it was found that a single nucleotide polymorphism in the FKBP5 gene increase the expression of the FKBP51 protein and have been associated with increased risk for neuropsychiatric disorders such as major depression and post-traumatic stress disorder. Moreover, it was also found that miR-511 robustly affected downstream protein levels of FKBP51, targeting FKBP5 and regulating neuronal differentiation⁸⁹. So, it could be interesting to evaluate the release and the action of the miR-511 once they are encapsulated into the layers of the manufactured nanoparticles. On the other hand, it was found that in case of infection or injury, the action potentials originating from the vagus nerve regulate T cells, which produce acetylcholine (ACh) that inhibits the production of pro-inflammatory cytokines. The transmembrane receptors for ACh (AChR) can be muscarinic AChR (mAChR) or nicotinic AChR (nAChR): one of the most abundant nAChR is $\alpha 7$ nAChR which is expressed in epithelial and endothelial cells, and it is essential for the cholinergic anti-inflammatory action. It was found that miR-124 is highly induced by $\alpha 7$ nAChR activation and it mediates the cholinergic anti-inflammatory action by inhibiting lipopolysaccharide (LPS)-induced production of pro-inflammatory cytokines⁹⁰. Moreover, the cytotoxicity could also be reduced by fine-tuning the deposition process. This might involve increasing the number of layers or harnessing the positive functional groups of chitosan. Additionally, it's worth exploring different concentrations of the polycation solution. Looking ahead, another interesting avenue for research could involve evaluating the simultaneous release of anti-inflammatory agents. This could include not only pharmaceutical drugs but also natural compounds like curcumin, which has the potential to enhance the natural antioxidant activity at sites of inflammation.

BIBLIOGRAPHY

1. Bisson JI, Olf M. Prevention and treatment of PTSD: the current evidence base. *Eur J Psychotraumatol.* 2021;12(1). doi:10.1080/20008198.2020.1824381
2. Posttraumatic Stress Disorder and Mild Brain Injury Controversies, Causes and Consequences Enhanced Reader.
3. Wang Z, Young MRI. PTSD, a disorder with an immunological component. *Front Immunol.* 2016;7(JUN):219. doi:10.3389/FIMMU.2016.00219/BIBTEX
4. Lindqvist D, Dhabhar FS, Mellon SH, et al. Increased pro-inflammatory milieu in combat related PTSD – A new cohort replication study. *Brain Behav Immun.* 2017;59:260-264. doi:10.1016/J.BBI.2016.09.012
5. Hoge CW, Castro CA, Messer SC, et al. Combat Duty in Iraq and Afghanistan, Mental Health Problems, and Barriers to Care. <https://doi.org/10.1056/NEJMoa040603>. 2004;351(1):13-22. doi:10.1056/NEJMoa040603
6. Bruenig D, Mehta D, Morris CP, et al. Genetic and serum biomarker evidence for a relationship between TNF α and PTSD in Vietnam war combat veterans. *Compr Psychiatry.* 2017;74:125-133. doi:10.1016/J.COMPPSYCH.2017.01.015
7. Kim TD, Lee S, Yoon S. Inflammation in Post-Traumatic Stress Disorder (PTSD): A Review of Potential Correlates of PTSD with a Neurological Perspective. *Antioxidants* 2020, Vol 9, Page 107. 2020;9(2):107. doi:10.3390/ANTIOX9020107
8. Malan S, Hemmings S, Kidd M, Martin L, Seedat S. Investigation of telomere length and psychological stress in rape victims. *Depress Anxiety.* 2011;28(12):1081-1085. doi:10.1002/DA.20903
9. Mellon SH, Gautam A, Hammamieh R, Jett M, Wolkowitz OM. Metabolism, Metabolomics, and Inflammation in Posttraumatic Stress Disorder. *Biol Psychiatry.* 2018;83(10):866-875. doi:10.1016/J.BIOPSYCH.2018.02.007

10. Pharmacotherapy for Post-traumatic Stress Disorder in Combat Veterans.
11. O'Donovan A, Cohen BE, Seal KH, et al. Elevated risk for autoimmune disorders in Iraq and Afghanistan veterans with posttraumatic stress disorder. *Biol Psychiatry*. 2015;77(4):365-374. doi:10.1016/J.BIOPSYCH.2014.06.015
12. O'Donovan A, Sun B, Cole S, et al. Transcriptional Control of Monocyte Gene Expression in Post-Traumatic Stress Disorder. *Dis Markers*. 2011;30(2-3):123. doi:10.3233/DMA-2011-0768
13. Gola H, Engler H, Sommershof A, et al. Posttraumatic stress disorder is associated with an enhanced spontaneous production of pro-inflammatory cytokines by peripheral blood mononuclear cells. Published online 2013. Accessed April 28, 2023. <http://www.biomedcentral.com/1471-244X/13/40>
14. Neylan TC, Sun B, Rempel H, et al. Suppressed monocyte gene expression profile in men versus women with PTSD. *Brain Behav Immun*. 2011;25(3):524-531. doi:10.1016/j.bbi.2010.12.001
15. ISSN 0100-879X. doi:10.1590/S0100-879X2012007500041
16. Wohleb ES, Powell ND, Godbout JP, Sheridan JF. Stress-induced recruitment of bone marrow-derived monocytes to the brain promotes anxiety-like behavior. *J Neurosci*. 2013;33(34):13820-13833. doi:10.1523/JNEUROSCI.1671-13.2013
17. O'Donovan A, Sun B, Cole S, et al. Transcriptional control of monocyte gene expression in post-traumatic stress disorder. *Dis Markers*. 2011;30(2-3):123-132. doi:10.3233/DMA-2011-0768
18. Michopoulos V, Powers A, Gillespie CF, Ressler KJ, Jovanovic T. Inflammation in Fear- and Anxiety-Based Disorders: PTSD, GAD, and Beyond. *Neuropsychopharmacology*. 2017;42(1):254-270. doi:10.1038/NPP.2016.146
19. Katrinli S, S Oliveira NC, Felger JC, Michopoulos V, Smith AK. The role of the immune system in posttraumatic stress disorder. doi:10.1038/s41398-022-02094-7

20. Ahmed-Leitao F, Spies G, van den Heuvel L, Seedat S. Hippocampal and amygdala volumes in adults with posttraumatic stress disorder secondary to childhood abuse or maltreatment: A systematic review. *Psychiatry Res Neuroimaging*. 2016;256:33-43. doi:10.1016/J.PSCYCHRESNS.2016.09.008
21. D'Autréaux B, Toledano MB. ROS as signalling molecules: mechanisms that generate specificity in ROS homeostasis. *Nature Reviews Molecular Cell Biology* 2007 8:10. 2007;8(10):813-824. doi:10.1038/nrm2256
22. Sena LA, Chandel NS. Physiological Roles of Mitochondrial Reactive Oxygen Species. *Mol Cell*. 2012;48(2):158-167. doi:10.1016/J.MOLCEL.2012.09.025
23. Kirtonia A, Sethi G, Garg M. The multifaceted role of reactive oxygen species in tumorigenesis. *Cellular and Molecular Life Sciences*. 2020;77(22):4459-4483. doi:10.1007/S00018-020-03536-5/FIGURES/9
24. Olf M. Sex and gender differences in post-traumatic stress disorder: an update. <https://doi.org/10.1080/2000819820171351204>. 2017;8(sup4):4. doi:10.1080/20008198.2017.1351204
25. Ravi M, Stevens JS, Michopoulos V. Neuroendocrine pathways underlying risk and resilience to PTSD in women. *Front Neuroendocrinol*. 2019;55:100790. doi:10.1016/J.YFRNE.2019.100790
26. Oyola MG, Handa RJ. Hypothalamic–pituitary–adrenal and hypothalamic–pituitary–gonadal axes: sex differences in regulation of stress responsivity. <https://doi.org/10.1080/1025389020171369523>. 2017;20(5):476-494. doi:10.1080/10253890.2017.1369523
27. Birkeland MS, Blix I, Solberg Ø, Heir T. Gender differences in posttraumatic stress symptoms after a terrorist attack: A network approach. *Front Psychol*. 2017;8(DEC). doi:10.3389/FPSYG.2017.02091/FULL
28. Asmundson GJG, Thorisdottir AS, Roden-Foreman JW, et al. A meta-analytic review of cognitive processing therapy for adults with posttraumatic stress disorder. *Cogn Behav Ther*. 2019;48(1):1-14. doi:10.1080/16506073.2018.1522371

29. Krediet E, Bostoën T, Breeksema J, van Schagen A, Passie T, Vermetten E. Reviewing the Potential of Psychedelics for the Treatment of PTSD. *International Journal of Neuropsychopharmacology*. 2020;23(6):385-400. doi:10.1093/ijnp/pyaa018
30. Smith R, Russo J, Fiegel J, Brogden N. antibiotics Antibiotic Delivery Strategies to Treat Skin Infections When Innate Antimicrobial Defense Fails. doi:10.3390/antibiotics9020056
31. Ibrahim AAE, Bagherani N, Smoller B, Bagherani N, Reyes-Barron C. Anatomy and Organization of Human Skin. In: *Atlas of Dermatology, Dermatopathology and Venereology*. Springer International Publishing; 2022:109-132. doi:10.1007/978-3-319-53811-2_3
32. Kolarsick PA, Ann Kolarsick M, Goodwin C. *Anatomy and Physiology of the Skin.*; 2006.
33. Aleemardani M, Trikić MZ, Green NH, Claeysens F. The importance of mimicking dermal-epidermal junction for skin tissue engineering: A review. *Bioengineering*. 2021;8(11). doi:10.3390/bioengineering8110148
34. Kendall AC, Nicolaou A. Bioactive lipid mediators in skin inflammation and immunity. *Prog Lipid Res*. 2013;52(1):141-164. doi:10.1016/J.PLIPRES.2012.10.003
35. Abdo JM, Sopko NA, Milner SM. The applied anatomy of human skin: A model for regeneration. *Wound Medicine*. 2020;28. doi:10.1016/j.wndm.2020.100179
36. Bangert C, Brunner PM, Stingl G. Immune functions of the skin. *Clin Dermatol*. 2011;29(4):360-376. doi:10.1016/j.clindermatol.2011.01.006
37. DeBenedictis C, Joubert S, Zhang G, Barria M, Ghohestani RF. *Immune Functions of the Skin.*; 2001.
38. Bacterial Skin and Soft Tissue Infections in Adults A Review of Their Epidemiology, Pathogenesis, Diagnosis, Treatment and Site Of Care.
39. Dryden MS. Skin and soft tissue infection: microbiology and epidemiology. *Int J Antimicrob Agents*. 2009;34(SUPPL. 1). doi:10.1016/S0924-8579(09)70541-2

40. Werner S, Grose R. Regulation of wound healing by growth factors and cytokines. *Physiol Rev.* 2003;83(3):835-870. doi:10.1152/PHYSREV.2003.83.3.835/ASSET/IMAGES/LARGE/9J0330256105.JPEG
41. Portou MJ, Baker D, Abraham D, Tsui J. The innate immune system, toll-like receptors and dermal wound healing: A review. *Vascul Pharmacol.* 2015;71:31-36. doi:10.1016/j.vph.2015.02.007
42. Sharma A, Pócsi I, Weindl G, Pfalzgraff A, Brandenburg K. Antimicrobial Peptides and Their Therapeutic Potential for Bacterial Skin Infections and Wounds. *Frontiers in Pharmacology* | www.frontiersin.org. 2018;1:281. doi:10.3389/fphar.2018.00281
43. Antonio J, Quaresma S. Organization of the Skin Immune System and Compartmentalized Immune Responses in Infectious Diseases. Published online 2019. doi:10.1128/CMR
44. Antonio J, Quaresma S. Organization of the Skin Immune System and Compartmentalized Immune Responses in Infectious Diseases. Published online 2019. doi:10.1128/CMR
45. Nestle FO, Di Meglio P, Qin JZ, Nickoloff BJ. Skin immune sentinels in health and disease. *Nat Rev Immunol.* 2009;9(10):679-691. doi:10.1038/nri2622
46. Reddy KVR, Yedery RD, Aranha C. Antimicrobial peptides: Premises and promises. *Int J Antimicrob Agents.* 2004;24(6):536-547. doi:10.1016/j.ijantimicag.2004.09.005
47. Luo Y, Song Y. Mechanism of antimicrobial peptides: Antimicrobial, anti-inflammatory and antibiofilm activities. *Int J Mol Sci.* 2021;22(21). doi:10.3390/ijms222111401
48. Nasir A, Gaspari A. The skin immune system. *Nanotechnology in Dermatology.* 2013;9781461450344:133-144. doi:10.1007/978-1-4614-5034-4_13/FIGURES/00133
49. Imada K, Leonard WJ. *The Jak-STAT Pathway.* www.elsevier.com/locate/molimm
50. Gonçalves-de-Albuquerque S da C, Pessoa-e-Silva R, Trajano-Silva LAM, et al. The equivocal role of Th17 cells and neutrophils on

- immunopathogenesis of leishmaniasis. *Front Immunol.* 2017;8(OCT). doi:10.3389/fimmu.2017.01437
51. Marrazzo P, O'leary C. Repositioning Natural Antioxidants for Therapeutic Applications in Tissue Engineering. *Bioengineering* 2020, Vol 7, Page 104. 2020;7(3):104. doi:10.3390/BIOENGINEERING7030104
 52. Polyphenols as natural antioxidants in cosmetics applications | Enhanced Reader.
 53. Oroian M, Escriche I. Antioxidants: Characterization, natural sources, extraction and analysis. *Food Res Int.* 2015;74:10-36. doi:10.1016/J.FOODRES.2015.04.018
 54. Abramovič H. Antioxidant Properties of Hydroxycinnamic Acid Derivatives: A Focus on Biochemistry, Physicochemical Parameters, Reactive Species, and Biomolecular Interactions. *Coffee in Health and Disease Prevention*. Published online 2015:843-852. doi:10.1016/B978-0-12-409517-5.00093-0
 55. Spencer JPE, Abd El Mohsen MM, Minihane AM, Mathers JC. Biomarkers of the intake of dietary polyphenols: strengths, limitations and application in nutrition research. *Br J Nutr.* 2008;99(1):12-22. doi:10.1017/S0007114507798938
 56. Arct J, Pytkowska K. Flavonoids as components of biologically active cosmeceuticals. *Clin Dermatol.* 2008;26(4):347-357. doi:10.1016/J.CLINDERMATOL.2008.01.004
 57. Silveira Coelho M, de las Mercedes Salas-Mellado M. Chemical Characterization of CHIA (*Salvia hispanica L.*) for Use in Food Products. *Journal of Food and Nutrition Research.* 2014;2(5):263-269. doi:10.12691/JFNR-2-5-9
 58. Kumar Y, Tarafdar A, Badgujar PC. Seaweed as a Source of Natural Antioxidants: Therapeutic Activity and Food Applications. Published online 2021. doi:10.1155/2021/5753391
 59. Gupta S, Abu-Ghannam N. Bioactive potential and possible health effects of edible brown seaweeds. *Trends Food Sci Technol.* 2011;22(6):315-326. doi:10.1016/J.TIFS.2011.03.011

60. Thiviya P, Gamage A, Gama-Arachchige NS, Merah O, Madhujith T. Seaweeds as a Source of Functional Proteins. *Phycology* 2022, Vol 2, Pages 216-243. 2022;2(2):216-243. doi:10.3390/PHYCOLOGY2020012
61. Jacobsen C, Sørensen ADM, Holdt SL, Akoh CC, Hermund DB. Source, Extraction, Characterization, and Applications of Novel Antioxidants from Seaweed. *Annu Rev Food Sci Technol.* 2019;10:541-568. doi:10.1146/ANNUREV-FOOD-032818-121401
62. Zhong Q, Wei B, Wang S, et al. marine drugs The Antioxidant Activity of Polysaccharides Derived from Marine Organisms: An Overview. Published online 2019. doi:10.3390/md17120674
63. Zhang Q, Li N, Liu X, Zhao Z, Li Z, Xu Z. The structure of a sulfated galactan from *Porphyra haitanensis* and its in vivo antioxidant activity. *Carbohydr Res.* 2004;339(1):105-111. doi:10.1016/j.carres.2003.09.015
64. The Antioxidant Activity of Polysaccharides Derived from Marine Organisms- An Overview.
65. Li Y, Fu X, Duan D, Liu X, Xu J, Gao X. Extraction and Identification of Phlorotannins from the Brown Alga, *Sargassum fusiforme* (Harvey) Setchell. *Mar Drugs.* 2017;15(2). doi:10.3390/md15020049
66. Akoh CC, Min DB. *Food Lipids : Chemistry, Nutrition, and Biochemistry.* M. Dekker; 2002.
67. Alfio VG, Manzo C, Micillo R. From fishwaste to value: An overview of the sustainable recovery of omega-3 for food supplements. *Molecules.* 2021;26(4). doi:10.3390/molecules26041002
68. Tsubaki S, Sakamoto M, Azuma J ichi. Microwave-assisted extraction of phenolic compounds from tea residues under autohydrolytic conditions. *Food Chem.* 2010;123(4):1255-1258. doi:10.1016/j.foodchem.2010.05.088
69. Goula AM. Ultrasound-assisted extraction of pomegranate seed oil - Kinetic modeling. *J Food Eng.* 2013;117(4):492-498. doi:10.1016/j.jfoodeng.2012.10.009

70. Abramovits W, Granowski P, Arrazola P. Applications of nanomedicine in dermatology: Use of nanoparticles in various therapies and imaging. *J Cosmet Dermatol.* 2010;9(2):154-159. doi:10.1111/j.1473-2165.2010.00492.x
71. Vinardell MP, Mitjans M. Nanocarriers for delivery of antioxidants on the skin. *Cosmetics.* 2015;2(4):342-354. doi:10.3390/cosmetics2040342
72. Manzano M, Vallet-Regí M. Mesoporous Silica Nanoparticles for Drug Delivery. *Adv Funct Mater.* 2020;30(2). doi:10.1002/adfm.201902634
73. Slowing II, Vivero-Escoto JL, Trewyn BG, Lin VSY. Mesoporous silica nanoparticles: Structural design and applications. *J Mater Chem.* 2010;20(37):7924-7937. doi:10.1039/c0jm00554a
74. Irají S, Rashidi L, Ganji F. *Functionalized Mesoporous Silica Nanoparticles as a Novel Antioxidant Delivery System.* Vol 12.; 2015.
75. Huh S, Wiench JW, Trewyn BG, Song S, Pruski M, Lin VSY. Tuning of particle morphology and pore properties in mesoporous silicas with multiple organic functional groups. *Chemical Communications.* 2003;3(18):2364-2365. doi:10.1039/b306255d
76. Wu SH, Hung Y, Mou CY. Mesoporous silica nanoparticles as nanocarriers. *Chemical Communications.* 2011;47(36):9972-9985. doi:10.1039/c1cc11760b
77. Tang Z, Kotov NA, Magonov S, Ozturk B. Nanostructured artificial nacre. *Nat Mater.* 2003;2(6):413-418. doi:10.1038/nmat906
78. Borges J, Mano JF. Molecular interactions driving the layer-by-layer assembly of multilayers. *Chem Rev.* 2014;114(18):8883-8942. doi:10.1021/cr400531v
79. Fuzzy nanoassemblies.
80. Malafaya PB, Silva GA, Reis RL. Natural-origin polymers as carriers and scaffolds for biomolecules and cell delivery in tissue engineering applications. *Adv Drug Deliv Rev.* 2007;59(4-5):207-233. doi:10.1016/j.addr.2007.03.012
81. Decher G, Hong JD, Schmitt J. *Thin Solid Films, 210/21 I.*; 1992.

82. Srivastava S, Kotov NA. Composite Layer-by-Layer (LBL) assembly with inorganic nanoparticles and nanowires. *Acc Chem Res.* 2008;41(12):1831-1841. doi:10.1021/ar8001377
83. Hu B, Guo Y, Li H, Liu X, Fu Y, Ding F. Recent advances in chitosan-based layer-by-layer biomaterials and their biomedical applications. *Carbohydr Polym.* 2021;271. doi:10.1016/j.carbpol.2021.118427
84. Lara-Espinoza C, Carvajal-Millán E, Balandrán-Quintana R, López-Franco Y, Rascón-Chu A. Pectin and pectin-based composite materials: Beyond food texture. *Molecules.* 2018;23(4). doi:10.3390/molecules23040942
85. Arauz J, Rivera-Espinoza Y, Shibayama M, Favari L, Flores-Beltrán RE, Muriel P. Nicotinic acid prevents experimental liver fibrosis by attenuating the prooxidant process. *Int Immunopharmacol.* 2015;28(1):244-251. doi:10.1016/j.intimp.2015.05.045
86. Zhang M, Zhang H, Li H, et al. Antioxidant Mechanism of Betaine without Free Radical Scavenging Ability. *J Agric Food Chem.* 2016;64(42):7921-7930. doi:10.1021/acs.jafc.6b03592
87. Chen Y, Mastalerz M, Schimmelmann A. Characterization of chemical functional groups in macerals across different coal ranks via micro-FTIR spectroscopy. *Int J Coal Geol.* 2012;104:22-33. doi:10.1016/j.coal.2012.09.001
88. Durazzo A, Gabrielli P, Manzi P. Qualitative study of functional groups and antioxidant properties of soy-based beverages compared to cow milk. *Antioxidants.* 2015;4(3):523-532. doi:10.3390/antiox4030523
89. Zheng D, Sabbagh JJ, Blair LJ, Darling AL, Wen X, Dickey CA. MicroRNA-511 binds to FKBP5 mRNA, which encodes a chaperone protein, and regulates neuronal differentiation. *Journal of Biological Chemistry.* 2016;291(34):17897-17906. doi:10.1074/jbc.M116.727941
90. Sun Y, Li Q, Gui H, et al. MicroRNA-124 mediates the cholinergic anti-inflammatory action through inhibiting the production of pro-inflammatory cytokines. *Cell Res.* 2013;23(11):1270-1283. doi:10.1038/cr.2013.116

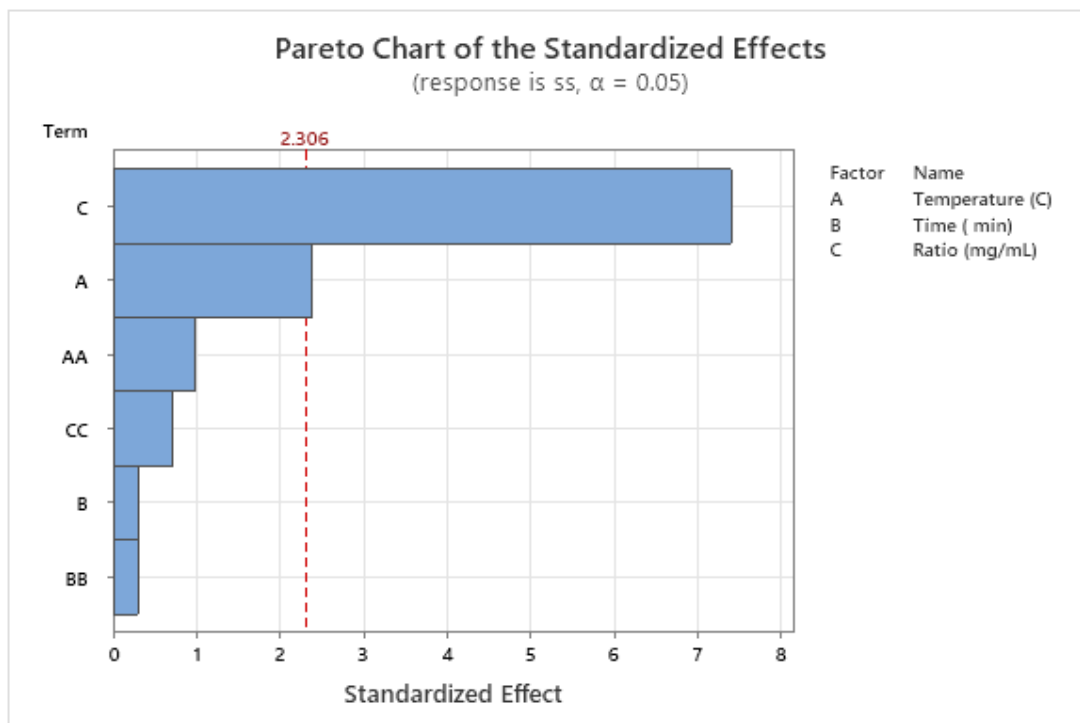
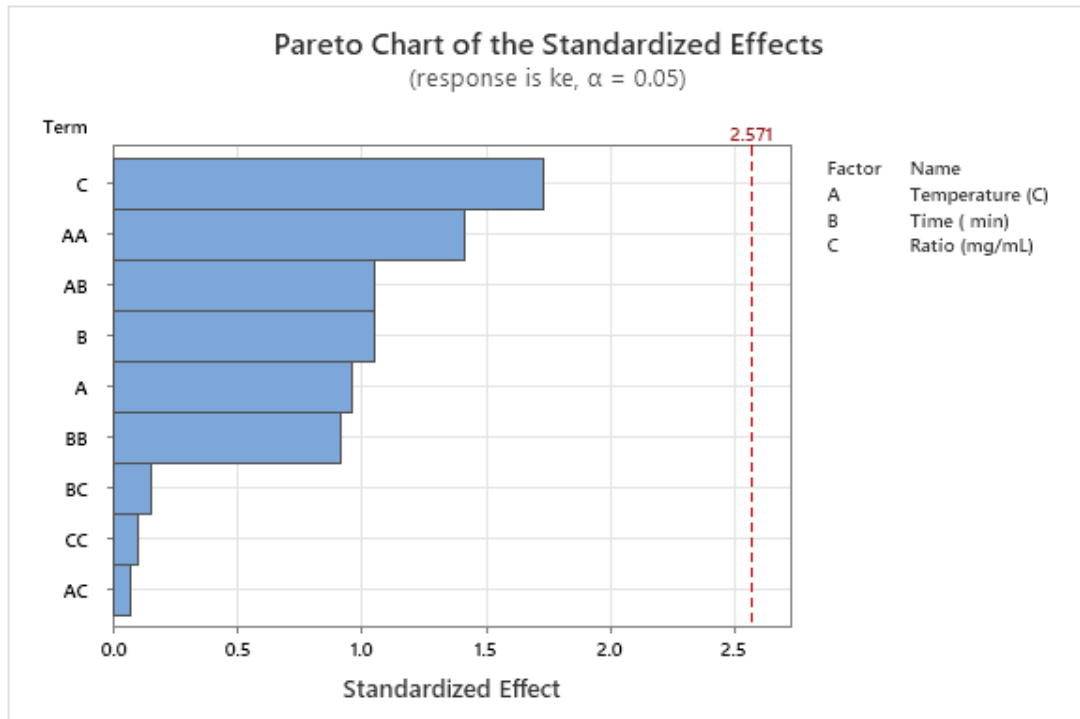
91. Mirata S, Asnaghi V, Chiantore M, et al. Photoprotective and Anti-Aging Properties of the Apical Frond Extracts from the Mediterranean Seaweed *Ericaria amentacea*. *Mar Drugs*. 2023;21(5). doi:10.3390/md21050306
92. Rodrigues D, Costa-Pinto AR, Sousa S, et al. *Sargassum muticum* and *osmundea pinnatifida* enzymatic extracts: Chemical, structural, and cytotoxic characterization. *Mar Drugs*. 2019;17(4). doi:10.3390/md17040209
93. De La Fuente G, Fontana M, Asnaghi V, et al. The remarkable antioxidant and anti-inflammatory potential of the extracts of the brown alga *cystoseira amentacea* var. *stricta*. *Mar Drugs*. 2021;19(1). doi:10.3390/md19010002
94. Cianciullo P, Maresca V, Sorbo S, Basile A. Antioxidant and antibacterial properties of extracts and bioactive compounds in bryophytes. *Applied Sciences (Switzerland)*. 2022;12(1). doi:10.3390/app12010160
95. Kumar Patra Sakti Kanta Rath Karmabeer Jena Vijaya Kumar Rathod Hrudayanath Thatoi J. *Evaluation of Antioxidant and Antimicrobial Activity of Seaweed (Sargassum Sp.) Extract: A Study on Inhibition of Glutathione-S-Transferase Activity*. Vol 32.; 2008.
96. Čmiková N, Galovičová L, Miškeje M, Borotová P, Kluz M, Kačániová M. Determination of Antioxidant, Antimicrobial Activity, Heavy Metals and Elements Content of Seaweed Extracts. *Plants*. 2022;11(11). doi:10.3390/plants11111493
97. Zheng D, Sabbagh JJ, Blair LJ, Darling AL, Wen X, Dickey CA. MicroRNA-511 binds to FKBP5 mRNA, which encodes a chaperone protein, and regulates neuronal differentiation. *Journal of Biological Chemistry*. 2016;291(34):17897-17906. doi:10.1074/jbc.M116.727941
98. Sun Y, Li Q, Gui H, et al. MicroRNA-124 mediates the cholinergic anti-inflammatory action through inhibiting the production of pro-inflammatory cytokines. *Cell Res*. 2013;23(11):1270-1283. doi:10.1038/cr.2013.116

APPENDIX

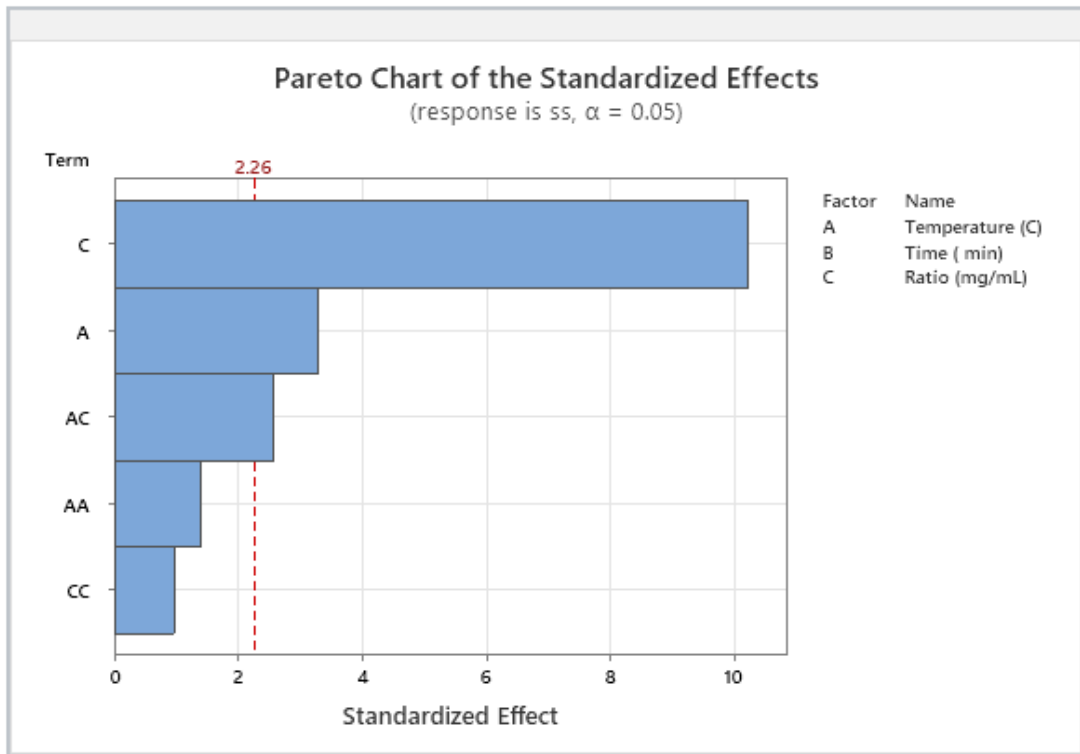
1. EVALUATION OF RELIABILITY OF THE FITTED MODELS

Pareto charts:

Organic Kelp (KE) and Sea Spaghetti (SS)

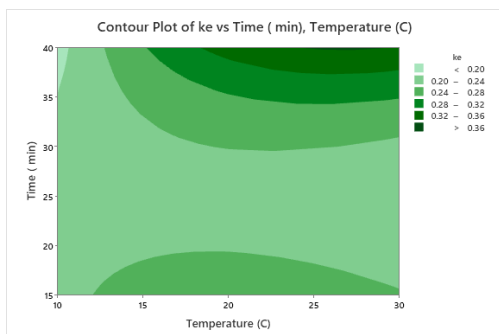
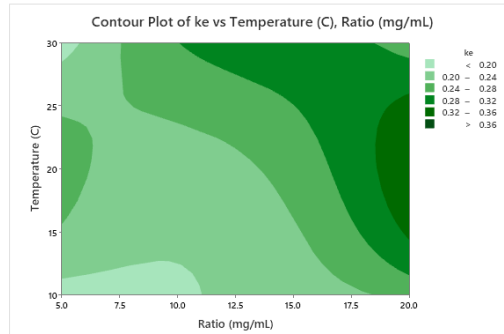
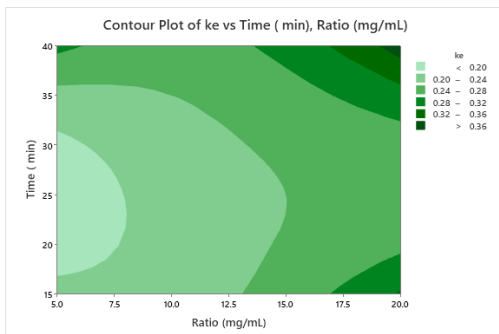


Spiral Wrack (SW)

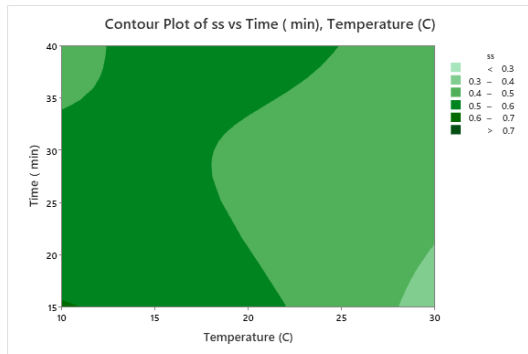
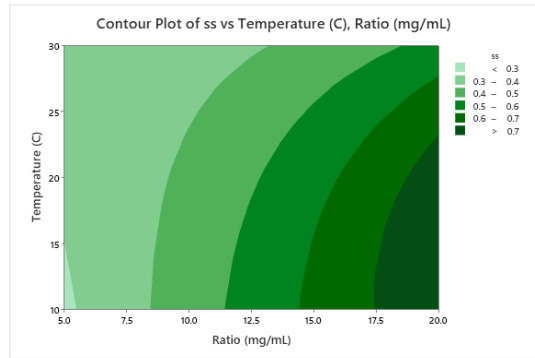
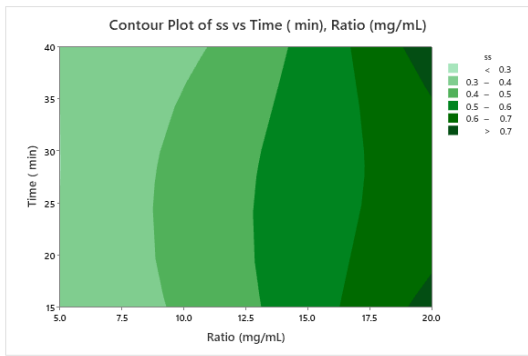


Contour Plots:

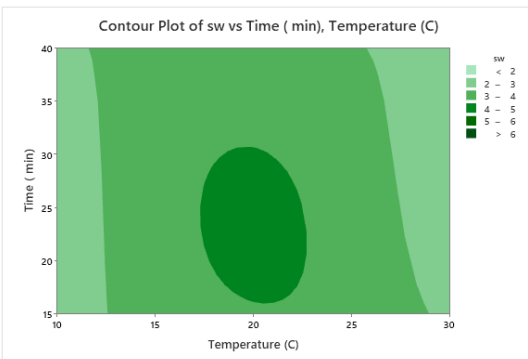
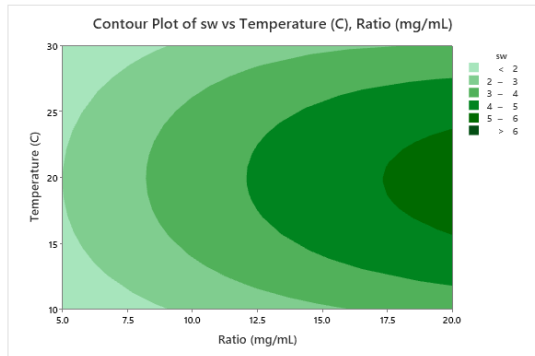
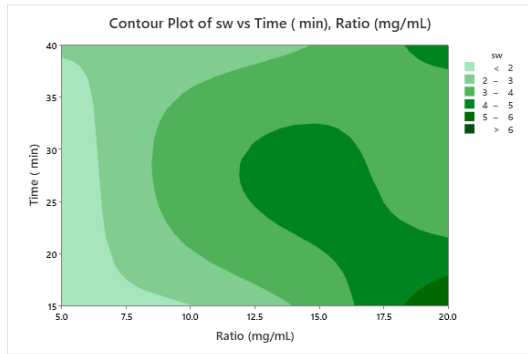
Organic Kelp (KE)



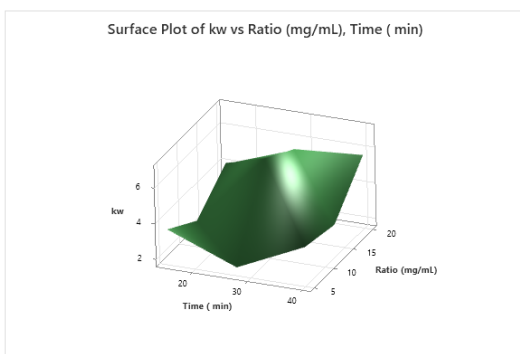
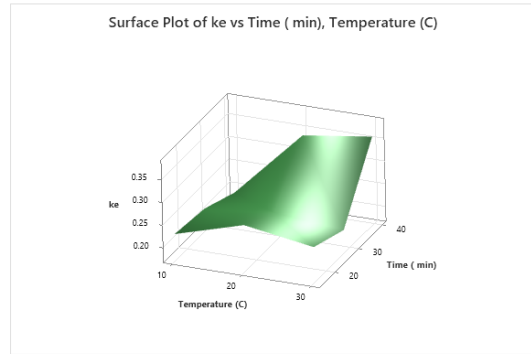
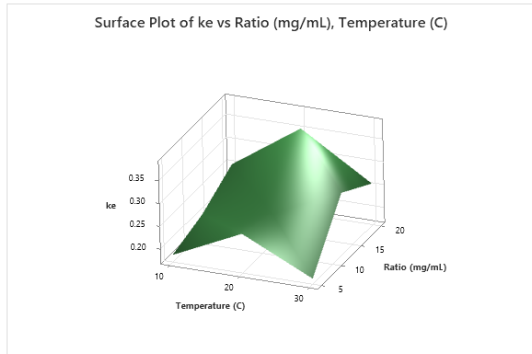
Sea Spaghetti (SS)



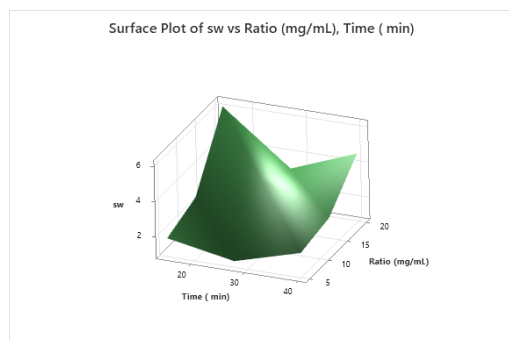
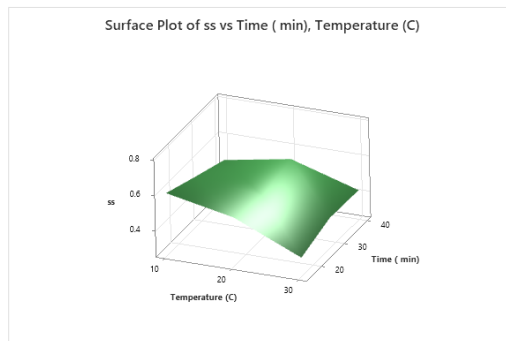
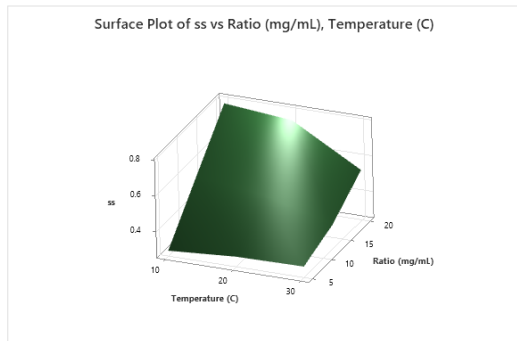
Spiral Wrack (SW)



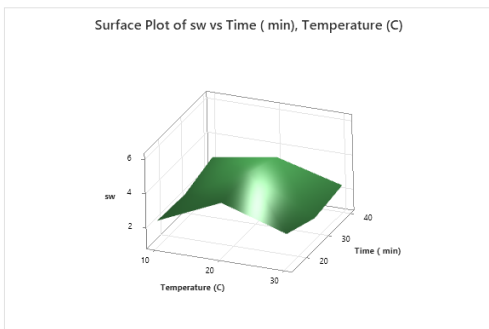
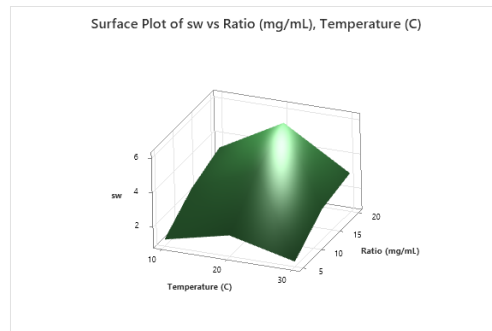
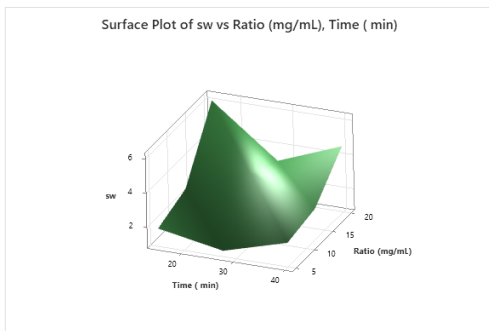
Surface Plots: Organic Kelp (KE)



Sea Spaghetti (SS)



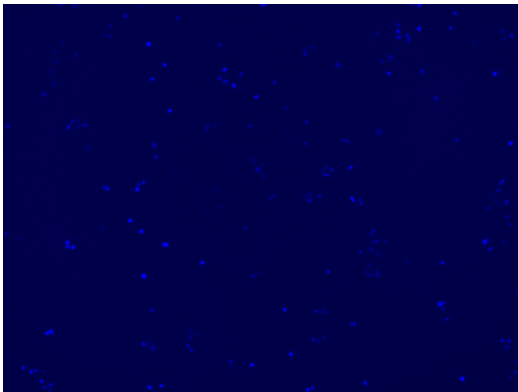
Spiral Wrack (SW)



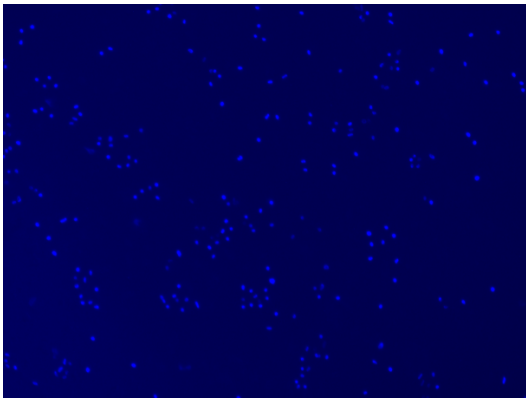
2. LIVE/DEAD ASSAY

Organic Kelp (KE)

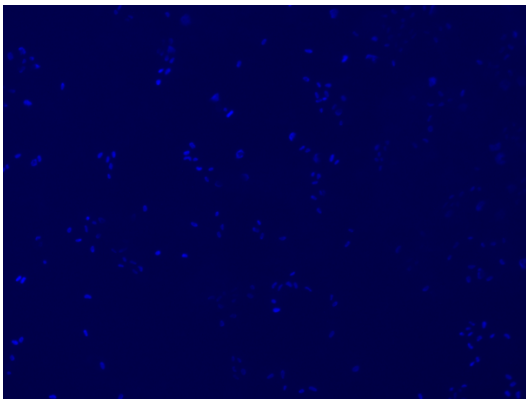
2mg/mL



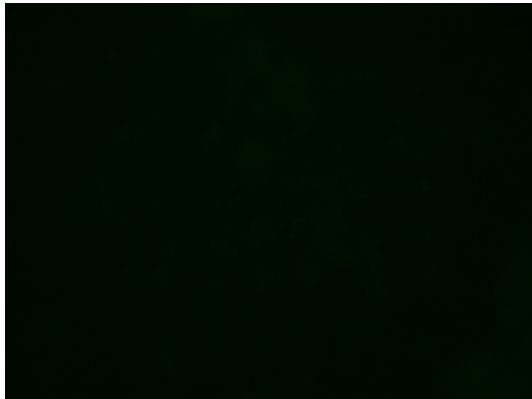
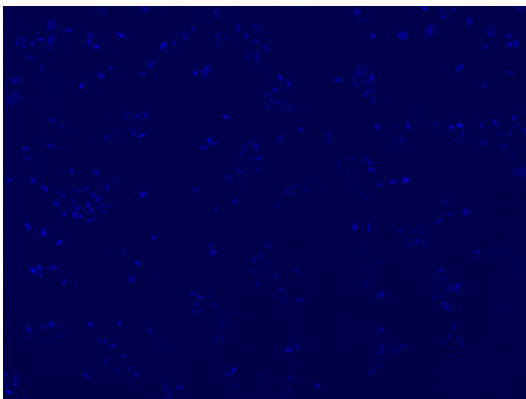
5mg/mL



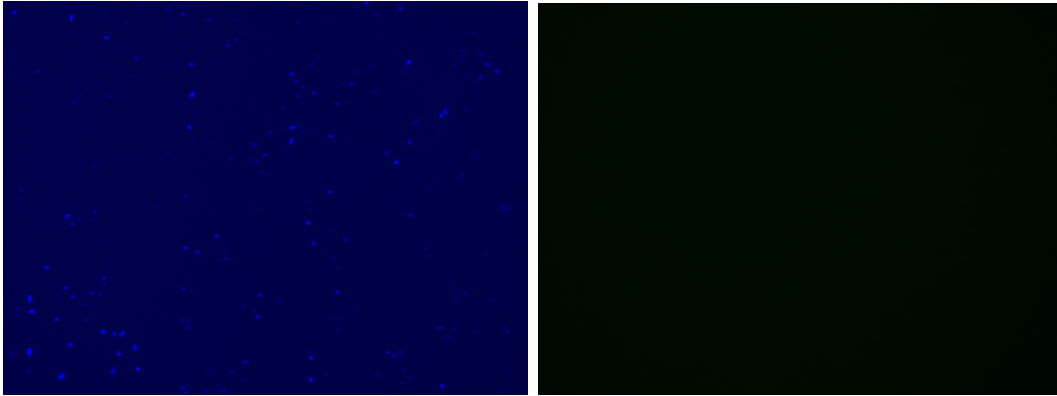
12.5mg/mL



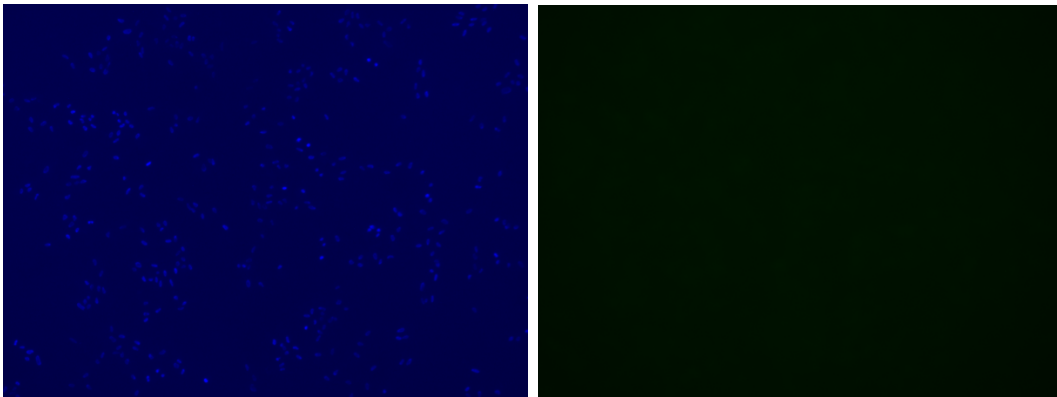
25mg/mL



50 mg/mL

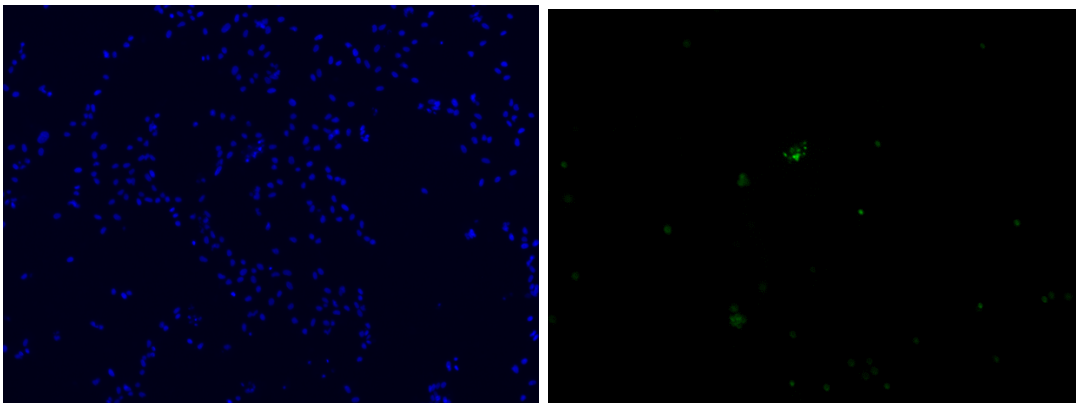


100mg/mL

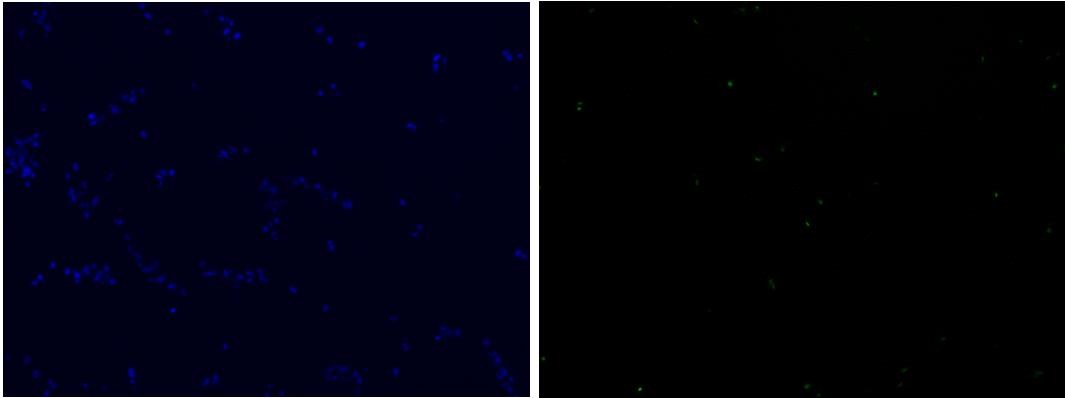


Sea Spaghetti (SS)

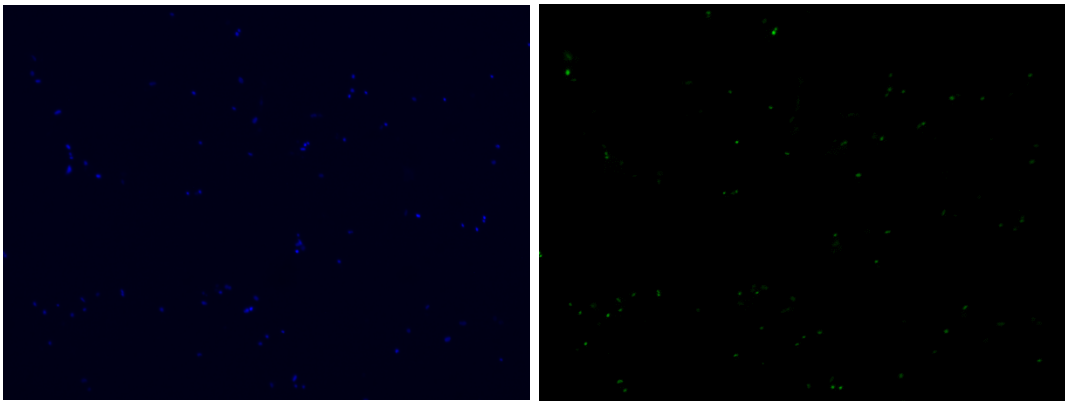
2mg/mL



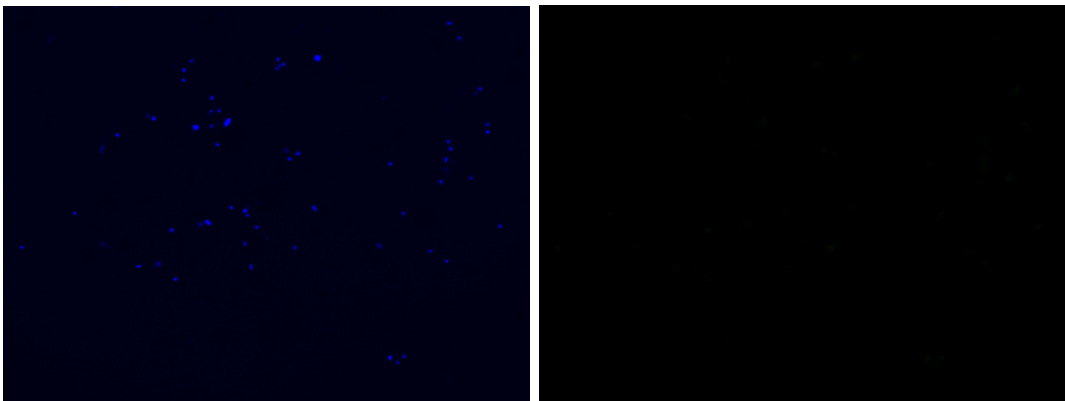
5mg/mL



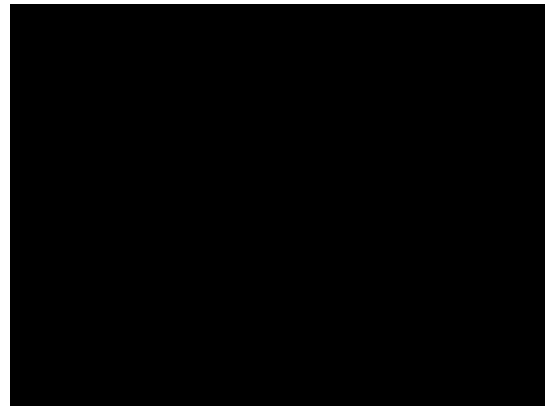
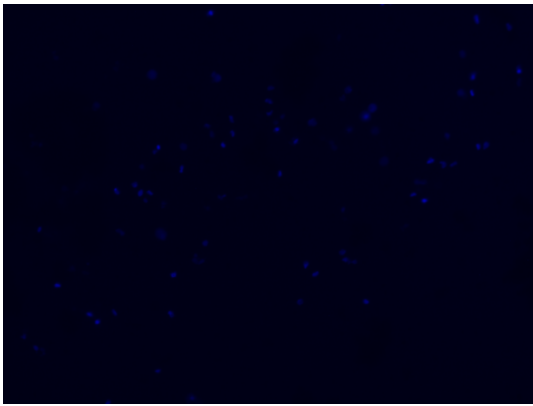
12.5 mg/mL



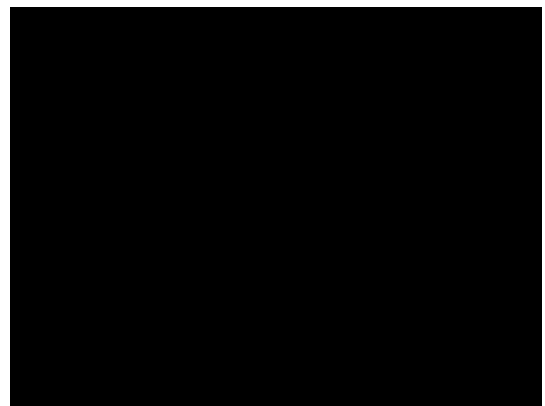
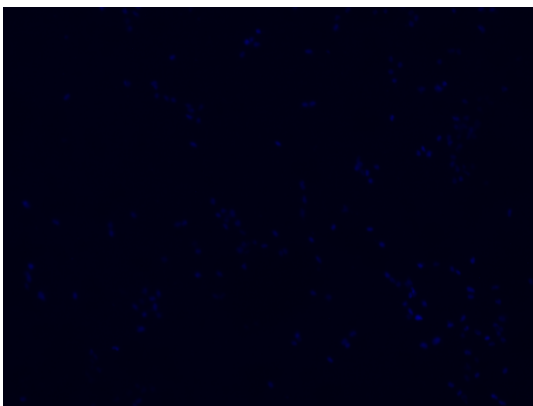
25mg/mL



50mg/mL

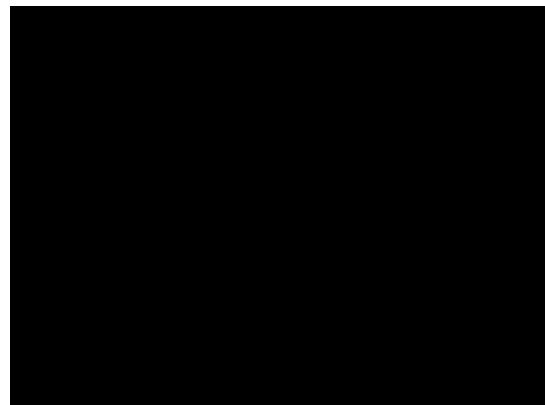
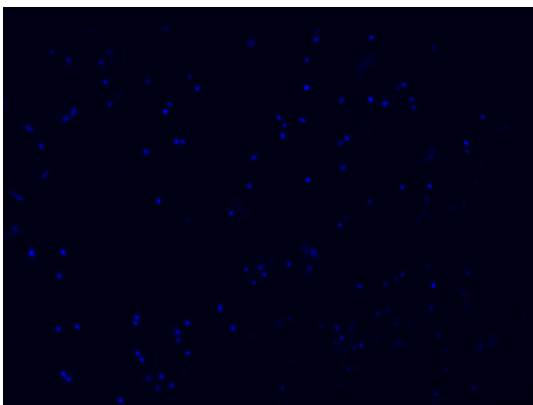


100mg/mL

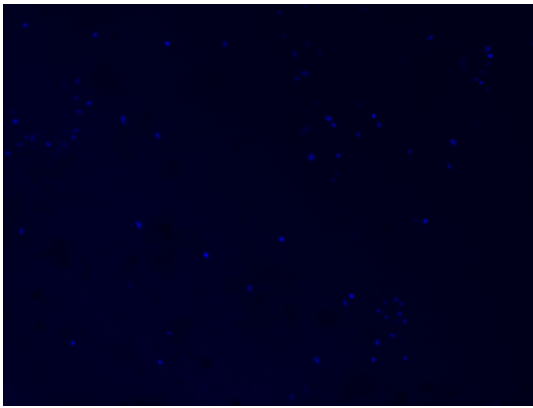


Spiral Wrack (SW)

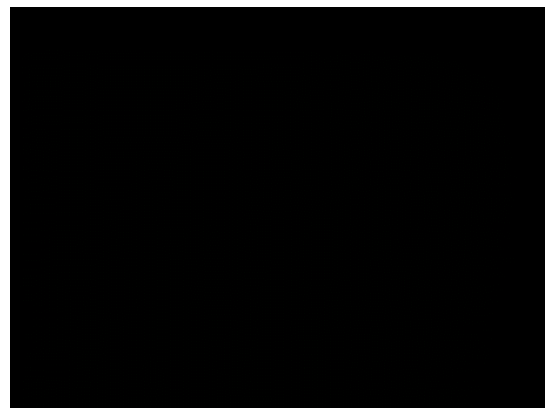
2mg/mL



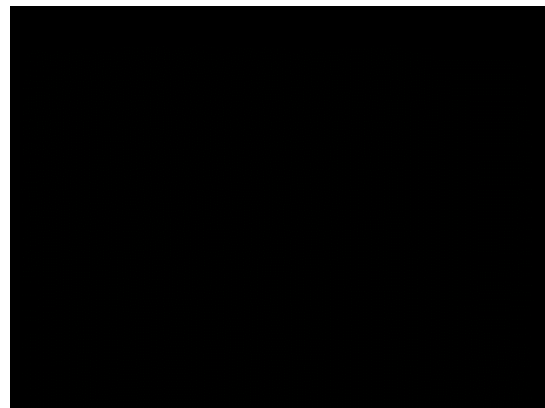
5mg/mL



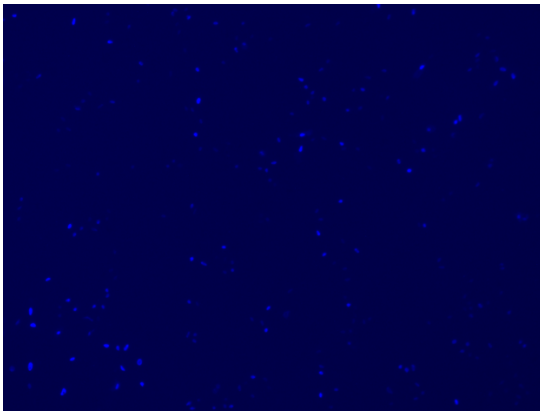
12.5mg/mL



25mg/mL



50mg/mL



100mg/mL

